Defense Threat Reduction Agency
8725 John J. Kingman Road, MS
6201 Fort Belvoir, VA 22060-6201

DTRA-TR-16-12

TECHNICAL REPORT

Probing Kill Mechanisms and Tuning Energetic Biocides

February 2018

HDTRA1-11-1-0072

Vincent T. Lee and
Michael Zachariah

Prepared by:
University of Maryland College
College Park, MD 20742

DESTRUCTION NOTICE:

Destroy this report when it is no longer needed.
Do not return to sender.

PLEASE NOTIFY THE DEFENSE THREAT REDUCTION AGENCY, ATTN: DTRIAC/ RD-NTF, 8725 JOHN J. KINGMAN ROAD, MS-6201, FT BELVOIR, VA 22060-6201, IF YOUR ADDRESS IS INCORRECT, IF YOU WISH IT DELETED FROM THE DISTRIBUTION LIST, OR IF THE ADDRESSEE IS NO LONGER EMPLOYED BY YOUR ORGANIZATION.

REPORT DOCUMENTATION PAGE

Form Approved
OMB No. 0704-0188

1. REPORT DATE *(DD-MM-YYYY)*	**2. REPORT TYPE**	**3. DATES COVERED** *(From - To)*
00-02-2018	Technical	August 2011 - July 2015

4. TITLE AND SUBTITLE

Probing Kill Mechanisms and Tuning Energetic Biocides

5a. CONTRACT NUMBER

5b. GRANT NUMBER
HDTRA1-11-1-0072

5c. PROGRAM ELEMENT NUMBER

6. AUTHOR(S)
Vincent T. Lee
Michael Zachariah

5d. PROJECT NUMBER

5e. TASK NUMBER

5f. WORK UNIT NUMBER

7. PERFORMING ORGANIZATION NAME(S) AND ADDRESS(ES)
University of Maryland College
College Park, MD 20742

8. PERFORMING ORGANIZATION REPORT NUMBER

9. SPONSORING / MONITORING AGENCY NAME(S) AND ADDRESS(ES)
Defense Threat Reduction Agency
8725 John J. Kingman Road, STOP 6201
Fort Belvoir, VA 22060-6201

10. SPONSOR/MONITOR'S ACRONYM(S)
DTRA

11. SPONSOR/MONITOR'S REPORT NUMBER(S)
DTRA-TR-16-12

12. DISTRIBUTION / AVAILABILITY STATEMENT

Distribution Statement A. Approved for public release; distribution is unlimited.

13. SUPPLEMENTARY NOTES

14. ABSTRACT

This project focuses on developing a methodology to accurately assess the time-temperature-kill relationships for spores under the exposure to biocidal agents. We will determine the relative role of thermal vs. biocidal stress and synergistic effects if any. Using energetic components that will yield biocidal agents in the reaction product, we will assess the reaction dynamics, post-analysis of the solid and gaseous products and correlate this with biocidal activity. We will conduct dynamic heating experiments to characterize by various microscopy and mass spectrometry methods, physical and chemical damage to spores. The kill mechanism for spores from short thermal pulses will be investigated for cellular or DNA damage. We will utilize data from the kill mechanism to rationally design more effective energetic biocide combinations.

15. SUBJECT TERMS

Bacillus spores, Heat neutralization, Sub-second heating, Solid and Gas biocides, Synergistic inactivation

16. SECURITY CLASSIFICATION OF:			**17. LIMITATION OF ABSTRACT**	**18. NUMBER OF PAGES**	**19a. NAME OF RESPONSIBLE PERSON**
a. REPORT	**b. ABSTRACT**	**c. THIS PAGE**	SAR	72	Douglas Dalton
Unclassified	Unclassified	Unclassified			**19b. TELEPHONE NUMBER** *(include area code)* 703-767-3054

Standard Form 298 (Rev. 8-98)
Prescribed by ANSI Std. Z39.18

UNIT CONVERSION TABLE

U.S. customary units to and from international units of measurement*

U.S. Customary Units	Multiply by → / ← Divide by†		International Units
Length/Area/Volume			
inch (in)	2.54	$\times 10^{-2}$	meter (m)
foot (ft)	3.048	$\times 10^{-1}$	meter (m)
yard (yd)	9.144	$\times 10^{-1}$	meter (m)
mile (mi, international)	1.609 344	$\times 10^{3}$	meter (m)
mile (nmi, nautical, U.S.)	1.852	$\times 10^{3}$	meter (m)
barn (b)	1	$\times 10^{-28}$	square meter (m^2)
gallon (gal, U.S. liquid)	3.785 412	$\times 10^{-3}$	cubic meter (m^3)
cubic foot (ft^3)	2.831 685	$\times 10^{-2}$	cubic meter (m^3)
Mass/Density			
pound (lb)	4.535 924	$\times 10^{-1}$	kilogram (kg)
unified atomic mass unit (amu)	1.660 539	$\times 10^{-27}$	kilogram (kg)
pound-mass per cubic foot (lb ft^{-3})	1.601 846	$\times 10^{1}$	kilogram per cubic meter (kg m^{-3})
pound-force (lbf avoirdupois)	4.448 222		newton (N)
Energy/Work/Power			
electron volt (eV)	1.602 177	$\times 10^{-19}$	joule (J)
erg	1	$\times 10^{-7}$	joule (J)
kiloton (kt) (TNT equivalent)	4.184	$\times 10^{12}$	joule (J)
British thermal unit (Btu) (thermochemical)	1.054 350	$\times 10^{3}$	joule (J)
foot-pound-force (ft lbf)	1.355 818		joule (J)
calorie (cal) (thermochemical)	4.184		joule (J)
Pressure			
atmosphere (atm)	1.013 250	$\times 10^{5}$	pascal (Pa)
pound force per square inch (psi)	6.984 757	$\times 10^{3}$	pascal (Pa)
Temperature			
degree Fahrenheit (^oF)	$[T(^oF) - 32]/1.8$		degree Celsius (^oC)
degree Fahrenheit (^oF)	$[T(^oF) + 459.67]/1.8$		kelvin (K)
Radiation			
curie (Ci) [activity of radionuclides]	3.7	$\times 10^{10}$	per second (s^{-1}) [becquerel (Bq)]
roentgen (R) [air exposure]	2.579 760	$\times 10^{-4}$	coulomb per kilogram (C kg^{-1})
rad [absorbed dose]	1	$\times 10^{-2}$	joule per kilogram (J kg^{-1}) [gray (Gy)]
rem [equivalent and effective dose]	1	$\times 10^{-2}$	joule per kilogram (J kg^{-1}) [sievert (Sv)]

*Specific details regarding the implementation of SI units may be viewed at http://www.bipm.org/en/si/.

†Multiply the U.S. customary unit by the factor to get the international unit. Divide the international unit by the factor to get the U.S. customary unit.

Abstract

This project focuses on developing a methodology to accurately assess the time-temperature-kill relationships for spores under the exposure to biocidal agents. We will determine the relative role of thermal vs. biocidal stress and synergistic effects if any. Using energetic components that will yield biocidal agents in the reaction product, we will assess the reaction dynamics, post-analysis of the solid and gaseous products and correlate this with biocidal activity. We will conduct dynamic heating experiments to characterize by various microscopy and mass spectrometry methods, physical and chemical damage to spores. The kill mechanism for spores from short thermal pulses will be investigated for cellular or DNA damage. We will utilize data from the kill mechanism to rationally design more effective energetic biocide combinations. Finally new types of proto-type nanosctructured energetic materials containing biocidal components will be synthesized and evaluated. The ultimate goal is to provide a data-base of exposure vs. effect that can be imported to a CFD formulation so that the combined effects of fluid entrainment, heat transfer and chemical composition can be used to model kill effectiveness in an arbitrary physical system.

Objective

Define the time-temperature-kill relationships for Bacillus spore inactivation at sub-second timescales that will be amenable to be implemented within the framework of a CFD simulation. This database may also contain information on the combustion dynamics and how new types of agents work.

In year 1, proposed Tasks 1-4 include the following:

Task 1: Develop experimental protocol
Task 2: Characterize Time-Temperature killing relationship
Task 3: Determine kill mechanisms
Task 4: Expose spores to gas-phase agents

In year 2, proposed Tasks 5-7 include the following:

Task 5: Characterize synergistic killing relationship with solid energetic biocide products
Task 6: Determine kill mechanisms with biocides
Task 7: Energetic Biocide Reaction Dynamics

Approach

Spores were immobilized on metal support and subjected to joule heating to different peak temperature, rates and biocides.

Work accomplished

In year 1, we established the experimental protocol of electrodeposition of *Bacillus* spores onto metal support. This is a novel approach to immobilize bacterial spores. A manuscript entitled "Quantitative attachment and detachment of bacterial spores from fine wires through pulsed voltammetry" was published in the Journal of Physical Chemistry B in 2012.

In year 2, we characterize the time-temperature-kill relationship by subjecting immobilized spores to resistive heating to different peak temperatures and at different peak heating rates. These results revealed an interesting observation that heating at different heating rates caused different time-temperature-kill relationships. The critical temperature for heat inactivation for heating rates below $1x10^4$ ˚C/sec matched results from conventional heating schemes that occur at lower heating rates. However, at rates above $1x10^5$ ˚C/sec, there is a significant improvement in thermal inactivation of *B. subtilis* spores. Morphological observations by SEM revealed that spores treated at the lower heating rate increasingly "melted" with increasing peak temperature. In contrast, SEM observation of spores at the higher heating rate revealed increasingly larger holes on the spore surface with increasing peak temperature. Decreasing the external pressure led to enlargement of the holes, whereas increase in the external pressure led to the formation of a surface protrusion. Using mutant spores obtained from the lab of Dr. Peter Setlow, we showed that lower heating rates caused DNA damage as spores lacking proteins responsible for DNA protection (sspA/sspB) or DNA repair (recA) were more sensitive to heat. These results are in agreement with the mechanism of spore inactivation by conventional heating schemes. A manuscript describing these finding entitled "Inactivation of bacterial spores subjected to sub-second thermal stress" was published in the Chemical Engineering Journal in 2015.

In year 3, we characterized the time-temperature-kill relationship of *B. thuringiensis* spores as these spores have features that are similar to *B. antracis* spores. Spores subjected to the two heating rates yielded similar time-temperature-kill relationships as observed earlier for Bs spores. Furthermore, we tested the synergistic effect of heat and chlorine, a gas phase biocide. The results showed that Cl_2 synergizes with heat at a heating rates below $1x10^4$ ˚C/sec by lowering the critical temperature by 150 ˚C, whereas at heating rate above $1x10^5$ ˚C/sec reduced the critical temperature by 50 ˚C. The synergistic effect of heat and Cl_2 was further characterized by determining the mechanism of action. Cl_2 gas reacts rapid with water vapor to form HCl and HOCl. By reducing the humidity of the heating chamber to 0% humidity, the synergistic effect of Cl_2 and heat can be completely reversed. These results indicate that HCl and HOCl participates in the synergistic killing with heat. By SEM, there was minimal morphological change associated with spores that were inactivated by Cl_2 and heat indicating the chlorine was not causing inactivation through large changes in the Bt spores. Interestingly, high heating rate (>10^5 ˚C) in the presence of Cl_2 gas caused the spore coat to shed from the underlying spore core. This morphology is in contrast to the "melting" morphology of spore coat treated with heat alone. Together, the SEM results indicate that heat and Cl_2 act fix the spore coat and preventing the ability of heat to melt

the spore. By energy dispersive spectroscopy (EDS) to determine the presence of Cl and C at different temperatures, the increase in Cl in the spores are correlated with increased spore inactivation. Furthermore, EDS analysis of the spore coat shed at high heating rate in the presence of Cl_2 revealed a high level of Cl. Since HOCl is chemically reactive to biological molecules, we propose a model in which HOCl is formed from reaction between Cl_2 and water vapor and heat activates the reactions between HOCl and the spore coat. As a consequence of this synergistic effect, the spores are inactivated at a lower temperature. A manuscript describing these findings entitled "Synergistic Effects of Ultrafast Heating and Gaseous Chlorine on the Neutralization of Bacterial Spores" has been submitted to Chemical Engineering Sciences.

In addition to the above works, the funds from the grant supported a collaborative study with the co-PI's lab to investigate the composites containing iodates and their biocidal activity on Bs spores. A manuscript entitled "Metal Iodate-based Energetic Composites and their Combustion and Biocidal Performance" was published in ACS Applied Material and Interfaces in 2015.

Papers published

1. Zhou, W., Watt, S.K., Tsai D.-H., **Lee, V.T.**, **Zachariah, M.R.** 2012 Quantitative attachment and detachment of bacterial spores from fine wires through pulsed voltammetry. *J Phys Chem B*. 117(6):1738-45. doi: 10.1021/jp307282q.

2. Wang, H., Jian, G., Zhou, W., DeLisio, J., **Lee, V.T.**, **Zachariah, M.R.** 2015. Metal Iodate-based Energetic Composites and their Combustion and Biocidal Performance. *ACS Appl Mater Interfaces*. 7(31):17363-70. doi: 10.1021/acsami.5b04589.

3. Zhou, W., Orr, M.W., Jian, G., Watt, S.K., **Lee, V.T.**, **Zachariah, M.R.** 2015 Inactivation of bacterial spores subjected to sub-second thermal stress. *Chemical Engineering Journal*. 279(2015):578–588. doi:10.1016/j.cej.2015.05.021.

4. Zhou, W., Orr, M.W., **Lee, V.T.**, **Zachariah, M.R.** Synergistic Effects of Ultrafast Heating and Gaseous Chlorine on the Neutralization of Bacterial Spores. *Chemical Engineering Science*. Submitted in 2015.

Students graduated

Wenbo Zhou, a graduate student in the Zachariah lab, is graduating in October, 2015.

Mona Orr, a graduate student in the Lee lab, is scheduled to graduate in Spring of 2016.

Sarah Watt, a technician in the Lee lab, is currently enrolled in University of Southern California Medical School.

Other accomplishments

The PI (Vincent Lee) received tenure and was promoted to Associate Professor in August of 2014 in the Department of Cell Biology and Molecular Genetics at the University of Maryland at College Park.

THE JOURNAL OF PHYSICAL CHEMISTRY B

Article

pubs.acs.org/JPCB

Quantitative Attachment and Detachment of Bacterial Spores from Fine Wires through Continuous and Pulsed DC Electrophoretic Deposition

Wenbo Zhou,[†] Sarah K. Watt,[‡] De-Hao Tsai,[†] Vincent T. Lee,*[,‡] and Michael R. Zachariah*[,†]

[†]Department of Chemistry and Biochemistry and Department of Mechanical Engineering, [‡]Department of Cell Biology & Molecular Genetics, University of Maryland, College Park, Maryland 20742, United States

Supporting Information

ABSTRACT: We demonstrate the uniform attachment of bacterial spores electrophoretically onto fine wires in liquids and subsequently quantitatively detached back into suspension. It was found that the use of a pulsed voltage method resulted in a uniform coverage of spores and prevented visible bubble formation resulting from water electrolysis which tended to dislodge the spores from the wires. By monitoring the electrophoretically derived current, this method could also be used to quantitatively measure the surface charges on spores and the deposition rate. The method is generic and should be applicable to the deposition of any charged biological material (e.g., spores, bacteria, viruses) onto metal surfaces.

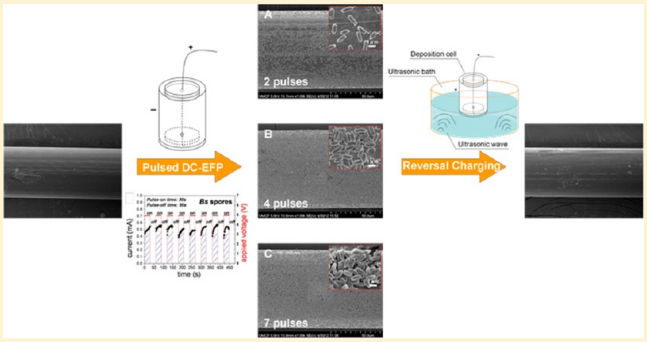

1. INTRODUCTION

Concerns on bioterrorism[1,2] have prompted efforts to discover, quantify, and compare neutralization methods such as heat,[3,4] chemical,[5] and other synergistic effects.[6−8] The extreme stress-resistance of bacterial spores[9] has provided the impetus to develop quantitative studies to more precisely define various neutralization mechanisms. Previous studies in defining spore neutralization have focused on heating under 100 °C in the absence of pressure or the combination of heat and pressure with inactivation time scale in the order of minutes.[10,11] In particular, a temperature−time relationship for spore inactivation for high temperatures (100−1000 °C) and short times (10 ms to 10 s) is still not available. The first approach to address this problem is to initiate thermal reactions in sealed chambers in which the temperature between 200 and 700 °C is monitored and correlated with the number of recovered viable spores.[4,12,13] These experiments are limited by the ability to precisely manipulate the temperature and exposure time. Another approach recently employed has been to disperse spores in the aerosol phase and subject them to high temperatures between ∼150 and >1000 °C and chemical environments.[3,14] However, there exists a temperature distribution in the aerosol flow in these studies, which causes a decrease in the precision of the temperature−viability relationship. A third approach is to immobilize spores on a surface that can be thermally varied in a precise manner. This approach can cover a larger temperature range[15] in short time scales and allows convenient enumeration of viable spores immediately after thermal exposure.

The latter method is only useful if a well-defined spore population can be coated on the surface. Typically, this might be accomplished in a liquid suspension either naturally[16−18] or by laboratory manipulation.[19,20] Bacteria naturally have various adhesins to promote attachment to plastic, glass, and metal surfaces to form biofilms.[16−18] In the laboratory, poly-L-lysine can be coated to impart a net positive charge on the surface to promote electrostatic interaction with the negatively charged exterior of most bacteria. However, neither mechanism can be utilized for the studies of spores, as spores are biological inert and often fail to attach to poly-L-lysine coated surfaces.[21] We sought to develop an alternative approach to attach spores onto wires using physical forces.

Previously, dielectrophoresis has been utilized in the manipulation of bacterial spores.[22] In the presence of an electric field gradient, a net force is imparted on the spore due to polarization, the magnitude of which is highly dependent on the material properties of the spore (including size),[23] the characteristics of the fluid (including ionic strength and dielectric permittivity of the solvent and solute),[24] and the field gradient.[25−28] Dielectrophoresis is contrasted with electrophoresis which can take place if the cell has a net charge, and is directly proportional to the magnitude of the field.[29,30] Most reported studies however modeled spore transport in liquids as

Special Issue: Electrophoretic Deposition

Received: July 23, 2012
Revised: October 15, 2012
Published: October 24, 2012

dx.doi.org/10.1021/jp307282q | J. Phys. Chem. B 2013, 117, 1738−1745

being net neutral in charge, and only considered the dielectrophoretic effect.[31−33] Actually, in aqueous dispersions, the glycoproteins and polysaccharides that comprise the exosporium (i.e., outer layer) are negatively charged. These negative charges arise from deprotonation of aldehydes (−RCOH), phosphodiester (−$(RO)_2$POOH), and carboxylic acids (−RCOOH), which have been detected by the infrared spectroscopy[34] and zeta potential analysis.[35]

Electrophoretic deposition (EPD) has been used in the past for a wide variety of bioparticles including bacteria,[36,37] protein inclusion bodies,[38] and yeast cells.[39] While the generic process of EPD of bioparticles is similar, the exact rates of attachment to the wire may be complicated by side effects including bubble formation,[40,41] surface chemistry,[42,43] electrode curvature effects,[44] and excretion of adhesive extracellular media[45,46] Bubble formation appears to be a significant problem for controlled and effective EPD. Two approaches have been reported to minimize this effect. AC-EPD has been found as a powerful method to mitigate the water electrolysis under some frequency conditions.[47,48] Pulsed DC-EPD has also been shown to obtain dense bubble-free deposits at suitable pulse widths and duty cycles.[49,50] From a practical standpoint, pulsed DC-EPD is a simpler approach that is easier to implement.

Besides the electrostatic interaction forces and the bubble formation effects on attachment, other forces may also contribute to the attachment of spores to surfaces. The Lifshitz−van der Waals force between the spore surface and the electrode surface can be described by the well-known Derjaguin−Landau−Verwey−Overbeek (DLVO) theory.[51] The image force which arises due to the induced dipole effect between the charged spore and the surface can also influence deposition and has been detected by atomic force microscopy.[52] While the Lifshitz−van der Waals force, the image force, and the electrostatic force all have an inverse square distance relationship, for the problem under consideration here, it has been shown that the dominant effect can be attributed to the electrostatic force.[53]

In this study, we will investigate electrophoretic attachment of uniform layers of spores to fine wires, and demonstrate reversible detachment. We demonstrate that, by applying a pulsed direct current (DC), we can quantify incremental spore attachment with time by measuring the electrical current to the wire electrode. The advantages of this charging mode will be shown over the continuous charging mode. By using the measured current which can be directly related to the spore flux to the surface, we are further able to validate a transport model and use the model to directly determine the average spore surface charge and spore deposition efficiency. This methodology developed here is to our knowledge the first demonstration of direct quantitative attachment and detachment of spores from fine wires.

2. EXPERIMENTAL APPROACH TO SPORE ATTACHMENT AND DETACHMENT

2.1. Spore Deposition Cell. The spore deposition cell is shown schematically in Figure 1. It is composed of four compartments: an outer PTFE tubular shell with sealed base, a stainless steel cylinder as the outer electrode, a central wire as the deposition surface and inner electrode, and two PTFE plates to center the wire. The stainless steel outer electrode has an inner diameter of 16 mm and a height of 20 mm. For the wire central deposition electrode, we use 76.2 μm platinum (Pt) (Omega Engineering, Inc.), since it is very stable in

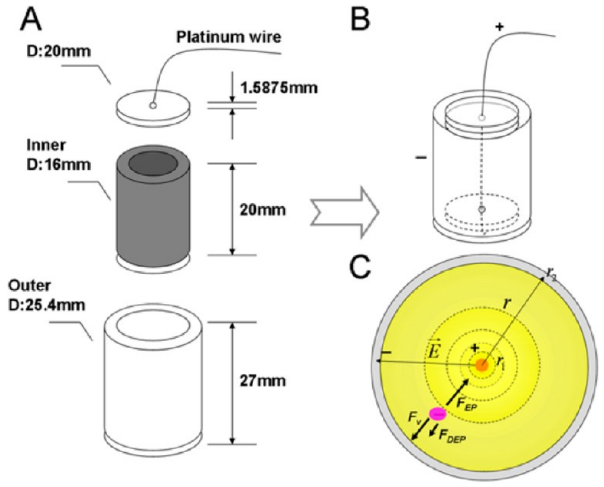

Figure 1. (A) Components of the spore deposition cell which includes an outer protection cylindrical shell, an inner stainless steel tube, two PTFE center-pierced plates, and the central wire. (B) Assembled cell in the spore coating process, with the wire as the anode and the stainless steel tube as the cathode. Part C shows the electric field distribution between two electrodes and the forces that the negatively charged spores experience in the liquid phase.

aqueous systems and will not be oxidized. The spore strain adopted in these studies is *Bacillus subtilis* (*Bs*) spores ATCC#6051 (see the optical microscopic image in Figure S1, Supporting Information), which were sporulated by growth in Difco Sporulation Medium (DSM) at 30 °C for 48 h. A 250 mL DSM was prepared which included 2 g of Bacto nutrient broth, 2.5 mL of 10% KCl, 0.375 mL of 1 M NaOH, and 2.5 mL of 1.2% $MgSO_4{\cdot}7H_2O$. The initial spore number concentration was regulated to be 8×10^9 CFU/mL.

The power supply and current detection were performed with a 6430 sub-femtoamp remote sourcemeter from Keithley. Ultrasonication employed a Branson model 5510 ultrasonic cleaner. Optical microscopic images were taken by a Zeiss AxioObserver microscrope using a 40× objective with phase contrast illumination. Scanning electronic microscopic (SEM) images were taken of spores on wires fixed with 2% glutaldehyde, dehydrated through a series of alcohol, and sputter coated with platinum. Images were captured with a Hitachi S4700 FESEM in the Laboratory of Biological Ultrastructure at the University of Maryland. To validate our spore charging measurement approach, we employed zeta-potential analyses from a Zetasizer Nano ZS (Malvern Instruments, U.K.) equipped with a 633 nm laser and a palladium dip cell module. A 500 μL portion of sample suspension was mixed with 250 μL of 10 mM ammonium acetate aqueous solution prior to the measurement.

2.2. Spore Attachment in Continuous and Pulsed DC Charging Modes. The fine wire was stabilized inside the spore deposition cell vertically, and the spore suspension was added into the cell to immerse the wire up to a depth of 1 cm. The central wire was connected with the positive pole of the power supply, and the outer stainless steel cylinder was connected to the negative pole. A variety of EPD measurements were performed with varying voltages and on-times, and real-time current data were stored. Comparably, fine wires with different compositions and diameters were tested to find an optimal one. In the pulsed DC charging mode, a series of pulsed on-times and off-times were controlled to differentiate

dx.doi.org/10.1021/jp307282q | J. Phys. Chem. B 2013, 117, 1738−1745

from the continuous charging mode, and the optimal pulsed charging condition for *Bs* spores ATCC#6051 was found.

2.3. Optical Microscopic and SEM Analyses. Wires coated with spores were observed under optical microscopy over glass slides and also by the naked eye. For the SEM analyses, samples were first fixed in 2% glutaraldehyde in buffer for 1 h at room temperature. Excess glutaraldehyde was removed in buffer by three washes of 10 min each. The samples were post fixed with 1−2% osmium tetroxide in the above buffer for at least 30 min, and then with double distilled water. After a series of dehydration processes in ethanol, the samples were treated with critical point drying with liquid carbon dioxide. Finally, samples were mounted to stubs and coated with gold/palladium alloy.

2.4. Spore Detachment. A very important aspect of this work was to develop the methodology to detach spores from the wire. To accomplish this, the wire loaded with spores was placed in a clean cell with distilled water and the wire oppositely biased to be the cathode. Simultaneously, the cell was immersed into an ultrasonic bath. The separate effects of opposite biasing and ultrasonication were compared. The detached spores were harvested for spore plate counting, as will be shown later. The treated wire was inspected by optical microscopic and SEM analyses to find if all the attached spores were removed from the surface.

2.5. Spore Plate Counting Assay. Spores detached from wires were counted by enumerating colony forming units (CFU) by plating serial dilutions on LB agar plates. Counting was repeated four times, and an averaged value was reported.

3. SPORE TRANSPORT MODEL

The use of the cylindrical deposition cell geometry enabled quantitative modeling, since the electric field is well described as

$$|\vec{E}| = \frac{\Delta U}{r \ln \frac{r_2}{r_1}} \tag{1}$$

where ΔU is the voltage difference between two electrodes, r is the radical distance from the center, and r_1 and r_2 are the diameters of the inner (wire) and outer cylindrical electrodes. In our design, r_1 = 0.0381 mm and r_2 = 8 mm. It is well-known that spores when introduced into an aqueous medium will acquire a net charge[34,35] and thus can be manipulated with an electric field. The electrophoretic force on a spore with q charges in an applied electric field is

$$F_{EP} = qE \tag{2}$$

The presence of the field will also induce polarization within the spore, which if the field is spatially invariant will impart no net force on the spore. However, in the presence of an electric field gradient, the spore will also experience a net dielectrophoretic force:[22]

$$F_{DEP} = 2\pi\varepsilon_m R^3 \,\mathrm{Re}(f)\nabla E^2 \tag{3}$$

where ε_m is the permittivity of the surrounding water (7.1×10^{-10} F/m) at room temperature, R is the radius of the spore, and $\mathrm{Re}(f)$ is the real part of the Clausius−Mossotti factor. In a DC field, this factor is directly related to the conductance of both the spore surface and the media:[22]

$$\mathrm{Re}(f) = \frac{\sigma_p - \sigma_m}{\sigma_p + 2\sigma_m} \tag{4}$$

Herein, σ_p and σ_m stand for the conductivities of spores and media. At room temperature, σ_p is 10^{-7} S/m (as the cell membrane[54]) and σ_m is 5.5×10^{-6} S/m. Hence, $\mathrm{Re}(f)$ is a negative value which implies that the direction of F_{DEP} is opposite to the direction of F_{EP}, as in Figure 1C. Meanwhile, the retarding force is caused by the viscous drag and can be evaluated with Stoke's law:

$$F_v = -6\eta\pi R u \tag{5}$$

where η is the viscosity of water (1.002×10^{-3} Pa·s) at room temperature and u is the velocity of spores. It should be noted that the *Bs* spores are not strictly spherical; thus, R in both eqs 3 and 5 is an effective radius (a spherical spore with this effective radius is defined to have the same volume as a real spore). From previous reports of spore volumes,[55] the effective R value for *Bs* spores is 0.336 μm. The spore motion can then be directly evaluated in a force balance:

$$\Delta F = m_s \frac{d^2 r}{dt^2} = F_{DEP} + F_{EP} + F_v \tag{6}$$

Since the inertia term is relatively small (i.e., the spore response time to any voltage perturbation is fast relative to the transit time), we can assume steady state ($\Delta F = 0$). The resulting governing equation becomes

$$\frac{dr}{dt} = \frac{A}{r} + \frac{B}{r^3} \tag{7}$$

where $A = \Delta U \cdot q/(0.101R)$, $B = 8.26 \times 10^{-9}(\Delta U)^2 R^2$.

The above equation describes the spore velocity at any radial location in the cell between two cylindrical electrodes and thus can be directly related to the experimental current data, since it is the motion of spores that contributes to the current formation. The time for spores with an initial distance $r + \Delta r$ away from the center to move a differential distance of Δr is from eq 7:

$$\Delta t = \frac{r^2 - (r + \Delta r)^2}{2A} + \frac{B}{2A^2} \ln \frac{A^2(r + \Delta r)^2 + AB}{A^2 r^2 + AB} \tag{8}$$

In this time interval, the total charge quantity passing through this differential distance Δr is

$$\Delta Q = q' C \Delta V = q' C \pi l[(r + \Delta r)^2 - r^2] \tag{9}$$

where C is the spore number concentration in the cell, l is the immersed depth of Pt wire inside the liquid (0.01m), and ΔV is the differential volume element around the wire. It should be noted that the charge q' is the effective overall charge after being shielded by counterions in the vicinity of the spore surface (i.e., the diffuse double layer). The importance of this is that the mobility of a spore is influenced by the thickness of the double layer that is dragged along with the spore. The current can be expressed as

$$I = \lim_{\Delta t \to 0} \left| \frac{\Delta Q}{\Delta t} \right| = \frac{2q' \pi C l (A r^2 + B)}{r^2} \tag{10}$$

Then, substituting for A and B above, the initial current observed can be expressed as

$$I_0 = \frac{0.622 C \Delta U}{R} q' q + 3.58 \times 10^{-7} C \Delta U^2 R^2 q' \tag{11}$$

Equation 11 is a simplified illustration of the current corresponding to the spore deposition rate but which does

dx.doi.org/10.1021/jp307282q | J. Phys. Chem. B 2013, 117, 1738−1745

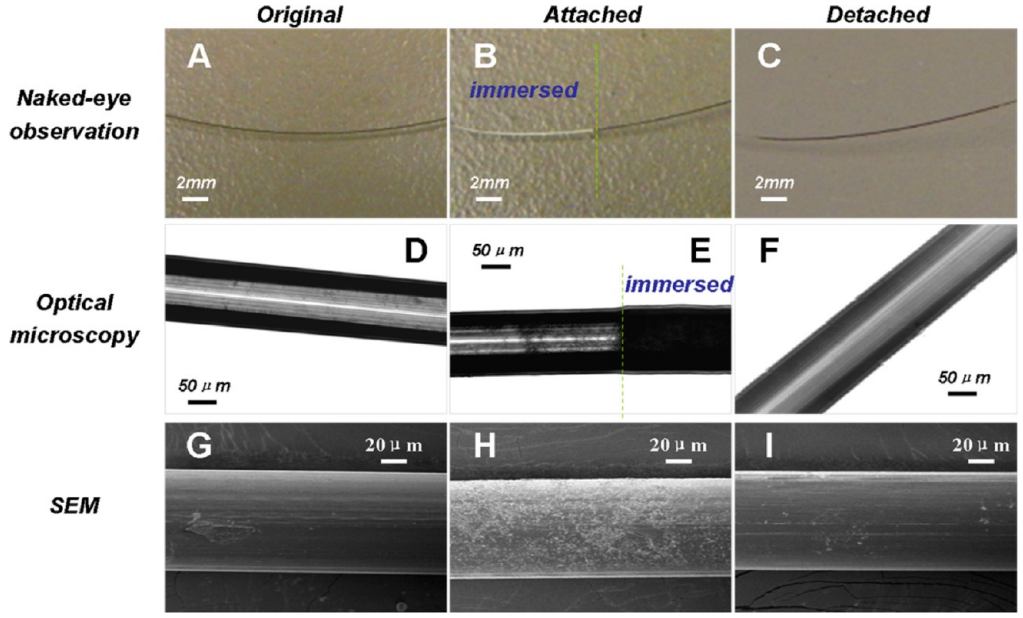

Figure 2. Parts A–C show Pt wires before coating, after coating, and after detaching. Parts D–F show optical microscopic images of Pt wires before coating, after coating, and after detaching. In both parts B and E, the immersed parts of the wire inside the spore suspension were marked. Parts G–I show SEM images of Pt wires before coating, after coating, and after detaching. The charging condition for spore attachment is 20 s at 20 V. The spore detaching condition is 10–15 min at reversed 60 V, combined with the ultrasonication.

not include possible effects due to particle–particle and particle–electrode interactions. Near the electrode, the spore transport may be complicated by electrohydrodynamic flows as well as electroosmotic flows due to the electric forces on charges from the electrode polarization layer and the equilibrium diffuse double layer near the spore.[56,57] However, since eq 11 describes the initial current when $t = 0$, the influence of those flows can be neglected. In the remainder of the paper, we analyze our experimental results in the context of the model resulting in eq 11.

4. RESULTS AND DISCUSSION

4.1. Spore Attachment in the Continuous DC Mode.

To exemplify the spore attachment in the continuous DC mode, a biased voltage of 20 V and a spore number concentration of 8×10^9 CFU/mL were adopted. The EPD conditions employed were chosen on the basis of prior work that showed that bacterial spores can withstand DC electric fields as high as 1500 V/cm and still maintain viability.[31] Before we proceeded with direct measurement of the current in evaluating spore deposition, we evaluated the temporal variation of current for pure water and the spore suspension in Figure S2 (Supporting Information). We found that steady state could be achieved on the order of 100 s, and that the measured current due to charge migration in the spore containing suspension was about an order of magnitude larger than that contributed to by pure water. This allows us to ignore the influence of the solvent in subsequent current measurements during EPD. Images of spore attachment are shown in Figure 2 for a deposition time of 20 s. The visual images (Figure 2A and B) show that, after DC biasing, an obvious white spore coating appeared in the immersed portion of the wire. Further optical microscopic images (Figure 2D and E) reflect the spore deposition in that region (the dark region represented the coverage of spores). SEM images (Figure 2G and H) show an evenly distributed and dense coating on the wire and more directly demonstrated the attachment of spores. The enlarged SEM images in Figure 3A and B also exhibit the structures of attached *Bs* spores on surfaces.

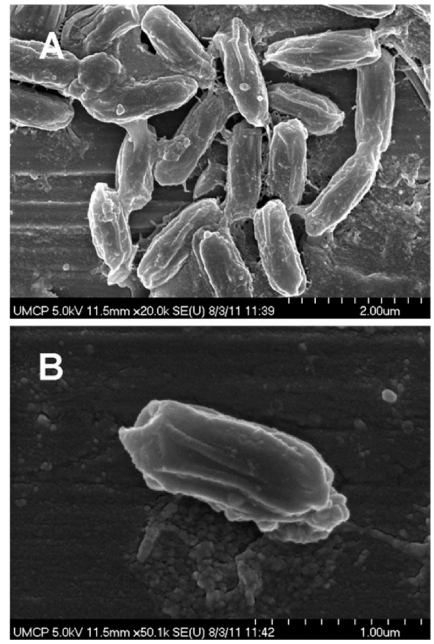

Figure 3. SEM images of *Bs* spores ATCC#6051 attached on Pt wires.

Nominally, we should expect that increasing the charging time would cause incremental increases in spore deposition to the surface. However, such a relationship was not linear especially after a relatively long time, and when a higher voltage was applied (Figure S3, Supporting Information). In those cases, the current–time curves show fluctuations which could be correlated to the generation of visible gas bubbles formed from water electrolysis[58] (Figure S4C, Supporting Informa-

dx.doi.org/10.1021/jp307282q | J. Phys. Chem. B 2013, 117, 1738–1745

tion). As a result, spore deposits became highly uneven along the wire surface, and subsequently were detached from the wire at high voltages, or long charging times (Figure S4A and B, Supporting Information). This prompted us to evaluate a pulsed deposition mode that will be described later.

4.2. Spore Detachment. To properly evaluate our eventual exposure studies (heat, chemicals), an efficient and quantitative method to detach the spores is necessary so that standard assays can be employed. We found that either reversed biasing the wire at −60 V for 5 min or ultrasonicating for 30 min allowed partial detachment of spores from the wire (Figure S5, Supporting Information). While some reports indicate that ultrasonication is known to harm spores[59,60] and repeated electric pulse cycling can also induce spore inactivation,[61,62] we operated at much shorter ultrasonication time and bias voltage which are ∼100× less than those studies. Similarly, pH changes which occur during deposition (Figure S6, Supporting Information) were evaluated for viability by exposing spores to a range of pH (5−10) (Figure S7, Supporting Information) and were found to have no effect. We found that the combination of reverse bias and ultrsonication would detach the spores completely.

The photographic, optical microscopic, and SEM images shown in Figure 2C, F, and I, respectively, demonstrate that all the *Bs* spores were removed from the surface after reversed biasing for 10−15 min at −60 V in an ultrasonic bath. Once the spores on the surface were removed into liquid, they could be enumerated by the plate counting method to determine the number of spores deposited on the wire. It should be noted that the reverse-bias charging time and voltage here are larger than those for spore attachment, which presumably accounts for the force required to overcome the binding energy between the spore and wire surface. Together, these results indicate that the combination of reversed biasing and ultrasonication is an effective means to completely remove spores deposited on the surface.

4.3. Spore Attachment in the Pulsed DC Mode. The fluctuation in the deposition current observed (Figure S3, Supporting Information) coincided with visible bubble formation (Figure S4C, Supporting Information). To mitigate this effect, we shifted our efforts to a pulsed DC mode, based on results of Besra et al.[50] who showed that, using a pulsed voltage strategy, an extension of an application used to deposit metal films could lead to a minimization of bubble formation and conformal deposits of small particles. We have adopted this strategy in order to generate a uniform and densely packed spore coating, by applying multiple electric pulses instead of a continuous DC bias. We have found that this leads to reproducible spore deposits by enabling consistent current measurements. In Figure 4, the measured temporal currents during deposition of *Bs* spores (ATCC#6051) at a voltage of 5 V are shown, with an on-time of 30 s followed by an off-time of 30 s. Over eight cycles of this experiment, the measured current was consistent between cycles, which implies that the ionic strength of the liquid was stable. The SEM images (Figure 5) reflect the increase of *Bs* spore attachment on the surface with the pulse number. After charging for two pulses, only partial coverage was achieved; however, these deposits were uniform. A monolayer of *Bs* spores could be formed after four pulses, and multiple layers of spores were found after seven pulses. Optical microscopic images (Figure S8, Supporting Information) also show that the *Bs* spore deposits increased as the pulses accumulated. After enumerating all the spores detached

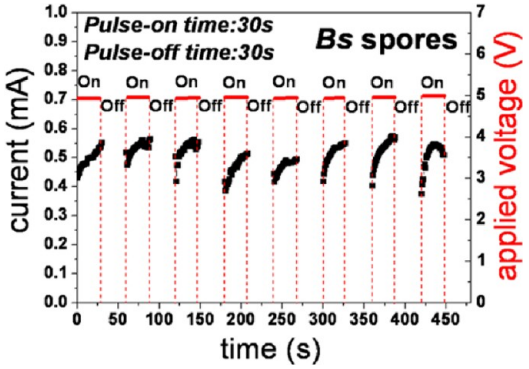

Figure 4. Current−time relationship in the pulsed DC charging mode for *Bs* spores (ATCC#6051). Both the charging time and the pulse-off time were 30 s, and the applied on-time voltage was 5 V. In our design, *Bs* spores were deposited to the surface for up to eight cycles.

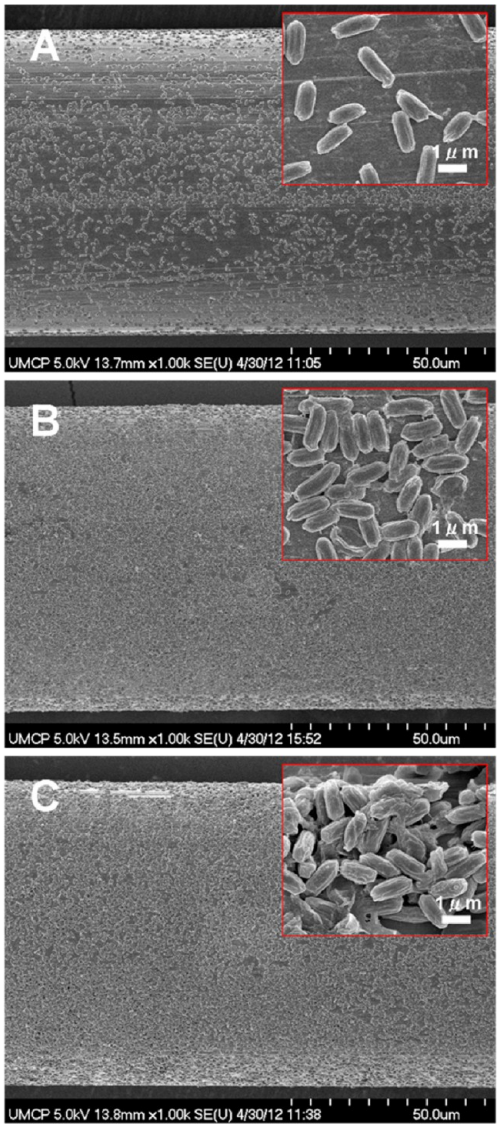

Figure 5. SEM images of *Bs* spore coating (ATCC#6051) on Pt wires after different biased DC pulses. Parts A, B, and C show the cases after 2, 4, and 7 pulses, respectively. Each DC pulse is set to last 30 s and stop for another 30 s before the next pulse. The enlarged SEM images are inserted which exhibit the different spore deposition densities on the surfaces.

dx.doi.org/10.1021/jp307282q | J. Phys. Chem. B 2013, 117, 1738−1745

from the surface, a linear relationship between the spore deposits and applied pulse number was found (Figure 6A). By

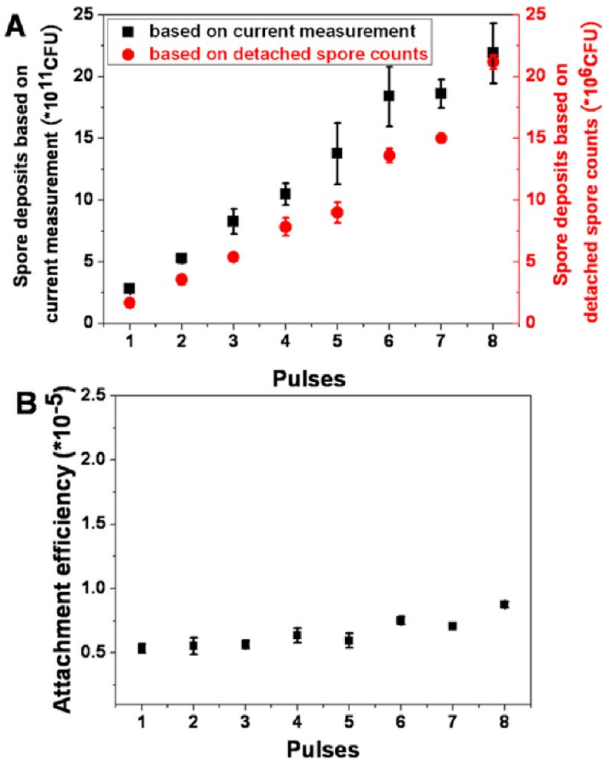

Figure 6. (A) *Bs* spore deposits (ATCC#6051) on the Pt wire after different pulses. The black points are for the spore deposits obtained from the current−time measurement, while the red points are from spore deposits counted from the detached spores. (B) Relationship between spore attachment efficiency and number of pulses for *Bs* spores. The spore attachment efficiency was calculated by the ratio of measured spore deposits (from the detached spore counting), over the idealized spore deposits (from the current−time data). Data were measured four times, which are reflected in the error bars.

our densely packing model (see the Supporting Information and Figure S9), the spore number and number density in one monolayer are 6.1×10^6 and 8×10^{12} m^{-2}, respectively, for *Bs* spores. As are reflected in Figure 6A, these are the spore deposits achieved after four biased pulses (on-time 30 s and off-time 30 s each).

It should be noted that, in this pulsed DC-EPD process up to eight cycles, the pH value of the spore suspension did not vary much (Figure S10, Supporting Information) which had no effect on the deposition rate and spore viability.

4.4. Calculations of the Spore Surface Charge and Deposition Efficiency. In principle, a measurement of the current is also a measure of spore transport to the wire (but not necessarily stick to), if one knows the average charge on a spore. From eq 11, the average charge on a spore can be measured by a prior knowledge of the spore concentration in the suspension and the initial current. A series of initial currents of the spore suspensions were collected under different applied potentials and spore concentrations, which were further subtracted from the initial current of a solution without spores and defined as the effective initial current of spores (I_0) and tabulated in Table 1. The corresponding surface charge (q) per spore is evaluated from eq 11.

However, we still need a relationship between q and q' to determine the fraction of the current associated with the diffuse double layer (Figure S11, Supporting Information). One approach is to find the electrical potential at the shear plane (i.e., the outer radius of solution ions that are carried along with the spore). The Helmholtz−Smoluchowski equation describes the relationship between the shear plane potential (ζ) and the mobility of spores (μ):[63]

$$\mu = \frac{\varepsilon_m}{\eta}\zeta \tag{12}$$

By equating the friction force (eq 5) to the electrophoretic force (eq 2) and also omitting the dielectrophoretic force (eq 3) (note: it has been found that the dielectrophoretic force is much smaller than the electrophoretic force), we can obtain

$$\zeta = \frac{q}{6\pi\varepsilon_m R} \tag{13}$$

In the spherical coordinates, the potential as a function of radial distance from the shear plane can be evaluated, from the simplified Poisson−Boltzmann equation:[63]

$$\zeta = \frac{q}{4\pi\varepsilon_m R_\zeta}\exp(-\kappa R_\zeta) \tag{14}$$

where R_ζ is the radius of the shear plane and κ is the inverse Debye length (1.0384×10^{-6} m^{-1}) in water at room temperature. By combining eqs 13 and 14, we obtain R_ζ = 0.35×10^{-6} m, thus slightly larger than the radius of one *Bs*

Table 1. Surface Charges and Numbers of Charges for *B. subtilis* Spores (ATCC#6051)[a]

concentration (CFU/mL)	voltage (V)	current (mA)	surface charge (C)	number of charges
3.77×10^6	5	0.0002 ± 0.0002	$(5.36 \pm 5.36) \times 10^{-14}$	$(3.35 \pm 3.35) \times 10^5$
8.59×10^7	5	0.0031 ± 0.0008	$(6.20 \pm 0.81) \times 10^{-14}$	$(3.88 \pm 0.51) \times 10^5$
7.67×10^9	5	0.1635 ± 0.0006	$(4.81 \pm 0.01) \times 10^{-14}$	$(3.00 \pm 0.01) \times 10^5$
	10	0.4459 ± 0.0311	$(5.61 \pm 0.20) \times 10^{-14}$	$(3.51 \pm 0.12) \times 10^5$
	20	0.8509 ± 0.1080	$(5.47 \pm 0.35) \times 10^{-14}$	$(3.42 \pm 0.22) \times 10^5$
	30	1.4584 ± 0.2005	$(5.85 \pm 0.40) \times 10^{-14}$	$(3.65 \pm 0.25) \times 10^5$
	40	1.7991 ± 0.2294	$(5.63 \pm 0.36) \times 10^{-14}$	$(3.52 \pm 0.23) \times 10^5$
1.53×10^{10}	5	0.1774 ± 0.0008	$(3.55 \pm 0.01) \times 10^{-14}$	$(2.22 \pm 0.00) \times 10^5$
	10	0.5162 ± 0.0179	$(4.28 \pm 0.07) \times 10^{-14}$	$(2.67 \pm 0.05) \times 10^5$
	20	1.1606 ± 0.0450	$(4.53 \pm 0.09) \times 10^{-14}$	$(2.83 \pm 0.05) \times 10^5$
	30	1.4610 ± 0.1474	$(4.15 \pm 0.21) \times 10^{-14}$	$(2.59 \pm 0.13) \times 10^5$
	50	3.1724 ± 0.2643	$(4.74 \pm 0.20) \times 10^{-14}$	$(2.96 \pm 0.12) \times 10^5$

[a]Note: the average value of surface charge is 5.01×10^{-14} C, and the average number of charges on the spore surface is 3.13×10^5.

dx.doi.org/10.1021/jp307282q | J. Phys. Chem. B 2013, 117, 1738−1745

spore (0.336×10^{-6} m). The quantity of charges between R and R_ζ can be calculated:

$$q - q' = -\int_R^{R_\zeta} \rho^* 4\pi r^2 \, dr \tag{15}$$

where ρ^* is the charge density in the diffuse layer which can be expressed from the Poisson equation:[63]

$$\rho^* = (-q)\frac{\kappa^2}{4\pi r} \exp(-\kappa r) \tag{16}$$

Finally, the spore surface charge can be found:

$$q = \frac{q'}{0.9964} \tag{17}$$

Equation 17 implies that the contribution of charges between the spore surface and the shear layer is negligible. Evaluation of eq 11 gives a value of $q = 5.01 \times 10^{-14}$ C. Accordingly, the average number of negative charges on the spore surface is 3.13×10^5 (Table 1). The result above is based on the assumption that the surface charge (or zeta potential) of spores in suspension does not vary during deposition, which is essentially what we observed experimentally (Figure S12, Supporting Information).

The most commonly used method to detect the surface charges of particles is through a measurement of the zeta-potential.[64] The zeta-potential measured for *Bs* spores yielded values of −33 mV, which accordingly gave a surface charge density of 0.0384 C/m^2. On the basis of the enlarged SEM images (Figure 3), it is reasonable to assume the spore as a prolate ellipsoid with a semilength axis c and a semiwidth axis a, from which the spore surface area can be estimated. It has been reported that, for *Bs* spores, $c = 0.535$ μm and $a = 0.24$ μm.[55] Together with the charge density data, the surface charges on the spores can be determined and are listed in Table 2. The table shows that the charge values obtained from our method and the zeta-potential assay are quite similar. Alternatively, Douglas[65] detected the surface charges of *Bs* spores through a mobility test in liquid (Table 2). These results suggest that our approach gives results that are consistent with other reported results, with the added benefit of being considerably simpler in terms of the sophistication of the instrumentation needed, and for our purposes the in situ nature of the measurement.

Table 2. Spore Surface Charge Densities, Real Surface Charges, and Number of Charges for *B. subtilis* Spores (ATCC#6051) from Different Methods

	surface charge density (C/m^2)	surface charge (C)	number of charges
zeta-potential method	0.0384	5.36×10^{-14}	3.34×10^5
our method	0.0358	5.01×10^{-14}	3.13×10^5
mobility method[65]	0.0167	2.34×10^{-14}	1.46×10^5

With a known shielded charge q', the net charge accumulation from our current measurement can be directly used to estimate the deposition rate. Accordingly, the deposited spore dose $N_{current}$ on the wire could be determined as (Figure 4)

$$N_{current} = \int_0^t dN_{current} = \frac{1}{q'}\int_0^t I(t)\, dt \tag{18}$$

In our pulsed DC-EPD model, the relationship between spore deposits based on the current measurement and pulses is shown in Figure 6A. $N_{current}$ for just one pulse is in the range of 10^{11} spores, which implies the formation of multiple spore layers. However, one densely packed monolayer of *Bs* spores (6.1×10^6) actually required four pulses. This leads to a somewhat surprising result that the deposition efficiency is only ~10^{-6} (Figure 6B). Thus, it appears that many spores apparently make it to the surface and become dislodged, possibly due to nonvisible gas generation at the electrode.[66] In spite of this low efficiency, the measured deposited spore amount is proportional to the calculated deposits based on the current (Figure 6B), consistent with the results of Hamaker.[67,68] On the basis of this model together with the verification from experiments, our result demonstrates that one is able to in reasonable short deposition time create a near conformal monolayer of spores and subsequently detach them.

5. CONCLUSION

We show in this study the ability to controllably deposit spores electrophoretically to fine wires using a pulsed voltage method which prevents electrolysis. Attached spores can be totally removed by a combination of reversing the electrical polarity and ultrasonicating the wire. We are also able to use this method to quantitatively measure the surface charge on spores and the deposition rate. The method is generic and should be applicable to the deposition of any biological material (e.g., spores, bacteria, viruses) onto metallic surfaces.

■ ASSOCIATED CONTENT

Supporting Information

Optical microscopic image of *Bs* spores; optical microscopic images of *Bs* spores in the continuous and pulsed DC-EPD modes; temporal current in the continuous DC-EPD mode; pH−time relationships during pulsed DC-EPD mode and reversal charging; dense spore packing model on a surface; scheme of the diffuse double layer of the spore surface; zeta potential−pH relationship in spore suspension. This material is available free of charge via the Internet at http://pubs.acs.org.

■ AUTHOR INFORMATION

Corresponding Author

*E-mail: vtlee@umd.edu (V.T.L.); mrz@umd.edu (M.R.Z.).

Notes

The authors declare no competing financial interest.

■ ACKNOWLEDGMENTS

This work was funded by a grant from DOD/DTRA (BRBAA08-Per5-H-2-0065). We express our gratitude to Mr. Tim Maugel in the Laboratory for Biological Ultrastructure at the University of Maryland, College Park, for his assistance with SEM images.

■ REFERENCES

(1) Christopher, G. W.; Cieslak, T. J.; Pavlin, J. A.; Eitzen, E. M. *J. Am. Med. Assoc.* **1997**, *278*, 412−417.
(2) Altas, R. M. *Annu. Rev. Microbiol.* **2002**, *56*, 167−185.
(3) Grinshpun, S. A.; Adhikari, A.; Li, C.; Reponen, T.; Yermakov, M.; Schoenitz, M.; Dreizin, E.; Trunov, M.; Mohan, S. *J. Aerosol Sci.* **2010**, *41*, 352−363.
(4) Gates, S. D.; McCartt, A. D.; Jeffries, J. B.; Hanson, R. K.; Hokama, L. A.; Mortelmans, K. E. *J. Appl. Microbiol.* **2011**, *111*, 925−931.

(5) McDonnell, G.; Russell, A. D. *Clin. Microbiol. Rev.* **1999**, *12*, 147−179.
(6) Reddy, N. R.; Tetzloff, R. C.; Solomon, H. M.; Larkin, J. W. *Innovative Food Sci. Emerging Technol.* **2006**, *7*, 169−175.
(7) Staack, N.; Ahrne, L.; Borch, E.; Knorr, D. *J. Food Eng.* **2008**, *89*, 319−324.
(8) Boudam, M. K.; Moisan, M. *J. Phys. D: Appl. Phys.* **2010**, *43*, 295202.
(9) Nicholson, W. L.; Munakata, N.; Horneck, G.; Melosh, H. J.; Setlow, P. *Microbiol. Mol. Biol. Rev.* **2000**, *64*, 548−572.
(10) Setlow, P. *J. Appl. Microbiol.* **2006**, *101*, 514−525.
(11) Setlow, P. *Trends Microbiol.* **2007**, *15*, 172−180.
(12) Gates, S. D.; McCartt, A. D.; Lappas, P.; Jeffries, J. B.; Hanson, R. K.; Hokama, L. A.; Mortelmans, K. E. *J. Appl. Microbiol.* **2010**, *109*, 1591−1598.
(13) McCartt, A. D.; Gates, S. D.; Jeffries, J. B.; Hanson, R. K.; Joubert, L. M.; Buhr, T. L. *Z. Phys. Chem.* **2011**, *225*, 1367−1377.
(14) Grinshpun, S. A.; Li, C.; Adhikari, A.; Yermakov, M.; Reponen, T.; Schoenitz, M.; Dreizin, E.; Hoffmann, V.; Trunov, M. *Aerosol Air Qual. Res.* **2010**, *10*, 414−424.
(15) Zhou, L.; Piekiel, N.; Chowdhury, S.; Zachariah, M. R. *Rapid Commun. Mass Spectrom.* **2009**, *23*, 194−202.
(16) Miller, M. B.; Bassler, B. L. *Annu. Rev. Microbiol.* **2001**, *55*, 165−199.
(17) Mitchell, J. G.; Kogure, K. *FEMS Microbiol. Ecol.* **2006**, *55*, 3−16.
(18) Reguera, G. *Trends Microbiol.* **2011**, *19*, 105−113.
(19) Colville, K.; Tompkins, N.; Rutenberg, A. D.; Jericho, M. H. *Langmuir* **2010**, *26*, 2639−2644.
(20) Fang, B.; Gon, S.; Park, M.-H.; Kumar, K.-N.; Rotello, V. M.; Nusslein, K.; Santore, M. M. *Langmuir* **2012**, *28*, 7803−7810.
(21) Wakeham, A.; Kennedy, R.; McCartney, A. J. *Aerosol Sci.* **2004**, *35*, 835−850.
(22) Lapizco-Encinas, B. H.; Rito-Palomares, M. *Electrophoresis* **2007**, *28*, 4521−4538.
(23) Urdaneta, M.; Smela, E. *J. Micromech. Microeng.* **2008**, *18*, 015001 (8pp).
(24) Markx, G. H.; Dyda, P. A.; Pethig, R. *J. Biotechnol.* **1996**, *51*, 175−180.
(25) Pohl, H. A.; Hawk, I. *Science* **1966**, *152*, 647−649.
(26) Benguigui, L.; Lin, I. J. *J. Electrost.* **1988**, *21*, 205−213.
(27) Huang, Y.; Pethig, R. *Meas. Sci. Technol.* **1991**, *2*, 1142−1146.
(28) Kazoe, Y.; Yoda, M. *Langmuir* **2011**, *27*, 11481−11488.
(29) Douglas, H. W. *Trans. Faraday Soc.* **1955**, *51*, 146−152.
(30) Resnick, M. A.; Tippetts, R. D.; Mortimer, R. K. *Science* **1967**, *158*, 803−804.
(31) Lapizco-Encinas, B. H.; Davalos, R. V.; Simmons, B. A.; Cummings, E. B.; Fintschenko, Y. *J. Microbiol. Methods* **2005**, *62*, 317−326.
(32) Gadish, N.; Voldman, J. *Anal. Chem.* **2006**, *78*, 7870−7876.
(33) Koklu, M.; Park, S.; Pillai, S. D.; Beskok, A. *Biomicrofluidics* **2010**, *4*, 034107.
(34) Chen, G.; Driks, A.; Tawfiq, K.; Mallozzi, M.; Patil, S. *Colloids Surf., B* **2010**, *76*, 512−518.
(35) Seale, R. B.; Bremer, P. J.; Flint, S. H.; McQuillan, A. J. *J. Appl. Microbiol.* **2010**, *109*, 1339−1348.
(36) Poortinga, A. T.; Busscher, H. J. *Biotechnol. Bioeng.* **2000**, *67*, 117−120.
(37) Neirinck, B.; Van Mellaert, L.; Fransaer, J.; Van der Biest, O.; Anne, J.; Vleugels, J. *Electrochem. Commun.* **2009**, *11*, 1842−1845.
(38) Novak, S.; Maver, U.; Peternel, S.; Venturini, P.; Bele, M.; Gaberscek, M. *Colloid Surface A.* **2009**, *340*, 155−160.
(39) Ammam, M.; Fransaer, J. *Electrochim. Acta* **2010**, *55*, 3206−3212.
(40) Hsu, P.-C.; Seol, S.-K.; Lo, T.-N.; Liu, C.-J.; Wang, C.-L.; Lin, C.-S.; Hwu, Y.; Chen, C. H.; Chang, L.-W.; Je, J. H.; Margaritondo, G. *J. Electrochem. Soc.* **2008**, *155*, D400−D407.
(41) Craig, V. S. J. *Soft Matter* **2011**, *7*, 40−48.
(42) Tauveron, G.; Slomianny, C.; Henry, C.; Faille, C. *Int. J. Food Microbiol.* **2006**, *110*, 254−262.
(43) Mercier-Bonin, M.; Dehouche, A.; Morchain, J.; Schmitz, P. *Int. J. Food Microbiol.* **2011**, *146*, 182−191.
(44) Granhag, L. M.; Finlay, J. A.; Jonsson, P. R.; Callow, J. A.; Callow, M. E. *Biofouling* **2004**, *20*, 117−122.
(45) Bower, C. K.; McGuire, J.; Daeschel, M. A. *Trends Food Sci. Technol.* **1996**, *7*, 152−157.
(46) Andersson, A.; Ronner, U. *Biofouling* **1998**, *13*, 51−67.
(47) Amman, M.; Fransaer, J. *Biosens. Bioelectron.* **2009**, *25*, 191−197.
(48) Neirinck, B.; Fransaer, J.; Van der Biest, O.; Vleugels, J. *Electrochem. Commun.* **2009**, *11*, 57−60.
(49) Besra, L.; Uchikoshi, T.; Suzuki, T. S.; Sakka, Y. *J. Am. Ceram. Soc.* **2008**, *91*, 3154−3159.
(50) Besra, L.; Uchikoshi, T.; Suzuki, T. S.; Sakka, Y. *J. Eur. Ceram. Soc.* **2009**, *29*, 1837−1845.
(51) Poortinga, A. T.; Bos, R.; Norde, W.; Busscher, H. J. *Surf. Sci. Rep.* **2002**, *47*, 1−32.
(52) Chung, E.; Yiacoumi, S.; Lee, I.; Tsouris, C. *Environ. Sci. Technol.* **2010**, *44*, 6209−6214.
(53) Walton, O. R. *KONA* **2008**, *26*, 129−141.
(54) Srivastava, S. K.; Gencoglu, A.; Minerick, A. R. *Anal. Bioanal. Chem.* **2011**, *399*, 301−321.
(55) Carrera, M.; Zandomeni, R. O.; Fitzgibbon, J.; Sagripanti, J.-L. *J. Appl. Microbiol.* **2007**, *102*, 303−312.
(56) Ristenpart, W. D.; Aksay, I. A.; Saville, D. A. *Langmuir* **2007**, *23*, 4071−4080.
(57) Ristenpart, W. D.; Aksay, I. A.; Saville, D. A. *J. Fluid Mech.* **2007**, *575*, 83−109.
(58) Atkins, P. *Physical Chemistry*, 6th ed.; W. H. Freeman and Company: New York, 1997.
(59) Burgos, J.; Ordonez, J. A.; Sala, F. *Appl. Microbiol.* **1972**, *24*, 497−498.
(60) Ordonez, J. A.; Burgos, J. *Appl. Environ. Microbiol.* **1976**, *32*, 183−184.
(61) Pagan, R.; Esplugas, S.; Gongora-Nieto, M. M.; Barbosa-Canovas, G. V.; Swanson, B. G. *Food Sci. Technol. Int.* **1998**, *4*, 33−44.
(62) Spilimbergo, S.; Dehghani, F.; Bertucco, A.; Foster, N. R. *Biotechnol. Bioeng.* **2003**, *82*, 118−125.
(63) Hiemenz, P. C.; Rajagopalan, R. *Principles of Colloid and Surface Chemistry*, 3rd ed.; Taylor & Francis Group: Boca Raton, FL, 1997.
(64) Tsai, D.-H.; Pease, L. F., III; Zangmeister, R. A.; Tarlov, M. J.; Zachariah, M. R. *Langmuir* **2009**, *25*, 140−146.
(65) Douglas, H. W. *Trans. Faraday Soc.* **1959**, *55*, 850−856.
(66) Bohmer, M. *Langmuir* **1996**, *12*, 5747−5750.
(67) Hamaker, H. C. *Trans. Faraday Soc.* **1940**, *36*, 279−87.
(68) Sarkar, P.; Nicholson, P. S. *J. Am. Ceram. Soc.* **1996**, *79*, 1987−2002.

Chemical Engineering Journal 279 (2015) 578–588

Contents lists available at ScienceDirect

Chemical Engineering Journal

journal homepage: www.elsevier.com/locate/cej

Inactivation of bacterial spores subjected to sub-second thermal stress

W. Zhou [a], M.W. Orr [c], G. Jian [b], S.K. Watt [c], V.T. Lee [c,*], M.R. Zachariah [a,b,*]

[a] Department of Chemical and Biomolecular Engineering, University of Maryland, College Park, MD 20742, USA
[b] Department of Chemistry and Biochemistry, University of Maryland, College Park, MD 20742, USA
[c] Department of Cell Biology & Molecular Genetics, University of Maryland, College Park, MD 20742, USA

HIGHLIGHTS

- A new approach to quantitatively apply high rate heat stress is developed.
- Spore inactivation with temperature followed a sigmoidal behavior with higher heating rates improving the neutralization efficiency.
- The peak temperature and not heating time was responsible for spore inactivation at ~10^4 °C/s.
- Viability reduction was mainly due to DNA damage at ~10^4 °C/s.
- Spore inactivation was mainly due to internal pressurization at ~10^5 °C/s.

GRAPHICAL ABSTRACT

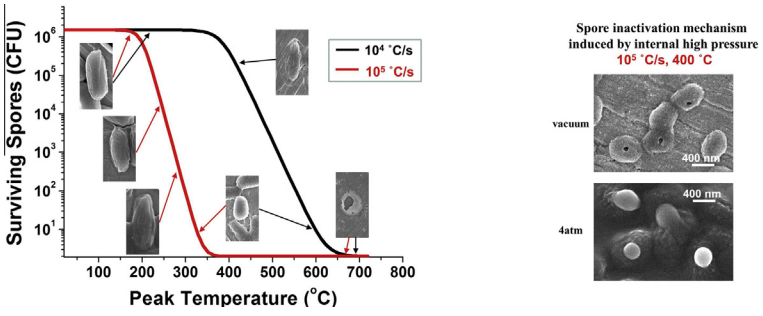

ARTICLE INFO

Article history:
Received 12 February 2015
Received in revised form 28 April 2015
Accepted 5 May 2015
Available online 14 May 2015

Keywords:
Bacterial spores
Inactivation
Ultrafast heating
Killing mechanism

ABSTRACT

Rapid heat pulse is the primary method for neutralizing large quantities of spores. Characterizing heat inactivation on a millisecond time scale has been limited by the ability to apply ultrafast, uniform heating to spores. Using our system for immobilization of spores on metal surfaces, bacterial spores were subjected to high temperatures (200–800 °C) and heating rates (~10^3 °C/s to ~10^5 °C/s). Spore inactivation increased with temperature and fit a sigmoid response. We observed the critical peak temperature (T_c) which caused a 2-fold reduction in spore viability was 382 °C and 199 °C for heating rates of ~10^4 °C/s and ~10^5 °C/s, respectively. Repetitive heating to the same peak temperature had little effect on viability. In contrast, stepwise heating to elevated peak temperatures inactivated spores in a manner similar to a single pulse heating to the same peak temperature. These results indicate that the maximum temperature rather than the overall heating time is primarily responsible for spore neutralization at ~10^4 °C/s heating rate. The mechanism of spore inactivation was further investigated at two heating rates (~10^4 °C/s and ~10^5 °C/s). Viability reduction was mainly due to DNA damage at the heating rate of ~10^4 °C/s as mutant strains defective for *sspA sspB* and *recA* were more sensitive to heat than the wide-type strains. At the higher heating rate (~10^5 °C/s), spore inactivation was correlated with physical damage from ultrafast vapor pressurization inside spores. This new approach of pulse heating generates a temperature, time, and kill relationship for *Bacillus* spores at sub-second timescales.

* Corresponding authors.
E-mail addresses: vtlee@umd.edu (V.T. Lee), mrz@umd.edu (M.R. Zachariah).

http://dx.doi.org/10.1016/j.cej.2015.05.021
1385-8947/

1. Introduction

Bacterial spores are a dormant cell type that are highly resistant to heat, moisture, pressurization, radiation and biocidal stresses [1–3]. Concerns regarding bio-terrorism [4] and possibly other public health risks [5,6] require the urgent development of methods for large scale inactivation of bacterial spores. The use of thermal destruction is a straightforward and convenient approach that has been investigated for the inactivation of spores in the liquid phase [7–16]. Conventional thermal inactivation methods require time periods up to minutes or even hours and are limited by a maximum temperature of 150 °C [8–10,11,13]. Maintaining these temperatures for the required time periods is unfeasible for large quantities of spores. Thus, stand-off neutralization methods which can sustain higher temperatures (>200 °C) for short periods of time (sub-seconds) are being considered, and these new temperature–time–kill histories of spore inactivation require evaluation. Aerosol methods have recently been employed to evaluate thermal and chemical kills of spores at extreme heating conditions [17–25]. These approaches have the advantage of isotropic and rapid heat transfer to individual spores, as well as controllable shorter heating times (milliseconds to seconds) and higher heating temperatures (>200 °C) [17–25]. However, there existed a temperature distribution within a population of spores in these studies, which allows for calculating the average resident time and temperature of the entire spore population, but not for individual spores. These studies evaluated the effect of peak temperature on spore viability. However, the effects of heating and cooling rates on spore inactivation were not discussed.

Precise measurements of heating rate and heating history can be achieved by an alternative method that heats spores immobilized on metal supports. Previous studies have shown that organic or inorganic nano/microparticles deposited on metal surfaces could be heated to a wide range of surface temperature (from ~100 °C to ~1800 °C) at a rate as high as $\sim 10^6$ °C/s [26–31]. In those studies, the heating time could be controlled with millisecond precision and the heating rate could be accurately tuned from $\sim 10^3$ °C/s to $\sim 10^6$ °C/s, allowing the application of uniform temperature to a deposited particle layer up to 5 μm thick [29] which exceeds the dimensions of a monolayer of bacterial spores. This approach allows accurate application of a uniform high temperature over millisecond time scales for individual spores, which will aid in determining the temperature–time–kill relationship of spores at high temperatures and sub-second timescales.

The mechanism of spore inactivation has been primarily studied in conventional heating schemes. Major mechanisms of spore inactivation occurred through damage to DNA and proteins [3]. Evidence supporting killing by DNA damage includes several studies that found mutants depleted in the *sspA sspB* genes (coding for α/β-type small, acid-soluble proteins (SASP)) and *recA* genes (coding for RecA) were sensitized to mutagenesis and inactivation under dry heating schemes [32–36]. In the dormant spores, SASP bind genomic DNA [32,33] to prevent depurination and strand breakage thereby confer resistance to dry heat and ultraviolet irradiation [34,35]. RecA participates in recombination repair to remove DNA lesions caused by dry heat [36]. In contrast, denaturation of some key proteins such as metabolic enzymes was found as the mechanism of spore killing in wet heat [8,37]. However, the specific proteins to which denaturation induces spore inactivation have not been identified [38]. A second mechanism of inactivation is through permeabilization of the spore membrane, cortex and coat (encoded by genes like *cotE*), as supported by several lines of evidence [3,39–44]. Damage to spore compartments after heating has been shown with compartment-specific staining techniques [45,46]. While the spore coat was identified as the primary barrier to oxidizing agents (hydrogen peroxide, hypochlorite, ozone, etc.) [47–49], the spore cortex plays a major role in maintaining spore resistance to heat [3,39]. Failure of the cortex structure leads to spore inactivation by two mechanisms. The first is the release of dipicolinic acid (DPA) associated with DNA damage during dry heating [40,41] and protein denaturation during wet heating [38]. The second is through rehydration of the spore protoplast [39,42]. Rehydration of the core will induce a concomitant reduction in spore heat resistance by disrupting SASP–DNA interaction and permitting protein denaturation [43,44]. Through these studies, the temperature–time–kill relationships for spores from several species have been characterized under conventional heating schemes [8–11,13]. However, the exact mechanism of spore inactivation during rapid heating, which is closer to conditions seen under combustion, is poorly understood. Recent studies of bacterial spores heated in hot air show that high-temperature gas induced severe damage to the spore core [50], and the extent of inactivation was attributed to the DNA damage [22].

In this work, we present the effect of fast heating pulses ($\sim 10^4$ °C/s and $\sim 10^5$ °C/s) on surface-immobilized spores as a complimentary approach to the aerosol studies. Our heating scheme possesses the advantages of precise measurement of heating time and rates, as well as uniform temporal temperature for individual spores. Using this heating scheme, we determined the effect of peak heating temperature and heat rate by assessing spore viability and morphology. The heating histories of spores were also investigated through repetitive exposures as a possible factor influencing spore inactivation. To investigate the mechanism of killing, spores carrying *sspA sspB*, *recA* or *cotE* mutations were tested to determine whether known mechanisms of spore inactivation contribute to spore viability in our heating scheme. Using these results, we propose a model for the thermal destruction of bacterial spores in the heating rates of $\sim 10^4$ °C/s and $\sim 10^5$ °C/s.

2. Materials and methods

2.1. Spore attachment on platinum wires

Bacillus subtilis (Bs) (ATCC#6051) were sporulated in Difco Sporulation Medium (DSM) at 30 °C for 48 h. The 250 ml of DSM included 2 g Bacto nutrient broth, 2.5 ml 10% KCl, 0.375 ml 1 M NaOH and 2.5 ml 1.2% $MgSO_4 \cdot 7H_2O$. The spore concentration was enumerated by plating to be 8×10^9 colony-forming units per milliliter (CFU/ml). The purity of spores was found more than 99%. For analysis of mechanism of killing, four isogenic Bs spore strains, namely, a wild-type strain (PS533) [36], a Δ*cotE* mutant strain lacking coat (PS3328) [48], a Δ*sspA* Δ*sspB* mutant strain lacking DNA protection mechanism (PS578) [32], and a Δ*recA* mutant strain lacking DNA repair mechanism (PS2318b) [36] were generously provided by Dr. Peter Setlow (University of Connecticut). A platinum (Pt) wire with a diameter of 76.8 μm (Omega Engineering, Inc.) was used to immobilize spores. An in-house spore deposition cell was manufactured for coating the wire with Bs spores electrophoretically (Fig. S1). By controlling the biased deposition voltage, pulse frequency, and charging time (from a 6340 sub-femtoamp remote sourcemeter, Keithley), a uniform monolayer of spores in the central region of the wire (~1 cm) could be obtained (Fig. 1A). The detailed information of the spore deposition cell and charging conditions can be found in our previous work [51].

2.2. Wire heating test

To subject spores to a defined thermal history, the spore coated Pt wire was connected to an in-house built power source, working

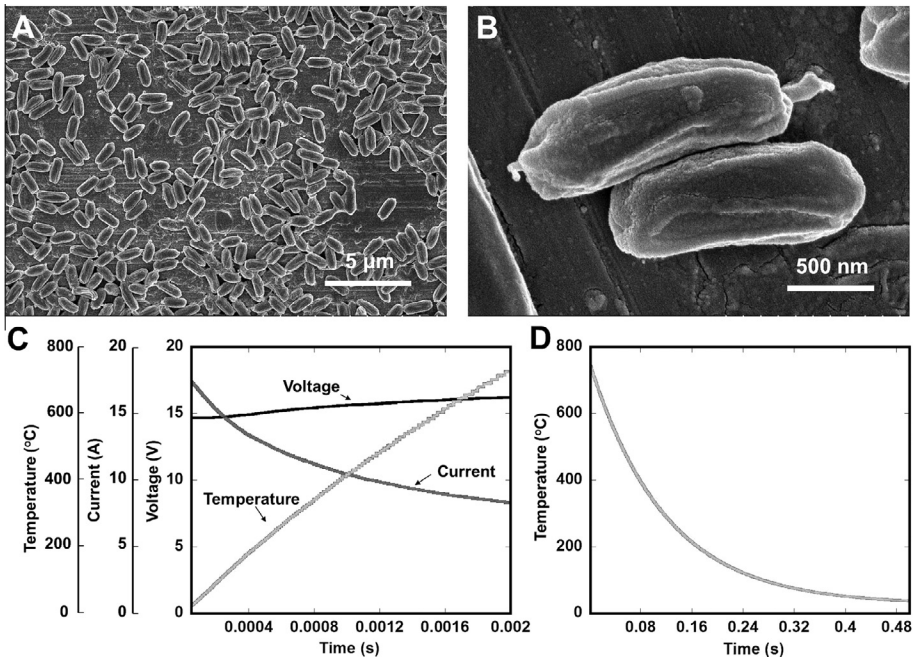

Fig. 1. (A) Electrophoretically deposited monolayer of Bs spores on the Pt wire as imaged by SEM. (B) High magnification SEM image of two immobilized spores. (C) Example of voltage, current and temperature temporal traces on the Pt wire surface in a 2 ms pulse test. The maximal temperature is ~740 °C in this case. (D) Surface temperature of the wire after cessation of the heating pulse.

as a temperature jump probe (Fig. S2). A pulse signal was generated to trigger the power supply prior to the heating of wire in air. The applied voltage (supplied from a 6291A DC power supply, HP) and the measured current (by a current probe AM503, Tektronix) were simultaneously recorded via an oscilloscope (LT344, LeCroy). The transient temperature on the wire during the heating period was measured based on the standard dynamic electric resistance temperature relationship (Callendar–Van Dusen equation) [52], in which the resistance measured from the applied voltage and the current was in a quadratic relationship with the transient temperature (see details in Supplemental text, Eqs. (S1)–(S9)). The maximum temperature (~200 °C to ~800 °C) and the heating rate (~10^3 °C/s to ~10^5 °C/s) can be precisely controlled by varying the applied voltage and the pulse time (2–50 ms). The corresponding profile of the wire in the cooled region was calculated according to an energy balance equation which was dominated by the heat conduction. The detailed content of the mathematical modeling can be found in the Supplemental information. The spore-coated Pt wire was replaced after each heating test, and the heated wires were processed for SEM imaging and determination of CFUs.

For wire heating tests in different pressures, two home-built chambers were used. The first chamber was connected to a vacuum pump for spore heating experiments under pressures as low as ~10^{-5} Pa, while the second chamber was connected to a high-pressure air source for experiments under pressures up to 4×10^5 Pa.

2.3. Determination of colony forming units

The number of viable spores that survived various heating conditions was enumerated by determining CFUs. Wires coated with heated or unheated spores were completely submerged in 1 ml of Lysogeny Broth (LB) media (10 g tryptone, 5 g yeast extract and 5 g NaCl per liter) and placed on a shaker at the 37 °C for three hours to allow for the germination and detachment of viable spores from the wire surface. After incubation, samples were serially diluted and plated on LB agar plates to determine viable CFUs. Each test included at least six replicates. The relationship of the recovered counts with time is shown in Fig. S3. Previous SEM images of unheated wires showed that ~10^6 spores were coated onto the platinum wires [51]. The three hours incubation time resulted in CFU counts that reflect the 10^6 spores on the wire.

The validity of this spore counting protocol was also evaluated by *in situ* phase contrast microscopy (Zeiss LSM 710, Germany) to monitor the germination of spores from wires. We found that Bs spores took 1 h before transition from phase bright to phase dark, and the 2 h to completely detach from wires. Additional experiments were performed on wire heated to temperatures >600 °C, a temperature that sterilizes Bs spores (see Fig. 2). Prolonged incubation of these heated wires for 24 h in LB at 37 °C failed to yield any growth.

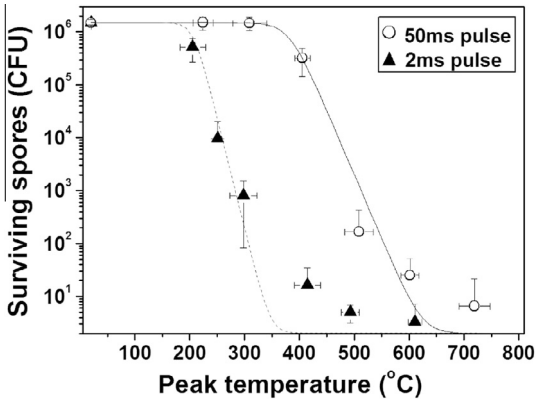

Fig. 2. Survival curves of Bs spores versus peak temperature for 2 ms and 50 ms heat pulses. Each experimental point represents the average of at least 6 replicates, and the standard deviations both in the measured spore viabilities and peak temperatures are indicated.

2.4. Spore morphological characterization

The heated wires were first mounted to stubs and then sputtered with gold/palladium alloy prior to the SEM using Hitachi S-4700). The dimensions of the spores were assessed by two parameters measured from SEM images, namely the aspect ratio (length divided by width) and the projected area (surface area inside the contour line of the cell body) of spores on the Pt surface. Statistical analyses are based on a spore population of >50.

2.5. Estimation of vapor pressurization inside spores

The vapor pressure and temperature relationship was calculated by a simple closed model assuming the spore allows for heat but not mass transfer. Empirical thermodynamics data of superheated vapor and steam were used to plot the standard curve of pressure rise with temperature (see details in the Supplemental information).

3. Results

3.1. Temperature profiles of the Pt wire surface

Precise definition of the temperature–time–kill relationship for Bs spores in sub-second time scales requires accurate and fast measurement of the spore temperature. Joule heating triggered by a strong electrical pulse enables us to quickly and accurately measure the transient temperature in a sub-second heating process. Our temperature–time measurement shows that the transient temperature on the wire surface during heating followed a closely linear ascending trace (Fig. 1C), while temperature–time calculation based on radial heat transfer estimates a slow exponential decaying trace when the pulse was turned off (Fig. 1D). The temperature of the ascending trace was measured from the time dependent variations of the applied voltage and current (see Eq. (S3) in the Supplemental information). By tuning the pulse time (2–50 ms) and applied voltage, different maximum temperatures (200–800 °C) and heating rates (~10^3 °C/s to ~10^5 °C/s) could be obtained (Fig. S5). The temperature decaying trace was calculated from a radial heat transfer model by assuming that most heat loss occurred by conduction from the cylindrical wire surface (see details in Supplemental text, Eqs. (S1)–(S9)). The surface temperature dropped exponentially after the voltage was turned off and returned to 40 °C after ~300 ms to ~500 ms (Table S1). While these cooling times are longer than the heating pulse times (2–50 ms), they are much shorter than the times employed in previous protocols [12,14].

Table 1
Fitting results for the variables in Eq. (1).

Heating conditions	k (°C^{-1})	T_c (°C)
2 ms heating pulse (~10^5 °C/s)	0.096	199
50 ms heating pulse (~10^4 °C/s)	0.056	382

3.2. Spore viability heated to fixed peak temperatures at two ramp rates

We assessed the effect of fast heating on the viability of Bs spores. When exposed to 50 ms fast heating pulse, spores reached peak temperatures between 200 °C to 800 °C which represents heat rates of 4×10^3 to 2×10^4 °C/s. Peak temperatures below 350 °C had minimal effect in the spore viability (Fig. 2). Once the temperature reached over 350 °C, the viability of spores decreased sharply by ~5 logs from 350 °C to 600 °C. Further increases in the peak temperature to ~700 °C reduced spore viability by 6 logs. These results indicate that 400 °C was the maximum peak temperature that the spores could resist in the 50 ms heating scheme.

When exposed to a 2 ms ultrafast heating pulse, spores reached peak temperatures between 200 °C to 800 °C, however, the heat rates were higher (1×10^5 to 4×10^5 °C/s). The spores were inactivated at a lower peak temperature (180 °C) and a reduction of 5 logs was achieved at 400 °C compared with 600 °C in 50 ms pulse heating. Finally, a complete viability reduction of 6 logs was reached at temperatures over 500 °C. These results indicate the ti me–temperature–kill relationships at different heating rates show similar sigmoidal response. However, the faster heating rate of ~10^5 °C/s potentiates spore inactivation and effectively reduces the peak temperature required for 6-log spore neutralization when compared to the heating rate of ~10^4 °C/s.

The viability data above were fitted with a standard sigmoid model used in traditional low rate heating experiments [53] as follows:

$$S = \frac{1}{1 + \exp(k(T - T_c))} \quad (1)$$

where S is the survival ratio of spores ($CFU_{final}/CFU_{initial}$), T is the peak temperature in a heating event, T_c is the critical peak temperature at which the spore viability is reduced by half, and k is the heat resistance parameter (larger k means spore viability is more temperature sensitive). In our study, the initial number of spores on the wire was measured as ~1.5×10^6 CFU. The fitted values of T_c and k are listed in Table 1. We found that the k value of the curve representing the spore destruction at the higher heating rates (~10^5 °C/s) was larger than that of the lower heating rates (~10^4 °C/s) (Table 2). In addition, T_c at the heating rates of

Table 2
Changes to spore physical dimensions after 2 ms and 50 ms pulse heating to different temperatures, with related viability loss.

Heating conditions	Length (μm)[a]	Width (μm)[a]	Aspect ratio	Projected area (μm^2)[b]	Viability (CFU)
Unheated	1.54 ± 0.17	0.62 ± 0.05	2.49 ± 0.37	0.82 ± 0.09	1.5×10^6
2 ms pulse, heat to 200 °C	1.47 ± 0.17	0.62 ± 0.02	2.38 ± 0.28	0.82 ± 0.10	7.8×10^5
2 ms pulse, heat to 240 °C	1.40 ± 0.14	0.61 ± 0.03	2.32 ± 0.31	0.82 ± 0.07	1.7×10^4
2 ms pulse, heat to 300 °C	1.49 ± 0.14	0.60 ± 0.04	2.43 ± 0.25	0.84 ± 0.11	5.7×10^1
2 ms pulse, heat to 410 °C	1.11 ± 0.11	0.56 ± 0.05	1.98 ± 0.21	0.52 ± 0.05	2.0×10^1
2 ms pulse, heat to 520 °C	0.69 ± 0.05	0.60 ± 0.07	1.16 ± 0.15	0.36 ± 0.04	0
50 ms pulse, heat to 170 °C	1.45 ± 0.13	0.59 ± 0.03	2.46 ± 0.29	0.79 ± 0.09	1.5×10^6
50 ms pulse, heat to 410 °C	1.11 ± 0.09	0.44 ± 0.04	2.57 ± 0.30	0.43 ± 0.02	2.4×10^5
50 ms pulse, heat to 570 °C	0.81 ± 0.10	0.54 ± 0.05	1.56 ± 0.21	0.44 ± 0.04	4.2×10^1

Data are derived from a random sample of 15 spores from totally more than 50 spores in SEM images.
[a] The length and width were measured as the longest distances along the longitudinal and transverse directions of the spore body.
[b] The projected area does not represent the spore volume, but acts as a comparable variable to evaluate changes in dimension under different heating conditions.

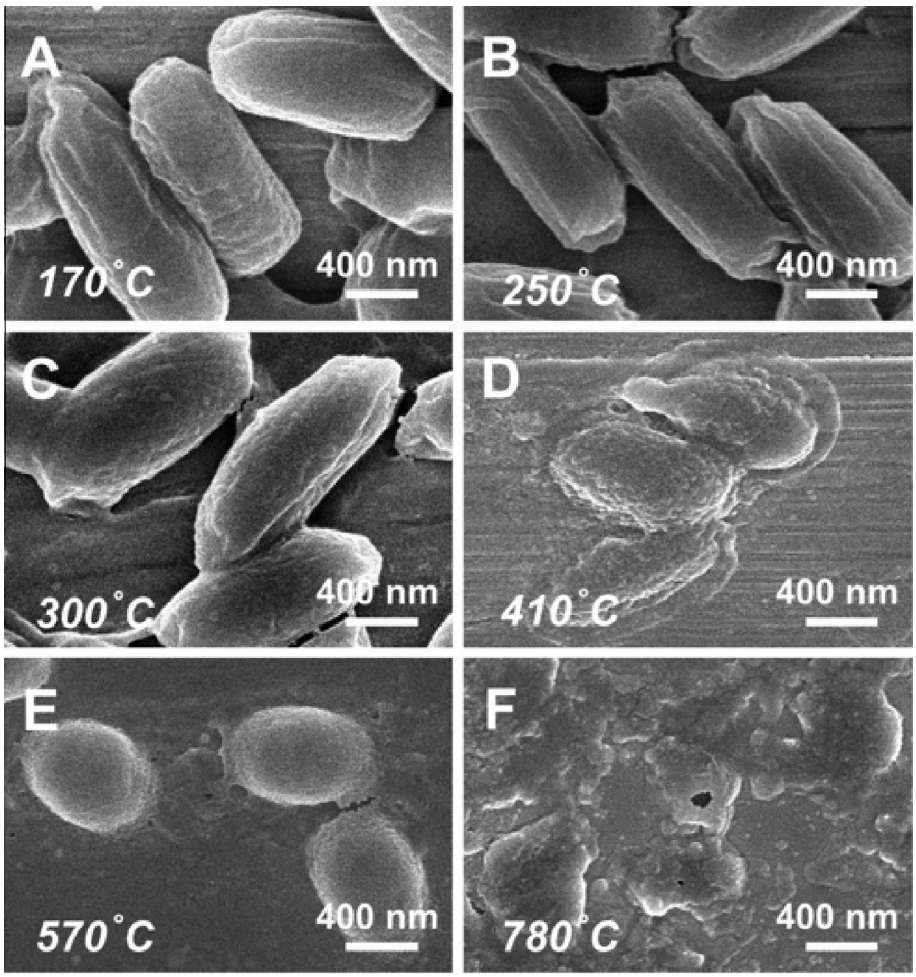

Fig. 3. SEM images of surface attached Bs spores after heat treatment triggered by a 50 ms pulse (~10^4 °C/s). Each image shows a representative morphological change of over 50 spores (see Fig. S6). The maximum temperatures exerted on spores are indicated (A–F).

~10^5 °C/s was lower than that at the heating rates of ~10^4 °C/s. Together, these results indicate that ultrafast heating rates (~10^5 °C/s) potentiate spore inactivation.

3.3. Spore morphology after heating to defined peak temperatures at two ramp rates

We assessed the morphological features of spores after heating. The unheated spores had characteristic longitudinal ridges along their surfaces (Fig. 1B). At the heating rates of ~10^4 °C/s, after fast heating to a peak temperature of up to 300 °C, the aspect ratio and the projected area remained constant (Fig. 3A and Table 2). Fast heating to 410 °C caused spores to shrink (projected area on surface decreased by 48% to 0.43 μm^2) (Fig. 3B). When heated to 570 °C (Fig. 3C), the spores were rounded (aspect ratio decreased by 37% to 1.56) without additional reduction in spore size (projected area decreased by 46% to 0.44 μm^2). The spore surface lost its integrity after fast heating to 780 °C (Fig. 3D). These results indicate that the severity of morphological change under the fast-heating and high temperature conditions correlates with spore viability at the heating rates of ~10^4 °C/s (Figs. 2 and 3 and relevant low magnification Fig. S6).

We also investigated the morphology of spores exposed to faster heating (2 ms pulses, ~10^4 °C/s). When heated to temperatures below 300 °C, the aspect ratio and surface area remained unchanged even though there was a large reduction in spore viability (Figs. 2 and 4B). At peak temperatures of 300 °C and above, pin holes and fissures were observed (Figs. 4C, S7 and S8). When heated to 410 °C, the aspect ratio decreased by 21% to 1.98 and the projected area decreased by 38% to 0.52 μm^2 (Fig. 4D). At a peak temperature of 520 °C, the aspect ratio further decreased by 53% to 1.16 and the projected area reduced by 56% to 0.36 μm^2 (Fig. 4E). By comparing spores exposed to the same peak temperature at two different heating rates, spores exposed to the faster heating rate (~10^5 °C/s) have minor morphological changes despite increased inactivation (Table 2, Figs. 3 and 4). These results indicate that the spore killing mechanisms in two heating rates are different.

3.4. Effect of repetitive fast heat pulses (~10^4 °C/s) on the spore morphology and viability

Our observations that faster heating rates and higher peak temperatures caused greater spore damage led us to propose a hypothesis that these two parameters have distinct effects on spores. To test this hypothesis, we devised two experiments to distinguish the effects of heating rate versus those of peak temperature. In the first experiment, we asked if repeated application of the same fast heating scheme resulted in accumulated damage to the spore (Fig. S9). The viability results show that spores exposed to 20 rounds of 200 °C in 50 ms decreased the survival rate by less than one order of magnitude, demonstrating that the viability loss in the

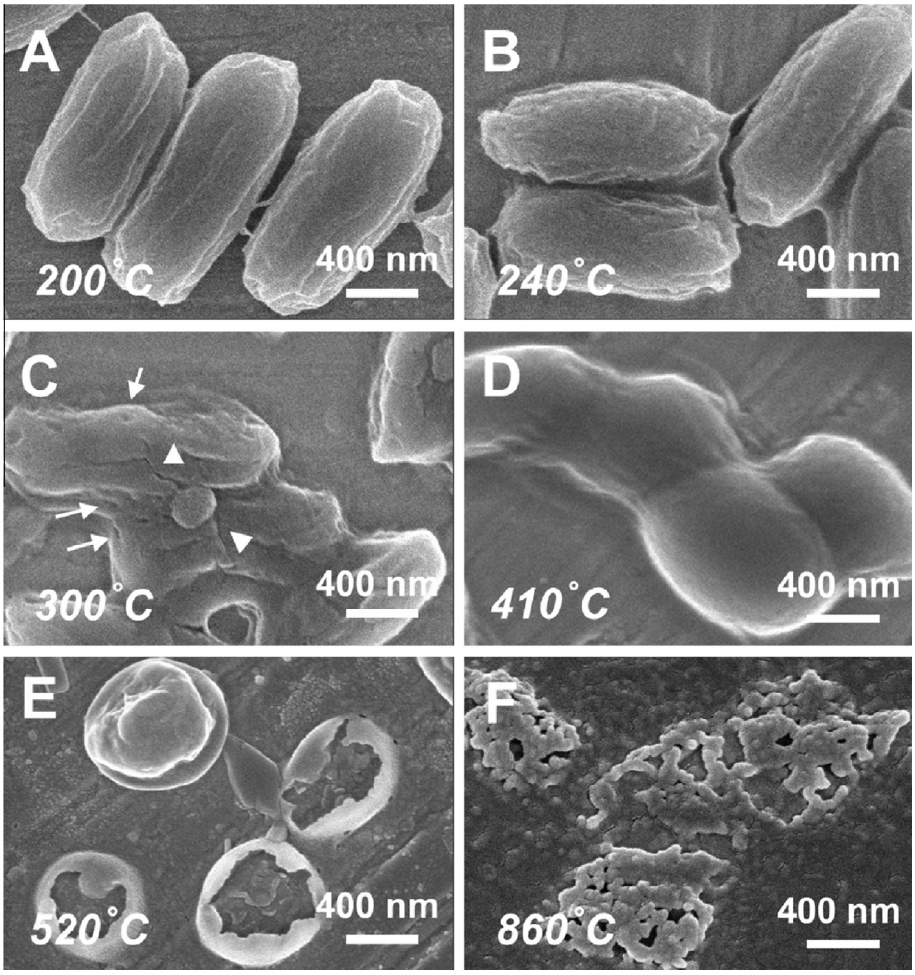

Fig. 4. SEM images of surface attached spores after heat treatment triggered by a 2 ms pulse (~10^5 °C/s). Each image shows a representative morphological change of over 50 spores (see Fig. S7). The maximum temperatures exerted on spores are indicated (A–F). In (C), the arrows and the arrow heads indicate the location of holes and fissures on the spore surfaces, respectively.

first pulse is not additive (Fig. 5). SEM results also confirmed that spores exposed to different heating cycles of 400 °C in 50 ms showed minor morphological differences or size changes (Figs. 5 and S10 and Table S3). In the second experiment, we asked if the repeated exposure of treated spores to higher peak temperatures caused additional damage to spores (Fig. S11). Pre-heating to 200 °C in 50 ms prior to pulse heating to 500 °C in 50 ms did not alter the viability of spores compared to just heating to 500 °C in 50 ms (Fig. 5A). The resulting SEM images (Fig. 5B–F) also show that melted and disintegrated spore structures appeared when the second and third pulse peak temperatures increased to 600 °C and 800 °C, respectively. These morphological changes could also be achieved by singular pulse heating to corresponding peak temperatures. Considering the total heating time in our experiments is less than 10 s, we propose that the heat accumulation is negligible compared with the reported heating time in traditional spore decontamination studies that was normally minutes or even hours [8–10,11,13]. These results demonstrate that maximum peak temperature, rather than repetitive heating, is the primary determinant for spore morphology and viability when exposed to fast heating rates (~10^4 °C/s).

3.5. Mechanism of inactivation by fast pulse heating (~10^4 °C/s) through analysis of mutant spores

To understand the mechanism of spore inactivation under our fast heating scheme (~10^4 °C/s), we have utilized wild-type strain PS533 [54] and three mutant spore strains: (1) Strain PS3328 lacks *cotE* gene [55] which encodes a protein required for outer coat assembly [56]; (2) Strain PS578 has deletions in *sspA sspB* genes [54] which encodes SASP that bind and protect DNA in spores [3,57]; Strain PS2318b lacks *recA* gene [36] which encodes a protein required for DNA repair. Wide-type spore strain (PS553) and PS3328 retained similar viability at 300 °C (Fig. 6). In contrast, PS2318b and PS578 mutants had significant viability reductions by 1–3 logs at peak temperatures around 300 °C (Fig. 6), indicating that the DNA-repair proteins and SASP protect the Bs spore against fast heating pulse. At peak temperatures >400 °C, wild-type and all the three mutant spores had similar viability reductions of ~4 logs (Fig. 6). Surface attached spores heated at ~10^4 °C/s under dry conditions had similar mechanism of killing as Bs spores heated in aerosols [22]. However at higher rates of ~10^5 °C/s, viabilities of most of mutant spores and wild-type spores were reduced similarly by ~4 logs at peak temperatures of as low as 300 °C, indicating that the spore killing mechanism at higher heating rates of ~10^5 °C/s is not only due to DNA damage (Fig. S12).

3.6. Heat inactivation of spores at ~10^5 °C/s under different external pressures

We hypothesized that ultrafast heating at rates >10^5 °C/s inactivate spores by increasing the internal pressure within the spore (see Section 4). We tested this hypothesis by heating spores exposed to different external pressures. When heated at rates

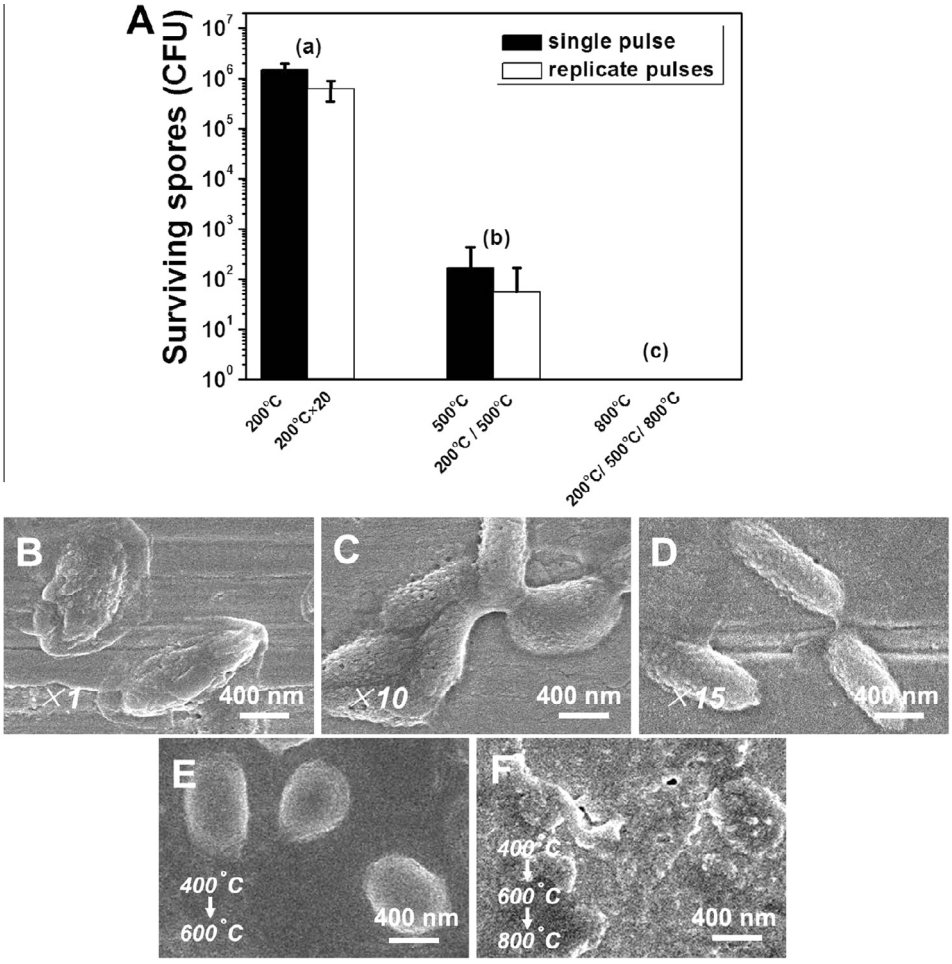

Fig. 5. Effect of repeat heat treatment on spore viability. (A–a) CFU of spores after being heated to 200 °C once (black bar) or 20 times (white bar) in the 50 ms pulse heating test. (A–b) CFU of spores after being heated to 200 °C followed by 500 °C (white bar), or directly heated to 200 °C (black bar) in the 50 ms pulse heating test. (A–c) CFU of spores after being heated in triplicates to 200 °C, 500 °C, and 800 °C subsequently (white bar), or directly heated to 800 °C (black bar) in the 50 ms pulse heating test. Bars are not shown in (A–c) since CFU = 0. Results are an average of at least 6 replicates and standard deviation is shown. In SEM images of (B)–(D), the heating pulse of 50 ms was tuned to yield the maximum temperature of ~400 °C. Samples were heated in (B), (C) and (D) for 1, 10 and 15 times, respectively. In (E), spores were first heated to 400 °C followed by a second pulse which heated spores to 600 °C. In (F), spores were heated to 400 °C, 600 °C and 800 °C under serial 50 ms pulses.

>10^5 °C/s in vacuum (1.3×10^{-5} Pa) with a peak temperature of 400 °C, holes formed on the spore surface indicating possible release of volatile species inside spores (Fig. 7). When spores were fast heated under 4 atm pressure (4.0×10^5 Pa) to 400 °C, bulges were observed on the surface of the spores indicating that volatile release was contained by the higher external pressure (Fig. 7). These results support our hypothesis that pressurization at heating rates of ~10^5 °C/s was associated with volatile release, thus contributing to spore inactivation.

4. Discussion

4.1. Temperature profiles of Bs spores on the Pt wire surface

Do Bs spores reach the same temperature as the Pt wire? Previous studies have revealed rapid heat transfer from the environment to the spore. Kumar et al. [58] showed that the spore took ~0.1 ms to reach the surrounding temperature of ~400 °C. Xing et al. [59] showed that the temperature could reach steady state in less than 0.5 ms. Since our spores are directly in contact with

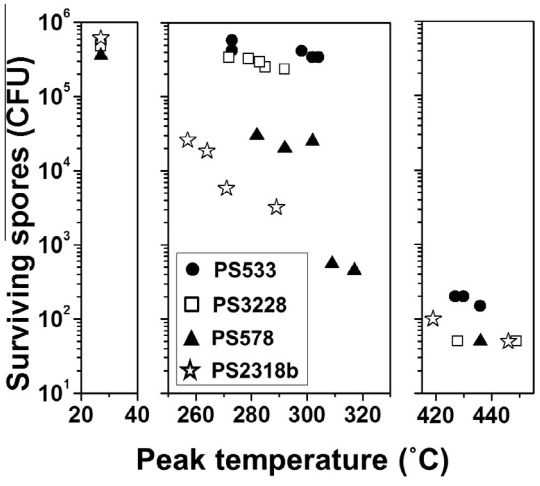

Fig. 6. Survival counts of the wide-type strain (PS533) and three mutant strains (PS3328 (Δ*cotE*), PS578 (Δ*sspA* Δ*sspB*) and PS2318b (Δ*recA*)) of Bs spores at elevated peak temperatures in the 50 ms pulse heating.

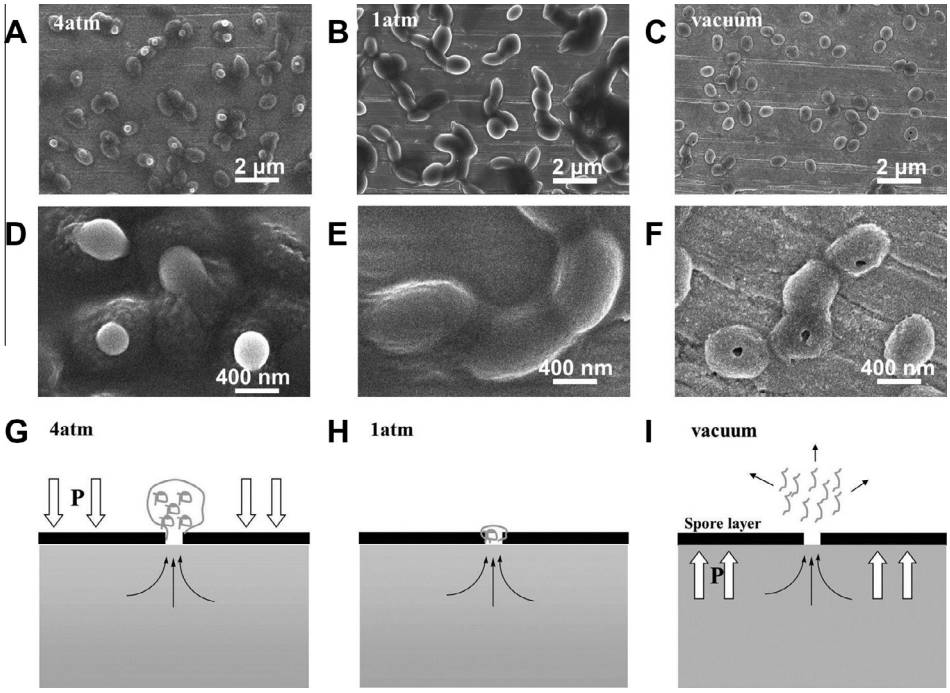

Fig. 7. Effect of external pressure towards the morphological changes of spores heated to 400 °C at a heating rate of ~10^5 °C/s. The pressures applied to spores in image (A), (B), and (C) are 4.0×10^5 Pa, 1.0×10^5 Pa, are 1.3×10^{-5} Pa, respectively. (D), (E), and (F) are the enlarged SEM images of (A), (B), and (C), respectively. (G), (H), and (I) are schematic drawings of the effect of external pressure towards distinct spore morphologies.

the wire (Fig. 1), the temperature increase of the spores will approximate the temperature increase of the wire in a 2–50 ms pulse heating process. We also assessed the accuracy of our temperature measurements and the distribution of heat along the length of the wire by using blackbody calibration, which showed that the wire temperature measurement fit to theoretical values precisely, especially below 1000 °C. Unlike the reported temperature measurements using thermocouples in the gas-phase spore inactivation studies that show a certain spatial temperature distribution [17–25], our results show a narrow temperature distribution along the entire length of the wire (see the evenly distributed temporal light intensity on wire in Fig. S4).

4.2. Spore viability heated to fixed peak temperatures under the same pulse time

There is intense interest in characterizing inactivation of *Bacillus* spores by sub-second heating pulses. Here we compare and contrast the results from thermal inactivation of spores affixed to solid surfaces to other studies. In general, sub-second heat inactivation of spores has a sigmoid temperature–kill relationship. Gates et al. [18] implemented pressure shocks to rapidly increase the air temperature around aerosolized Bs spores to 200–700 °C within 2–45 ms. The loss of viability occurred at ~200 °C, followed by decrease by 5 logs from 200 °C to 500 °C. Further reduction in viability at higher temperatures was minimal. Grinshpun et al. [19,20] exposed aerosolized Bs spores to hot air flow (150–1000 °C) and controlled the entire exposure time to be around 0.2–1 s. Due to rapid heat transfer into aerosolized spores [58], the exact time to reach peak temperature could be much shorter. Similarly, the viability of spores started to decrease at 200–250 °C. From 250 °C to 370 °C, the viability dropped exponentially by 5 logs. Recently, Xing et al. [59] utilized a conductive heating system to rapidly heat *Bacillus anthracis* spores placed on a gold foil in 0.1 s. They found that the viability decreased exponentially with temperature, with a reduction of 5 logs from 300 °C to ~700 °C. All these studies show clear correlations between temperature, heating time and spore inactivation efficiency. Although the temperature–kill curves from previous studies [18–20,59] are similar to our results (Fig. 2), the spore inactivation mechanisms are different. Grinshpun et al. [19,20] heated aerosolized dry spores through a top-hat heating scheme and found the primary contribution to spore inactivation was the peak temperature and the heating time. Gates et al. [18] killed spores in a gas dynamic heating scheme induced by mechanical shocks, in which the high pressure and top-hat temperature have synergistic effect on spore inactivation. However, the heating rate was not directly measured in these studies as an important factor. Our studies demonstrate that ~10^5 °C/s heating schemes can potentiate spore inactivation (Fig. 2).

The sigmoid nature of spore destruction kinetics is consistent with the kill curves within other time–kill models. Spores are resistant to applied heat during a short period of time, while suffered from rapid inactivation by 3–6 logs when the heating time is elongated [60]. Further increasing the heating time can induce complete inactivation of the few surviving spores [53]. Compared with these well-studied time–kill models, studies of temperature–kill relationships have been limited due to the narrow temperature range of conventional heating methods. Our temperature–kill results demonstrate a similar sigmoid feature for spore inactivation. There are also three stages relative to the T_c. At temperatures well below the T_c, spores are resistant to thermal damage. At temperatures near the T_c, the spores are readily inactivated and the survival ratio drops logarithmically. At temperature well above the T_c, the remaining spores are completely inactivated.

4.3. Relationship of spore morphology heated to defined peak temperatures at two ramp rates

We observed two different morphological changes at the two different heating rates. When heated at ~10^4 °C/s rate that is similar to other heating scheme studies, we find that increasing

severity of morphological change correlates with decrease in spore viability. Our results here demonstrate that when Bs spores heated to 400 °C at ~10^4 °C/s, a reduction of 38–42% in the projected area of spores was induced (Table 2). This reduction in projected area matches the ratio of areas of the spore cortex and the spore coat from previous observations made by TEM of spore thin sections [2,61,62]. From these TEMs, we calculated the projected areas of the intact spore with coat and the spore that has shed the coat, and estimated the reduction in the projected area to be between 32% and 40% based on the removal of the coat (Table S2). In contrast when spores exposed to ~10^5 °C/s heating rate, the spore viability decreased rapidly at temperatures above 200 °C. However, the aspect ratio and projected area remain unchanged. The exact correlation between the mechanical changes of spores from morphological studies and the spore inactivation efficiency remains to be determined. These results suggest that spores exposed to these higher heating rates (~10^5 °C/s) are inactivated by a different mechanism than spores inactivated at ~10^4 °C/s.

4.4. Spore inactivation at fast heating rates (~10^4 °C/s) through DNA damage

We determined the mechanism of heat inactivation of spores affixed on surfaces by utilizing mutant strains defective for DNA protection, DNA repair and coat assembly. We used the fast heating rate (~10^4 °C/s) that allows detection of increased sensitivity in mutant spores. Our results show that DNA damage is a major contributor to inactivation of surface attached dry spores in the fast heat scheme, which is consistent with the mechanism for inactivation of aerosolized spores exposed to extreme dry heat [22,50]. Spore coat is not required for heat resistance in this heating scheme which agrees with results by Setlow et al. [3,63] that demonstrated that decoated spores had similar heat resistance to the wide-type spores. Instead, they found that the spore coat was mainly involved in resistance to some biocidal chemicals [47–49]. In agreement with the *cotE* mutant analysis, our morphological studies also show that when heated at ~10^4 °C/s spores with melted coats at 400 °C had minimal reduction in viability (Fig. 3B). Together, our results indicate that surface attached spores heated in our fast heating scheme (~10^4 °C/s) behave similar to dry spores heated in other aerosol heating schemes [17–25].

4.5. Spore inactivation at heating rates of ~10^5 °C through rapid pressurization inside spore

Our results yield an interesting finding: when heated to the same peak temperature, higher heating rates of ~10^5 °C/s potentiate thermal inactivation of spores as compared to ~10^4 °C/s (see the temperature range from 250 °C to 450 °C in Fig. 2). What is the basis for enhanced spore inactivation by these higher heating rates? Since the peak temperature in these two heating schemes is the same, the observed enhanced killing of Bs spores must be due to the rate of heating (Fig. 2). We propose that this effect is due to vaporization of the internal contents of the spore, i.e. water, DPA and other volatiles. SEM images of spores heated at the ~10^4 °C/s revealed that the spores had minimal morphological change until >400 °C (Fig. 3 and Table 2). In contrast, SEM images of spores heated at ~10^5 °C/s formed the cracks and fissures at temperatures as low as 300 °C (Figs. 4C and S8). Spore viability was reduced at a lower peak temperature of 240 °C (Fig. 2) without detectable morphological change (Fig. 4), suggesting that transient holes may form in the spore coat that is not detectable by SEM (Fig. 4B). We tested whether pressurization events are occurring on the heated spore by testing the effect of external pressure on spore morphology. Spores on a wire were heated to the same peak temperature at ~10^5 °C/s in three different pressures: (1) vacuum, (2) atmospheric (1 atm), and (3) four atmosphere (4 atm) pressure. Under vacuum, the spores displayed an exaggerated morphology in which large holes were formed (Fig. 7C and F). In contrast, SEMs of spores heated in excess external pressure showed 'balloons' on the surface of spores indicating that the external pressure contained the expansion of explosive volatiles (Fig. 7A and D).

Based on these observations, one possible mechanism for enhanced killing at ultrafast heating rates is the *dynamic* internal pressure generated by violent vaporization of volatiles, including water that imposes dynamic shock on spores. To estimate the *dynamic* internal pressure within spores during these heating events, we assumed that water is the primary volatile component in the cell since water comprises ~30% of the spore core mass [64]. Assuming minimal diffusive loss, and all liquid water is vigorously vaporized after 200 °C due to the rapid heating rates, *dynamic* pressure is a function of peak temperature [65]. Using the amount of water presented in the spore core and the volume of the spore core, the *dynamic* pressures at 240 °C and 400 °C are estimated to be 308 MPa and 404 MPa, respectively (Fig. S13). Based on our killing curves (Fig. 2) and morphological changes (Figs. 3 and 4), the maximum *dynamic* internal pressures that spores can sustain (without significant reduction of viability and failure of spore coat) are 308 MPa at a heating rate of ~10^5 °C/s, and 404 MPa at a heating rate of ~10^4 °C/s. This huge difference in the yield stresses indicates that the assumption of minimal diffusive loss of volatiles from the spore core must be incorrect. If we assume the diffusive rate of water through the spore coat keeps constant at v (MPa/ms) during the temperature range of 240–400 °C, the real yield stress of spore coat (σ_{yield}) at both heating rates can be express as:

$$\sigma_{yield} = P_1 - vT_1 = P_2 - vT_2 \quad (2)$$

P_1 (308 MPa) and P_2 (404 MPa) are the maximum *dynamic* internal pressures of spores at heating rates of ~10^5 °C/s and ~10^4 °C/s, respectively. T_1 (2 ms) and T_2 (50 ms) are the pulse heating times at heating rates of ~10^5 °C/s and ~10^4 °C/s, respectively. The results are v = 2 MPa/ms and σ_{yield} = 304 MPa. Considering that the water diffusion rate (2 MPa/ms) is closer to the pressurization rate (8 MPa/ms) at ~10^4 °C/s, but much smaller than the pressurization rate (154 MPa/ms) at ~10^5 °C/s, it is easy to understand the potentiation of thermal inactivation at higher heating rates by internal pressurization. A similar explanation for spore inactivation was reported by Xing et al. [59]. They found that the spore surface was ruptured after rapid heating to 300 °C for 10 s, suggesting the vaporized content inside spores cannot promptly diffuse out and therefore the pressure-induced mechanical stresses exceed the yield stress of spores. The authors measured the temporal modulus of spores with temperature and found the modulus to be ~400 MPa at 275 °C [66]. We should also note that the maximum hydrostatic pressures (400–800 MPa) employed in the industrial high-pressure sterilization approaches [67–69] are larger than our aforementioned result (304 MPa). This suggests that the dynamic yield stress of spores could be smaller than that under static pressure.

Given the approximations used in our estimates, and the fact that the tensile stress of the spore exterior layers is probably also temperature sensitive (decreases as the structure melts at high temperatures), our result indicates that spores in ultrafast-heat (~10^5 °C/s) and high-temperature processes are more susceptible to increased internal pressures and liable to lose both viability and morphological integrity. It should be noted that such critical heating rates may also be different for other spores, depending upon the degree of dehydration and the permeability of water in the spores.

5. Conclusion

Surface immobilized bacterial spores subjected to sub-second and ultrahigh heating conditions were characterized for spore inactivation and morphological changes. There are two key determinants in spore inactivation. First, maximal peak temperature greater than 700 °C led to 6 logs reduction in spore viability. Second, ultrafast heating of the initial pulse exceeding $\sim 10^5$ °C/s potentiates spore inactivation. Repetitive heating had no discernible effect on spore morphology and survival rate, implying that damage is not cumulative in sub-second heat exposures. At fast heating rates ($\sim 10^4$ °C/s), mutant spores that lack *sspA sspB* and *recA* genes were more susceptible to inactivation, indicating that DNA damage contributes to spore inactivation at $\sim 10^4$ °C/s. At higher heating rates of $\sim 10^5$ °C/s, rapid pressurization inside spores is the major contributor to inactivation. The exact correlation between the mechanical changes of spores from morphological studies, and the spore inactivation efficiency remains to be determined. The temperature–time–kill correlation described for spores undergoing a pulse heating process ($\sim 10^3$ °C/s to $\sim 10^5$ °C/s) can be utilized for generating novel strategies to inactivate biological warfare threats due to bacterial spores.

Acknowledgements

This work was funded by a grant from DOD/DTRA (BRBAA08-Per5-H-2-0065). It is greatly thankful to Dr. Peter Setlow from University of Connecticut Health center for kindly providing the wild-type and mutant Bs spores. We also thank Mr. Tim Maugel in the Laboratory for Biological Ultrastructure at the University of Maryland, College Park, for his assistance of shooting SEM images.

Appendix A. Supplementary data

Supplementary data associated with this article can be found, in the online version, at http://dx.doi.org/10.1016/j.cej.2015.05.021.

References

[1] G.W. Gould, History of science – spores Lewis B Perry memorial lecture 2005, J. Appl. Microbiol. 101 (2006) 507–513.
[2] W.L. Nicholson, N. Munakata, G. Horneck, H.J. Melosh, P. Setlow, Resistance of *Bacillus* endospores to extreme terrestrial and extraterrestrial environments, Microbiol. Mol. Biol. Rev. 64 (2000) 548–572.
[3] P. Setlow, Spores of *Bacillus subtilis*: their resistance to and killing by radiation, heat and chemicals, J. Appl. Microbiol. 101 (2006) 514–525.
[4] E. Nadasi, T. Varjas, I. Prantner, V. Virag, I. Ember, Bioterrorism: warfare of the 21st century, Gene Ther. Mol. Biol. 11 (2007) 315–320.
[5] Y. Gilbert, C. Duchaine, Bioaerosols in industrial environments: a review, Can. J. Civ. Eng. 36 (2009) 1873–1886.
[6] V. Kummer, W.R. Thiel, Bioaerosols – sources and control measures, Int. J. Hyg. Environ. Health 211 (2008) 299–307.
[7] T.L. Buhr, A.A. Young, Z.A. Minter, C.M. Wells, D.C. McPherson, C.L. Hooban, C.A. Johnson, E.J. Prokop, J.R. Crigler, Test method development to evaluate hot, humid air decontamination of materials contaminated with *Bacillus anthracis* ΔSterne and *B. thuringiensis* Al Hakam spores, J. Appl. Microbiol. 113 (2012) 1037–1051.
[8] W.H. Coleman, D. Chen, Y.-Q. Li, A.E. Cowan, P. Setlow, How moist heat kills spores of *Bacillus subtilis*, J. Bacteriol. 189 (2007) 8458–8466.
[9] R. Conesa, P.M. Periago, A. Esnoz, A. Lopez, A. Palop, Prediction of *Bacillus subtilis* spore survival after a combined non-isothermal–isothermal heat treatment, Eur. Food Res. Technol. 217 (2003) 319–324.
[10] O. Couvert, S. Gaillard, N. Savy, P. Mafart, I. Leguerinel, Survival curves of heated bacterial spores: effect of environmental factors on Weibull parameters, Int. J. Food Microbiol. 101 (2005) 73–81.
[11] J. Iciek, A. Papiewska, M. Molska, Inactivation of *Bacillus stearothermophilus* spores during thermal processing, J. Food Eng. 77 (2006) 406–410.
[12] J.-H. Mah, D.-H. Kang, J. Tang, Morphological study of heat-sensitive and heat-resistant spores of *Clostridium* sporogenes, using transmission electron microscopy, J. Food Prot. 71 (2008) 953–958.
[13] T.J. Montville, R. Dengrove, T. de Siano, M. Bonnet, W. Schaffner, Thermal resistance of spores from virulent strains of *Bacillus anthracis* and potential surrogates, J. Food Prot. 68 (2005) 2362–2366.
[14] N.E.M. Mustafa, U. Keller, U. Malkus, D. Harmsen, R. Reichelt, A.A. Hussein, S.M. El-Sanousi, Morphological changes induced by wet–heat in *Bacillus cereus* endospores, Curr. Res. Bacteriol. 3 (2010) 214–226.
[15] J.S. Novak, V.K. Juneja, B.A. McClane, An ultrastructural comparison of spores from various strains of *Clostridium perfringens* and correlations with heat resistance parameters, Int. J. Food Microbiol. 86 (2003) 239–247.
[16] F.T. Tabit, E. Buys, The effects of wet heat treatment on the structural and chemical components of *Bacillus sporothermodurans* spores, Int. J. Food Microbiol. 140 (2010) 207–213.
[17] S.D. Gates, A.D. McCartt, P. Lappas, J.B. Jeffries, R.K. Hanson, L.A. Hokama, K.E. Mortelmans, *Bacillus* endospores resistance to gas dynamic heating, J. Appl. Microbiol. 109 (2010) 1591–1598.
[18] S.D. Gates, A.D. McCartt, J.B. Jeffries, R.K. Hanson, L.A. Hokama, K.E. Mortelmans, Extension of *Bacillus* endospore gas dynamic heating studies to multiple species and test conditions, J. Appl. Microbiol. 111 (2011) 925–931.
[19] S.A. Grinshpun, A. Adhikari, C. Li, T. Reponen, M. Yermakov, M. Schoenitz, E. Dreizin, M. Trunov, S. Mohan, Thermal inactivation of airborne viable *Bacillus subtilis* spores by short-term exposure in axially heated air flow, J. Aerosol Sci. 41 (2010) 352–363.
[20] S.A. Grinshpun, C. Li, A. Adhikari, M. Yermakov, T. Reponen, M. Schoenitz, E. Dreizin, V. Hoffmann, M. Trunov, Method for studying survival of airborne viable microorganisms in combustion environments: development and evaluation, Aerosol Air Qual. Res. 10 (2010) 414–424.
[21] S.A. Grinshpun, A. Adhikari, M. Yermakov, T. Reponen, E. Dreizin, M. Schoenitz, V. Hoffmann, S. Zhang, Inactivation of aerosolized *Bacillus atrophaeus* (BG) endospores and MS2 viruses by combustion of reactive materials, Environ. Sci. Technol. 46 (2012) 7334–7341.
[22] E. Johansson, A. Adhikari, T. Reponen, M. Yermakov, S.A. Grinshpun, Association between increased DNA mutational frequency and thermal inactivation of aerosolized *Bacillus* spores exposed to dry heat, Aerosol Sci. Technol. 45 (2011) 376–381.
[23] J.H. Jung, J.E. Lee, S.S. Kim, Thermal effects on bacterial bioaerosols in continuous air flow, Sci. Total Environ. 407 (2009) 4723–4730.
[24] Y.H. Lee, B.U. Lee, Inactivation of airborne *E. coli* and *B. subtilis* bioaerosols utilizing thermal energy, J. Microbiol. Biotechnol. 16 (2006) 1684–1689.
[25] A.D. McCartt, S.D. Gates, J.B. Jeffries, R.K. Hanson, L.M. Joubert, T.L. Buhr, Response of *Bacillus thuringiensis* Al Hakam endospores to gas dynamic heating in a shock tube, Z. Phys. Chem. 225 (2011) 1367–1377.
[26] N. Piekiel, M.R. Zachariah, Decomposition of aminotetrazole based energetic materials under high heating rate conditions, J. Phys. Chem. A 116 (2012) 1519–1526.
[27] K.T. Sullivan, N.W. Piekiel, S. Chowdhury, C. Wu, M.R. Zachariah, C.E. Johnson, Ignition and combustion characteristics of nanoscale Al/$AgIO_3$: a potential energetic biocidal system, Combust. Sci. Technol. 183 (2011) 285–302.
[28] C. Wu, K. Sullivan, S. Chowdhury, G. Jian, L. Zhou, M.R. Zachariah, Encapsulation of perchlorate salts within metal oxides for application as nanoenergetic oxidizers, Adv. Funct. Mater. 22 (2012) 78–85.
[29] G. Young, N. Piekiel, S. Chowdhury, M.R. Zachariah, Ignition behavior of α-AlH_3, Combust. Sci. Technol. 182 (2010) 1341–1359.
[30] L. Zhou, N. Piekiel, S. Chowdhury, M.R. Zachariah, T-jump/time-of-flight mass spectrometry for time-resolved analysis of energetic materials, Rapid Commun. Mass Spectrom. 23 (2009) 194–202.
[31] L. Zhou, N. Piekiel, S. Chowdhury, M.R. Zachariah, Time-resolved mass spectrometry of the exothermic reaction between nanoaluminum and metal oxides: the role of oxygen release, J. Phys. Chem. C 114 (2010) 14269–14275.
[32] J.M. Mason, P. Setlow, Essential role of small, acid-soluble spore proteins in resistance of *Bacillus subtilis* spores to UV light, J. Bacteriol. 167 (1986) 174–178.
[33] W.L. Nicholson, B. Setlow, P. Setlow, Binding of DNA in vitro by a small, acid-soluble spore protein from *Bacillus subtilis* and the effect of this binding on DNA topology, J. Bacteriol. 172 (1990) 6900–6906.
[34] P. Setlow, I will survive: protecting and repairing spore DNA, J. Bacteriol. 174 (1992) 2737–2741.
[35] B. Setlow, P. Setlow, Small, acid-soluble proteins bound to DNA protect *Bacillus subtilis* spores from killing by dry heat, Appl. Environ. Microbiol. 61 (1995) 2787–2790.
[36] B. Setlow, P. Setlow, Role of DNA repair in *Bacillus subtilis* spore resistance, J. Bacteriol. 178 (1996) 3486–3495.
[37] W.H. Coleman, P. Setlow, Analysis of damage due to moist heat treatment of spores of *Bacillus subtilis*, J. Appl. Microbiol. 106 (2009) 1600–1607.
[38] P. Zhang, L. Kong, P. Setlow, Y.-Q. Li, Characterization of wet–heat inactivation of single spores of *Bacillus* species by dual-trap Raman spectroscopy and elastic light scattering, Appl. Environ. Microbiol. 76 (2010) 1796–1805.
[39] D.L. Popham, J. Helin, C.E. Costello, P. Setlow, Analysis of the peptidoglycan structure of *Bacillus subtilis* endospores, J. Bacteriol. 178 (1996) 6451–6458.
[40] H. Fairhead, B. Setlow, P. Setlow, Prevention of DNA damage in spores and in vitro by small, acid-soluble proteins from *Bacillus* species, J. Bacteriol. 175 (1993) 1367–1374.
[41] B. Setlow, S. Atluri, R. Kitchel, K. Koziol-Dube, P. Setlow, Role of dipicolinic acid in resistance and stability of spores of *Bacillus subtilis* with or without DNA-protective α/β-type small acid-soluble proteins, J. Bacteriol. 188 (2006) 3740–3747.

[42] B. Setlow, E. Melly, P. Setlow, Properties of spores of *Bacillus subtilis* blocked at an intermediate stage in spore germination, J. Bacteriol. 183 (2001) 4894–4899.
[43] S. Nakashio, P. Gerhardt, Protoplast dehydration correlated with heat resistance of bacterial spores, J. Bacteriol. 162 (1985) 571–578.
[44] P. Gerhardt, R.E. Marquis, Spore thermoresistance mechanisms, in: Regulation of Procaryotic Development, American Society for Microbiology, DC, 1986. pp. 43–63.
[45] S. Kozuka, K. Tochikubo, Permeability of dormant spores of *Bacillus subtilis* to malachite green and crystal violet, J. Gen. Microbiol. 137 (1991) 607–613.
[46] P. Zhang, L. Kong, G. Wang, P. Setlow, Y.Q. Li, Monitoring the wet–heat inactivation dynamics of single spores of *Bacillus* species by using Raman tweezers, differential interference contrast microscopy, and nucleic acid dye fluorescence microscopy, Appl. Environ. Microbiol. 77 (2011) 4754–4769.
[47] E. Melly, A.E. Cowan, P. Setlow, Studies on the mechanism of killing of *Bacillus subtilis* spores by hydrogen peroxide, J. Appl. Microbiol. 93 (2002) 316–325.
[48] S.B. Young, P. Setlow, Mechanisms of killing of *Bacillus subtilis* spores by hypochlorite and chlorine dioxide, J. Appl. Microbiol. 95 (2003) 54–67.
[49] S.B. Young, P. Setlow, Mechanisms of *Bacillus subtilis* spore resistance to and killing by aqueous ozone, J. Appl. Microbiol. 96 (2004) 1133–1142.
[50] B. Setlow, S. Parish, P. Zhang, Y.Q. Li, W.C. Neely, P. Setlow, Mechanism of killing of spores of *Bacillus anthracis* in a high-temperature gas environment, and analysis of DNA damage generated by various decontamination treatments of spores of *Bacillus anthracis*, *Bacillus subtilis* and *Bacillus thuringiensis*, J. Appl. Microbiol. 116 (2013) 805–814.
[51] W. Zhou, S.K. Watt, D.-H. Tsai, V.T. Lee, M.R. Zachariah, Quantitative attachment and detachment of bacterial spores from fine wires through continuous and pulsed DC electrophoretic deposition, J. Phys. Chem. B 117 (2013) 1738–1745.
[52] P.R.N. Childs, Practical Temperature Measurement, Butterworth Heinemann, London, UK, 2001.
[53] J.N. Junior, P.R. de Massaguer, Thermal death kinetics of *B. stearothermophilus* spores in sugarcane must, J. Food Proc. Eng. 30 (2007) 625–639.
[54] B. Setlow, K.A. McGinnis, K. Ragkousi, P. Setlow, Effects of major spore-specific DNA binding proteins on *Bacillus subtilis* sporulation and spore properties, J. Bacteriol. 182 (2000) 6906–6912.
[55] M. Paidhungat, K. Ragkousi, P. Setlow, Genetic requirements for induction of germination of spores of *Bacillus subtilis* by Ca^{2+}-dipicolinate, J. Bacteriol. 183 (2001) 4886–4893.
[56] A. Driks, S. Roels, B. Beall, C.P. Moran Jr., R. Losick, Subcellular localization of proteins involved in the assembly of the spore coat of *Bacillus subtilis*, Genes Dev. 8 (1994) 234–244.
[57] P. Setlow, Small, acid-soluble spore proteins of *Bacillus* species: structure, synthesis, genetics, function, and degradation, Ann. Rev. Microbiol. 42 (1988) 319–338.
[58] R. Kumar, S. Saurav, E.V. Titov, D.A. Levin, R.F. Long, W.C. Neely, P. Setlow, Thermo-structural studies of spores subjected to high temperature gas environments, Int. J. Heat Mass Transf. 54 (2011) 755–765.
[59] Y. Xing, A. Li, D.L. Felker, L.W. Burggraf, Nanoscale structural and mechanical analysis of *Bacillus anthracis* spores inactivated with rapid dry heating, Appl. Environ. Microbiol. 80 (2014) 1739–1749.
[60] M. Peleg, M.B. Cole, Reinterpretation of microbial survival curves, Crit. Rev. Food Sci. Nutr. 38 (1998) 353–380.
[61] A. Driks, *Bacillus subtilis* spore coat, Microbiol. Mol. Biol. Rev. 63 (1999) 1–20.
[62] H. Takamatsu, K. Watabe, Assembly and genetics of spore protective structures, Cell Mol. Life Sci. 59 (2002) 434–444.
[63] S. Ghosh, B. Setlow, P.G. Wahome, A.E. Cowan, M. Plomp, A.J. Malkin, P. Setlow, Characterization of spores of *Bacillus subtilis* that lack most coat layers, J. Bacteriol. 190 (2008) 6741–6748.
[64] T.C. Beaman, P. Gerhardt, Heat resistance of bacterial spores correlated with protoplast dehydration, mineralization, and thermal adaptation, Appl. Environ. Microbiol. 52 (1986) 1242–1246.
[65] S.I. Sandler, Chemical, Biochemical, and Engineering Thermodynamics, John Wiley & Sons Inc., Hoboken, NJ, 2006.
[66] A.G. Li, Y. Xing, L.W. Burggraf, Thermal effects on surface structures and properties of *Bacillus anthracis* spores on nanometer scales, Langmuir 29 (2013) 8343–8354.
[67] E.P. Black, P. Setlow, A.D. Hocking, C.M. Stewart, A.L. Kelly, D.G. Hoover, Response of spores to high-pressure processing, Compr. Rev. Food Sci. Food Saf. 6 (2007) 103–119.
[68] H.-W. Huang, H.-M. Lung, B.B. Yang, C.-Y. Wang, Responses of microorganisms to high hydrostatic pressure processing, Food Control. 40 (2014) 250–259.
[69] Z. Zhang, B. Jiang, X. Liao, J. Yi, X. Hu, Y. Zhang, Inactivation of *Bacillus subtilis* spores by combining high-pressure thermal sterilization and ethanol, Int. J. Food Microbiol. 160 (2012) 99–104.

ACS APPLIED MATERIALS & INTERFACES

Research Article

www.acsami.org

Metal Iodate-Based Energetic Composites and Their Combustion and Biocidal Performance

H. Wang,[†] G. Jian,[†] W. Zhou,[†] J. B. DeLisio,[†] V. T. Lee,[‡,§] and M. R. Zachariah*[,†]

[†]Department of Chemical and Biomolecular Engineering and Department of Chemistry and Biochemistry, University of Maryland, College Park, Maryland 20742, United States

[‡]Department of Cell Biology and Molecular Genetics, University of Maryland, College Park 20740, Maryland, United States

Supporting Information

ABSTRACT: The biological agents that can be weaponized, such as *Bacillus anthracis*, pose a considerable potential public threat. Bacterial spores, in particular, are highly stress resistant and cannot be completely neutralized by common bactericides. This paper reports on synthesis of metal iodate-based aluminized electrospray-assembled nanocomposites which neutralize spores through a combined thermal and chemical mechanism. Here metal iodates ($Bi(IO_3)_3$, $Cu(IO_3)_2$, and $Fe(IO_3)_3$) act as a strong oxidizer to nanoaluminum to yield a very exothermic and violent reaction, and simultaneously generate iodine as a long-lived bactericide. These microparticle-assembled nanocomposites when characterized in terms of reaction times and temporal pressure release show significantly improved reactivity. Furthermore, sporicidal performance superior to conventional metal-oxide-based thermites clearly shows the advantages of combining both a thermal and biocidal mechanism in spore neutralization.

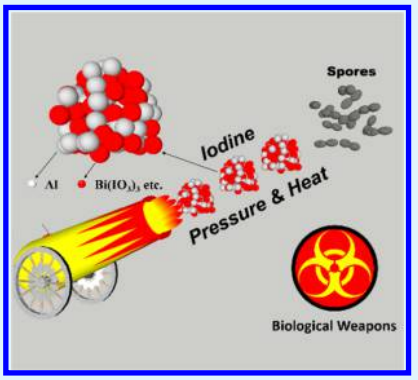

KEYWORDS: *energetic materials, metal iodate, nanothermite, biocidal, electrospray*

1. INTRODUCTION

Thermites is a class of energetic materials that can undergo fast redox reaction between a fuel (e.g., Al) and an oxidizer (CuO, Fe_2O_3, Bi_2O_3, etc.), which ,once initiated, release large amounts of thermal energy.

$$\mathrm{Al} + \frac{3}{2}\mathrm{MO} \rightarrow \frac{1}{2}\mathrm{Al_2O_3} + \frac{3}{2}\mathrm{M} + \Delta H \quad (1)$$

Decreasing the reactant length scales from the micron to the nanoscale greatly increases the interfacial contact and reduces the diffusion distance between fuel and oxidizer, resulting in as much as ~1000× higher reactivity.[1−6] The thermochemical properties of the materials used result in energy densities, for the most common mixtures, that are a factor of 2 or more higher on a volumetric basis than conventional organic-based energetic materials (e.g., TNT or RDX).[7−22]

The potential threats from biological-based weapons, such as those employing *Bacillus anthracis*, pose a significant challenge to global security. Of particular concern are spores of virulent bacteria that are highly stress resistant and cannot be completely killed by high-pressure processing (HPP), heat, or toxic chemicals such as iodophor.[23−25] Conventional energetic materials produce a thermal event over a relatively short time, which may not be sufficient for total inactivation. Thus, a strategy has developed in which, in addition to the thermal event, a remnant biocidal agent delivered simultaneously would have a much longer exposure time resulting in a more effective inactivation. As such, both silver- or halogen-containing thermites, even difluoroiodate compound-based explosives, have been considered as biological agent defeating ingredients.[26−29] The two most common methods of incorporating biocidal agents into energetic systems are to either directly add silver or halogen into the metallized energetic materials or to employ silver- or iodine-containing oxidizers into the thermite formulation.[30−32] The latter option has the potential for Ag and I to act as part of the energy release landscape rather than as a passive species. Some extremely strong oxidizers of the latter kind, such as $NaIO_4/KIO_4$, do not release iodine, while others like I_2O_5 and $AgIO_3$ have storage issues because of their hygroscopicity and light sensitivity.[31,32] The ideal oxidizer should (1) be easy to handle and (2) decompose to allow the oxygen to react with the fuel and release molecular iodine.

$$\mathrm{Al} + \frac{1}{2}\mathrm{M(IO_3)} \rightarrow \frac{1}{2}\mathrm{Al_2O_3} + \frac{1}{2}\mathrm{M} + \frac{1}{4}\mathrm{I_2} + \Delta H \quad (2)$$

In this paper, three metal iodate nanoparticles, $Bi(IO_3)_3$, $Cu(IO_3)_2$, and $Fe(IO_3)_3$, were synthesized and subsequently assembled with aluminum nanoparticles using an electrospray technique to create microsized nanothermites. The confined burning pressure of the metal iodate-based thermite was found to be ~5× higher than conventional Al/CuO nanothermite. The rapid reaction mechanism and the iodine release from the metal-iodate-based thermite was investigated using rapid heating mass spectrometry. The effectiveness of synthesized

Received: May 26, 2015
Accepted: July 10, 2015
Published: July 10, 2015

DOI: 10.1021/acsami.5b04589
ACS Appl. Mater. Interfaces 2015, 7, 17363−17370

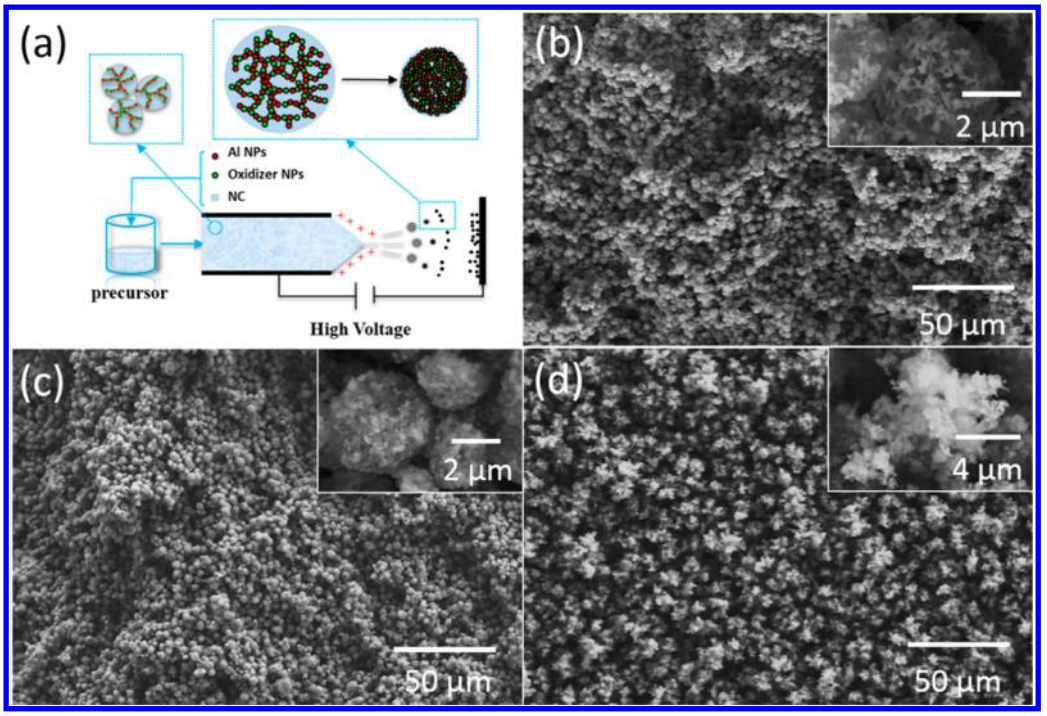

Figure 1. (a) Schematic of electrospray approach. (b–d) Low- and high-magnification SEM images of (b) Al/$Bi(IO_3)_3$ composites, (c) Al/$Cu(IO_3)_2$ composites, and (d) Al/$Fe(IO_3)_3$ composites. Note: all the above composites contain 5% NC (by weight).

iodate-based thermites as a biocidal agent was tested, and results show superior performance in the inactivation of spores.

2. EXPERIMENTAL SECTION

Chemicals. Copper oxide (~50 nm), bismuth oxide (90–210 nm), and iron oxide (~50 nm) were purchased from Sigma-Aldrich, and aluminum (ALEX, ~50 nm) was purchased from Argonide Corp. Al nanoparticles contain ~70% active aluminum (by weight), which is confirmed by thermogravity analysis.[33] Collodion solution (4–8% nitrocellulose, i.e., NC, in ethanol/diethyl ether, by weight) was purchased from Fluka Corp., and diethyl ether (99.8%)/ethanol (99.8%) mixture (volume ratio: 1:3) was employed to dissolve the collodion. The copper iodate, bismuth iodate, and iron iodate nanoparticles were synthesized by the following procedures. The formation energies of these oxidizers were calculated on the basis of the data at https://materialsproject.org/. The formation energies of $Bi(IO_3)_3$, $Cu(IO_3)_2$, and $Fe(IO_3)_3$ are calculated as −1282, −725, and −1293 kJ/mol, respectively.

Synthesis of the Copper Iodate Nanoparticles. Copper iodate nanoparticles were synthesized by milling copper(II) nitrate trihydrate (Sigma-Aldrich) and potassium iodate (Sigma-Aldrich) mixture (mass ratio: 1:3). After the milling process, the sample was washed with 30 mL of deionized water, and centrifuged for 30 min at 13 500 rpm (Hermle Z300). The whole process was repeated 4 times to enable full removal of any impurities. The sample was then dried at 100 °C overnight. The yield of copper iodate nanoparticles using this milling process was ~75%.

Preparation of the Bismuth Iodate and Iron Iodate Nanoparticles. Bismuth iodate ($Bi(IO_3)_3$) and iron iodate ($Fe(IO_3)_3$) nanoparticles were synthesized by a precipitation method. $Bi(IO_3)_3$ nanoparticles were synthesized by the following process: 485 mg bismuth nitrate pentahydrate ($Bi(NO_3)_3{\cdot}5H_2O$) was dissolved in 8 mL nitric acid solution (2 M), and 528 mg iodic acid (HIO_3) was dissolved in 8 mL deionized (DI) water. These were then mixed by dropwise addition of $Bi(NO_3)_3$ solution. The yield of bismuth iodate nanoparticles using this milling process was ~90%. $Fe(IO_3)_3$ nanoparticles were synthesized by mixing the $Fe(NO_3)_3$ solution and HIO_3 solution (1:3, by mole) at concentrations of 25 and 66 mg/mL, respectively. The obtained brown solution was kept at 100 °C overnight, and the subsequent yellow-green precipitate was collected and further washed and dried for characterization, with a yield of ~75%. Both of the $Bi(IO_3)_3$ and $Fe(IO_3)_3$ powders were handled with the same washing, centrifuging, drying, and breaking process as the $Cu(IO_3)_2$.

Preparation of the Physically Mixed Metal Iodate and Metal-Oxide-Based Composites. The traditional approach to create a nanocomposite thermite is by physical mixing. For example, to make the bismuth-iodate-based thermite, 160 mg $Bi(IO_3)_3$ powder was dispersed in 1.8 mL of ethanol and sonicated for 60 min. Then, 51 mg of aluminum nanoparticles (and 0.20 mL collodion for the case of added NC, from Fluka Corp.) is added and sonicated for another 60 min. The suspension was stirred for 24 h, and then allowed to air-dry in a hood. The dry powder was then gently broken to a fine powder. A similar procedure was employed for the other iodates, but the mass was adjusted to maintain a stoichiometry.

Electrospray Procedure. The electrospray assembly process is essentially as previously described in ref 22. For example to make the bismuth-iodate-based thermite 160 mg $Bi(IO_3)_3$ powder was dispersed in 1.8 mL of ethanol and sonicated for 60 min. To this was added 51 mg of aluminum nanoparticles (and 0.20 mL collodion for the case with NC), and the mixture was sonicated for another 60 min. Then, after stirring for 24 h, the suspension was ready to be electrosprayed. The electrospray system consisted of a syringe pump to feed the precursor at a constant speed of 4.5 mL/h, through a stainless steel 0.43 mm inner diameter needle. The distance between the needle and substrate was 10 cm, with an applied voltage of 19 kV.

SEM/EDS, TEM, and TGA/DSC. Scanning electron microscope (SEM) characterization was conducted with a Hitachi SU-70 instrument coupled to an energy dispersive spectrometer (EDX). Transmission electron microscope (TEM) analysis employed a JEOL 2100F field-emission instrument. Thermogravimetry/differential scanning calorimetry (TG/DSC) results were obtained with a TA Instruments Q600 at a rate of 10 °C/min up to a maximum temperature of 1000 °C in a nitrogen atmosphere.

Combustion Cell and Burning Products. The details of combustion cell experiment can be found in refs 5 and 34. A confined combustion cell with a constant volume (~13 cm^3) was used to measure the pressure and burn time of the samples. In this study, 25.0 mg of the loose thermite sample was placed inside a cell and was

DOI: 10.1021/acsami.5b04589
ACS Appl. Mater. Interfaces 2015, 7, 17363–17370

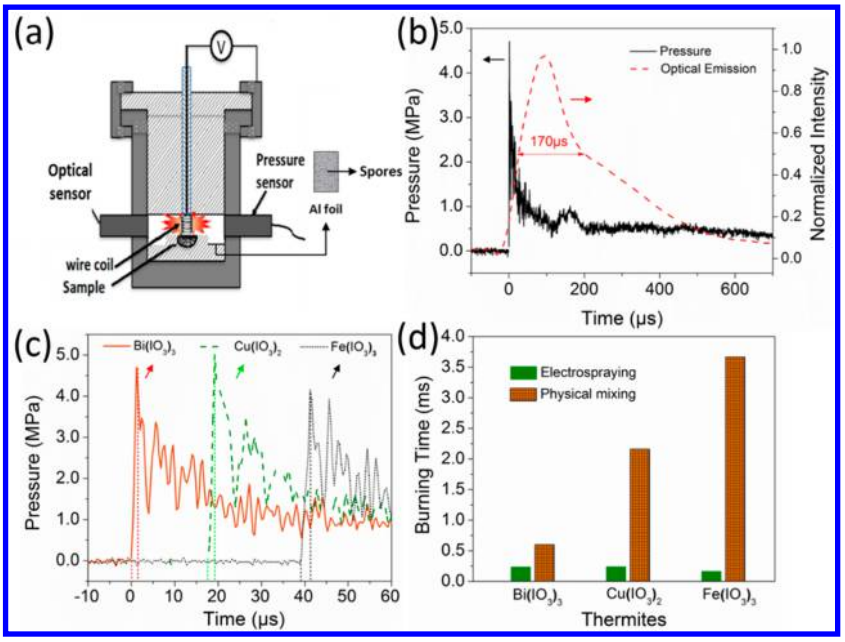

Figure 2. (a) Schematic of combustion cell. (b) Pressure and optical emission profiles of the Al/$Bi(IO_3)_3$ nanothermite composites. (c) Pressure profiles of the three metal-iodate-based thermites. (d) Burning times of metal-iodate-based nanothermite composites. Note: The pressure traces of $Cu(IO_3)_2$- and $Fe(IO_3)_3$-based thermites have been offset to the right, for better readability.

ignited by a nichrome coil on top of the loose powder. An attached piezoelectric pressure sensor (PCB) together with an in-line charge amplifier and signal conditioner were used to record the pressure history. The optical emission history was simultaneously collected by a lens tube assembly, containing a planoconvex lens (f = 50 mm) and a photodetector to collect the broadband emission. The burn time was defined as the peak width at half height of the optical emission.

T-Jump Ignition and Time-Resolved Mass Spectrometry Measurement. The details of the time-of-flight mass spec system used can be found in refs 5 and 33−35. In a typical experiment, a fine Pt wire (76 μm in diameter, 10 mm in length) was coated with a thin layer of sample (3−5 mm in length). An applied voltage of ∼24 V was put across the wire to rapidly heat to ∼1800 K at a heating rate of 5 × 10^5 K s^{-1}. The wire temperature can be calculated by determining the resistance changing with time. Time-resolved mass spectra were used for characterization of the species produced during the rapid heating. A Vision Research Phantom v12.0 digital camera was employed to capture the burning of the thermite in air. The resolution used was 256 × 256 pixels, and the frame rate used was 67 065 fps (14.9 μs per frame).

Spore Inactivation. The above combustion cell was employed as a container to evaluate the spore inactivation effectiveness of the samples. First, metal-iodate-based thermite was placed in the cell of the internal chamber in the combustion cell (Figure 2a). Aluminum foil was adopted as the substrate for *Bacillus thuringiensis* spores, a known surrogate for *Bacillus anthracis*. A 10 μL portion of spore solution (∼7 × 10^5/μL, ∼1.4 μg) was dripped onto the foil surface followed by spreading and drying. Aluminum foils deposited with or without spores were placed close to the wall of the chamber, ∼15 mm from thermite sample. After ignition, the combustion cell was kept closed for 30 min, following which the foils were extracted and sent for bacterial spore counting assay. Before the test, explosion-product-loaded control foils were deposited with the same amount of spores. Each foil was then immersed in 1 mL of fresh Lysogeny Broth (LB) medium and incubated at 37 °C for 3 h. Our preliminary test reveals that this time period is necessary for the initially immobile living spores to detach from the foil and germinate in the media, enabling us to measure the spore counts quantitatively later. Since the exact range of spore viability was unknown, a serial dilution was used. A 100 μL portion of the medium was extracted and diluted subsequently, with each dilution of a factor of 10. Then 10 μL of these diluted media with different bacteria concentrations were spread in parallel lines on an agar plate. Agar plates were kept overnight at room temperature prior to numeration of the colony forming units (CFUs) in each line. The final counts of spores in each sample were obtained statistically in terms of these serial CFUs. Each experiment was repeated in triplicate.

3. RESULTS AND DISCUSSION

3.1. Metal-Iodate-Based Thermite Synthesis and Assembly. In this work, micron-scale metal-iodate-based energetic composites were produced by electrospraying a precursor solution containing nanoscale components, comprising fuel (nano-Aluminum), the biocidal oxidizer (metal iodates), and a small quantity of energetic binder nitrocellulose. As shown in Figure 1a, because of the combined action of electrostatic forces and surface tension, the precursor suspension shatters into nearly monodiserse microsized droplets. Subsequent rapid evaporation of the solvent drives gelling process within the droplet until the aggregate particles jam, creating a porous structure. More details of the electrospray assembly technique can be found in our prior work.[22,36]

The metal iodate nanoparticles used in this study include bismuth iodate (∼90 nm), iron iodate (∼70 nm), and copper iodate (∼65 nm), which were prepared by either precipitation or milling (see Experimental Section and Supporting Information). For comparison purposes, physically mixed metal-iodate-based nanothermites were also prepared, and the SEM images can be found in Figure S9 in the Supporting Information.

Figure 1b−d shows typical SEM images of the three metal-iodate-based thermites. The obtained Al/$Bi(IO_3)_3$ (Figure 1b) composites have a size distribution of 3−5 μm, have a porous structure, and contain a well-dispersed mixture of the fuel and oxidizer nanoparticles. Al/$Cu(IO_3)_2$ composites have similar structure features and a relatively narrow size of 2−4 μm (Figure 1c), respectively, while the Al/$Fe(IO_3)_3$ composites

DOI: 10.1021/acsami.5b04589
ACS Appl. Mater. Interfaces 2015, 7, 17363−17370

(Figure 1d) were found to have a more open structure, with a larger size ranging from 5 to 7 μm.

3.2. Reactivity of Metal-Iodate-Based Nanothermite. The reactivity of nanothermite was assessed in a constant volume combustion cell (13 cm^3), from which the pressure history and optical emission during combustion can be obtained simultaneously. Figure 2a shows the schematic of the combustion cell, which is composed of a pressure sensor and an optical detector. Pressurization rates obtained from the pressure history data, which mimic the burning rate, are used to evaluate the reactivity. Burning times were also obtained by measuring the peak width at half-maximum (fwhm) of the optical emission trace.[5,37] Supporting Information Table S1 summarizes the combustion cell results for all the nanothermites in this study.

Figure 2b shows the pressure and optical-emission trace for Al/$Bi(IO_3)_3$ composites. The peak pressure and burning time are ~4.7 MPa and ~170 μs, respectively. The burning time is considerably longer than the corresponding pressure rise time, implying that decomposition of iodates occurs prior to the primary reaction of the thermite, suggesting that the thermite burning rate is limited by the aluminum fuel release, rather than oxidizer availability. The temporal pressure of the three metal-iodate-based nanothermites are shown in Figure 2c. All three pressure traces show a rapid rise, of ~1 μs, achieving a peak pressure of 4−5 MPa with the Cu > Bi > Fe.

For comparison, the reactivity of metal iodates thermite prepared by conventional physical mixing method was also evaluated. The pressurization rate results of metal-iodate-based thermites produced by two approaches were listed in Table 1.

Table 1. Peak Pressure, Pressurization Rate, and Burning Time of Metal-Iodate-Based Nanothermites Made by Electrospraying (ES) and Physical Mixing (PM)[a]

thermite	pressure (MPa)	pressurization (GPa/s)	burning time (μs)
ES Al/$Bi(IO_3)_3$	4.5	3816	235
PM Al/$Bi(IO_3)_3$	0.73	53	298
ES Al/$Cu(IO_3)_2$	4.9	3966	238
PM Al/$Cu(IO_3)_2$	0.14	0.07	2162
ES Al/$Fe(IO_3)_3$	4.0	3186	161
PM Al/$Fe(IO_3)_3$	0.17	0.10	3667

[a]All the composites contain 5% NC (by weight). 25.0 mg sample in each test.

The results show that the pressurization rate of electrosprayed Al/$Bi(IO_3)_3$ composites is approximately 2 orders of magnitude higher than the physical mixed thermites, while the Al/$Cu(IO_3)_2$ and Al/$Fe(IO_3)_3$ systems are more than 4 orders of magnitude higher, relative to the physically mixed thermites. The increase in reactivity of the electrosprayed sample can be attributed to the unique porous inner structure combined with energetic gas generator nitrocellulose which we have previously shown minimizes sintering among nanoparticles.[22]

Similar to what we have observed for Al/CuO composites,[22] the physically mixed $Bi(IO_3)_3$, $Cu(IO_3)_2$, and $Fe(IO_3)_3$ nanothermites have a much longer burning time than that of the corresponding electrosprayed nanothermites, as Figure 2d shows.

The reactivity difference between metal-iodate-based and metal oxide-based thermites was compared. The peak pressure and pressurization rate of the two thermites were simultaneously obtained, as listed in Table 2. The reactivity of the metal-iodate-based thermite is much higher than the reactivity of the corresponding metal-oxide-based thermite even though the size of metal iodate nanoparticles is larger. Specifically, the so-called weak thermite, Al/Fe_2O_3, has a pressure and pressurization rate of only 0.06 MPa and 0.02 GPa/s, respectively. While the corresponding iron-based iodate, Al/$Fe(IO_3)_3$, achieves 1.9 MPa and 590 GPa/s, as shown in Figure 3a. As discussed in our previous work,[38] Al/Fe_2O_3 nanothermite combustion pressure and optical emission signals appear concurrently (Figure 3b), and it has been suggested that oxidizer decomposition is the rate limited step. In contrast, Al/$Fe(IO_3)_3$ features a very rapid pressure increase followed by a prolonged optical emission profile, indicating the burning is rate limited by the aluminum fuel. These results show the advantages of using strong oxidizers, with rapid oxygen release kinetics in nanothermite formulations.

The adiabatic flame temperatures (AFT) of the three metal-iodate- and metal-oxide-based thermites have been calculated and are listed in Table 2. Since there are no experimental data for thermochemical properties of these metal iodates, the theoretical estimate results were adopted.[39] These results are then employed in the Cheetah code, assuming the sample is in the maximum density and the volume of the burning product is constant.[40,41] Generally, the flame temperatures of the three metal-iodate-based thermite reactions are roughly the same, ~4050 K, which is >1000 K higher than that of the corresponding metal-oxide-based thermites. The high reaction temperature can largely improve the potential biocidal performance for its additional thermal activities which can synergistically function with the released iodine.

To investigate the ignition mechanism, the nanothermite samples were coated on a Pt wire with a diameter of 76 μm and joule heated in air at a heating rate of 5×10^5 K s^{-1}, as schematically shown in Figure 4a. The Al/$Bi(IO_3)_3$ composites reveal a violent reaction, with an ignition temperature of 590 °C. The ignition temperatures of $Cu(IO_3)_2$-based and $Fe(IO_3)_3$-based nanothermites is 560 and 550 °C, respectively,

Table 2. Pressure Cell Results of Physically Mixed Nanothermites[a]

oxidizer	pressure (MPa)	pressurization (GPa/s)	burning time (μs)	AFT (K)	stoichiometric ratio
Bi_2O_3, 90−210 nm	1.0	54	240	2333	1.3
$Bi(IO_3)_3$, ~90 nm	2.3	770	150	4062	1.0
CuO, ~50 nm	1.1	100	220	3054	1.0
$Cu(IO_3)_2$, ~200 nm	1.8	225	170	4061	1.0
Fe_2O_3, ~50 nm	0.06	0.02	3330	3027	1.0
$Fe(IO_3)_3$, ~70 nm	1.9	590	170	4043	1.0

[a]Sample mass: 25.0 mg. All the composites contain no NC. The AFT of Al/Bi_2O_3 thermite is only 3031 K. (Because this was a fuel lean mixture, stoichiometric ratio = 1, to optimize pressurization rate.)

DOI: 10.1021/acsami.5b04589
ACS Appl. Mater. Interfaces 2015, 7, 17363−17370

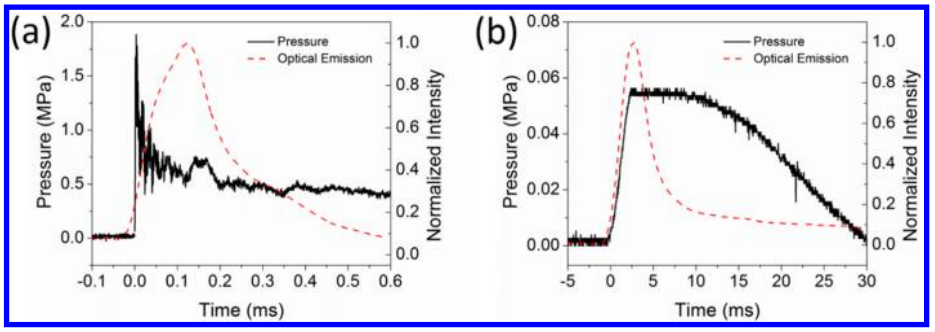

Figure 3. Pressure and optical emission profiles of (a) $Al/Fe(IO_3)_3$ and (b) Al/Fe_2O_3 nanothermite reactions.

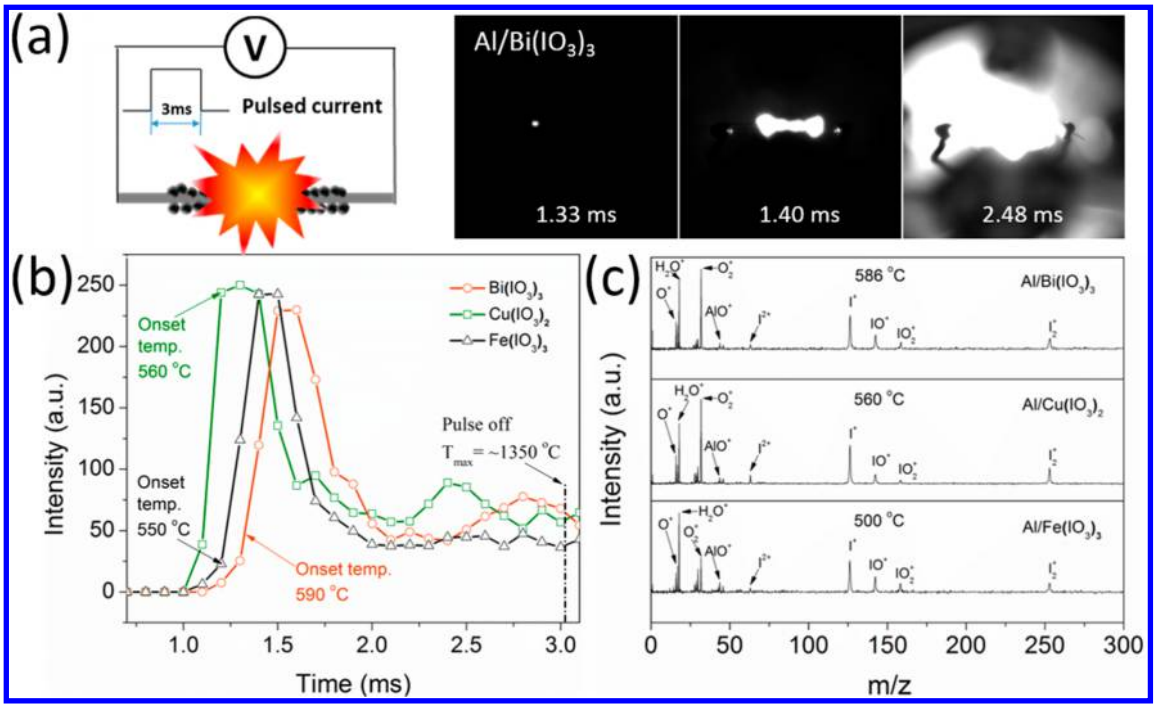

Figure 4. (a) T-Jump wire ignition method, and burning snapshots of $Al/Bi(IO_3)_3$ composites. (b) Temporal profile of oxygen release upon heating the three different metal iodates. (c) T-Jump TOFMS results for the $Bi(IO_3)_3$-based, $Cu(IO_3)_2$-based, and $Fe(IO_3)_3$-based thermite made by electrospray (5% NC, by weight). Note: The heating pulse time was 3.0 ms.

which is much lower than that of corresponding CuO-based (770 °C) and Fe_2O_3-based nanothermites (1140 °C). The low ignition temperature is indicative that the metal iodate salts release oxygen at a relatively low temperature.[5] To further confirm this, the wire within the extraction region of a mass spectrometer, i.e., T-jump/time-of-flight mass spectrum (T-Jump/TOFMS), was employed to investigate the oxygen release properties of the three metal iodates.[37]

Reactivity of a thermite can be evaluated by the explosion characterization parameters such as peak pressure, pressurization rate, and burn time in a confined container (Figure 2a). Especially, the pressurization rate is directly proportional to the burn rate of the thermite. In the previous work, it is found that the reactivity is closely related to its oxygen release behavior at high heating rates.[42] Figure 4b shows the temporal profile for oxygen from metal iodates in T-Jump/TOFMS, from which the oxygen release temperature can be obtained, and the oxygen release behavior of different oxidizers at high heating rates can be compared. It is found that the onset temperature of oxygen release for $Bi(IO_3)_3$, $Cu(IO_3)_2$, and $Fe(IO_3)_3$ nanoparticles is 490, 450, and 475 °C, respectively, and thus insensitive to structure. Interestingly, it is worth noting that while $Bi(IO_3)_3$ releases oxygen at 490 °C, and Bi_2O_3 releases gas phase oxygen at ~1350 °C, they both show a similar ignition temperature of ~590 °C.[43] The results imply that $Bi(IO_3)_3$ and Bi_2O_3 have different initiation mechanisms. For $Bi(IO_3)_3$, it is obvious that oxygen release from oxidizer contributes to the ignition of nanothermite, while its condensed phase appears to be the initiation mechanism for the Al/Bi_2O_3 nanothermite.

As Figure 4b shows, all of the oxygen release traces show a rapid rise. The oxygen release from $Cu(IO_3)_2$ initiates at 450 °C, and reaches it maximum in 0.20 ms, significantly outperforming the commercial CuO nanoparticles, whose rise time is 1.0 ms,[33] revealing its fast oxygen release kinetics at high heating rates. Oxygen release profiles of $Fe(IO_3)_3$ and $Bi(IO_3)_3$ nanoparticles are very similar to that of $Cu(IO_3)_3$, implying, not surprisingly, that all metal iodate nanoparticles release oxygen in a similar manner. It is worth noting that the decomposition of iodates occurs prior to the thermite ignition, suggesting that gas phase oxygen release is critical to ignition.

The metal-iodate-based nanothermites were also rapidly heated in the T-Jump/TOFMS to determine temporal

DOI: 10.1021/acsami.5b04589
ACS Appl. Mater. Interfaces 2015, 7, 17363−17370

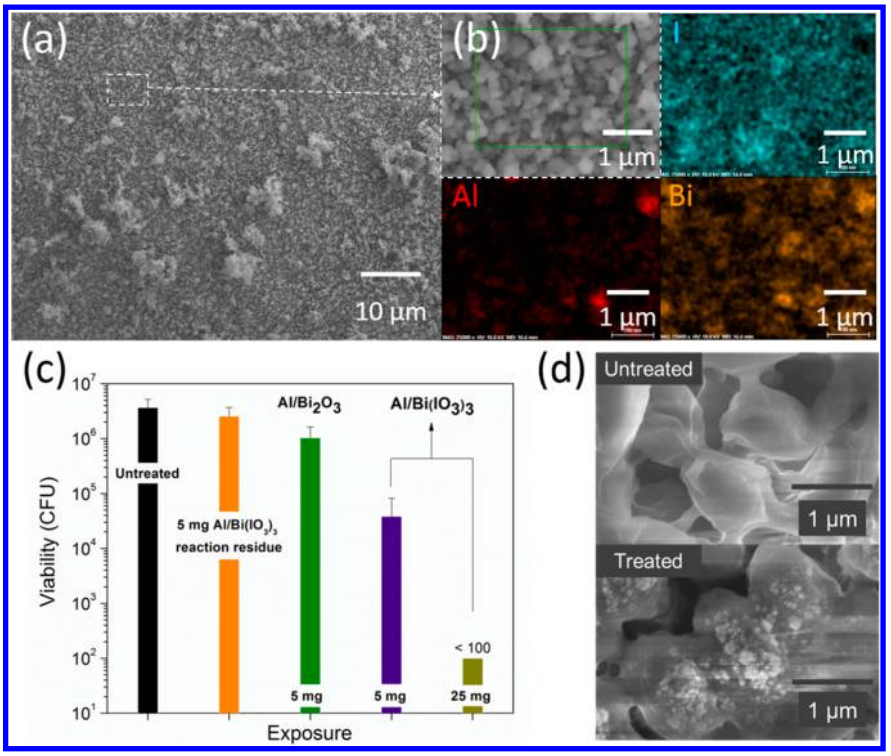

Figure 5. (a, b) SEM and energy dispersive X-ray spectroscopy (EDS) results of $Al/Bi(IO_3)_3$ thermite reaction products. (c) CFU counts from the spores treated by 5.0 mg $Al/Bi(IO_3)_3$ postcombustion products, 5.0 mg Al/Bi_2O_3 thermite reaction, and 5.0 mg and 25.0 mg $Al/Bi(IO_3)_3$ thermite reactions. (d) SEM images of spores before (top) and after (bottom) undergoing the $Al/Bi(IO_3)_3$ thermite reaction (5.0 mg). Note: all the composites are produced by electrospraying with 5% NC (by weight). The labeled numbers in part c are survival ratios of spores.

speciation. As shown in Figure 4c, iodine and oxygen species are detected in all three metal-iodate-based thermites reactions. The intensities of oxygen and iodine species, in all of the samples, reach their maximum values between 500 and 600 °C, revealing the major weight loss event happening during that period, and is consistent with TGA results (Supporting Information).

3.3. Sporicidal Performance. The ability of metal-iodate-based thermites to produce high heat, pressure, and iodine makes them ideal biocidal energetic materials with potential synergistic killing mechanisms. To test the sporicidal performance of metal iodate-based thermites, a spore inactivation experiment was conducted in the combustion cell (V = 13 cm^3, see Figure 2a). Aluminum foil coupons deposited with or without ~7×10^6 CFU *Bacillus thuringiensis* spores were placed within the combustion chamber around the wire coil that ignites the thermite reaction. The control experiment of $Al/Bi(IO_3)_3$ thermite reaction without spores shows that iodine was released after reaction and uniformly dispersed within the layer of postcombustion products (Figure 5a,b). By loading different quantities of $Al/Bi(IO_3)_3$ thermite in the combustion cell, the survival ratios of *Bacillus thurigiensis* spores on coupons were measured after the thermite reactions (Figure 5c). Spores exposed to 5.0 mg and 25.0 mg of thermite reaction products had a 2 log or a >4 log reduction in their viability (i.e., the ability to form bacterial colonies), respectively. Alternatively, similar tests by employing the reaction of 5.0 mg Al/Bi_2O_3 thermites show that the viability of spores decreased by 28%. The major difference of these two thermite systems is that iodate-based composites can generate free iodine through a thermite reaction, which has been widely confirmed as a biocidal agent. Therefore, except for the pressure and thermal stresses which were also generated from the combustion of Al/Bi_2O_3 thermites, the combustion of $Al/Bi(IO_3)_3$ thermites exposes spores to the additional biocidal stress of iodine. We estimated that the released iodine efficiently contributed to 27% loss of spore viability (28% − 1%), while the other effects from pressure, heat, and other reaction products such as Al_2O_3 and Bi contributed to the majority of the loss as confirmed by the result after the Al/Bi_2O_3 reaction (Figure 5c). Figure 5c shows that the postreaction products of Al_2O_3 and Bi induced viability reduction of spores by 30%, implying that the other heat and pressure stresses contributed to a 42% loss of spore viability (72% − 30%). Given that other reactions of metal iodate thermites ($Al/Bi(IO_3)_3$ and $Al/Cu(IO_3)_2$) also led to uniform iodine release (Supporting Information Figures S13 and S14) and demonstrate higher sporicidal capabilities compared with the corresponding oxide-based thermite reactions (Supporting Information Figure S15), it is proposed that the metal iodate thermite system can be recognized as an effective biocidal agent.

The SEM images of spores (Figure 5d) further demonstrate that fine particles were deposited on the spore surfaces after the 5.0 mg $Al/Bi(IO_3)_3$ thermite reaction. There is some precedent for cell death in the absence of morphological damage.[43] However, interestingly, there is no gross morphological change in the spores after the thermite reaction, suggesting that the thermite reaction has not compromised the spore structure, although the viability has been reduced by 2 orders of magnitude (Figure 5c). Previously, we have shown that, during rapid heating, spores maintained most of their viability until the spore coat was melted.[44] Herein, it is further found that, by applying iodine, the spores were killed before changing morphologies, indicating the superiority in efficacy of the

DOI: 10.1021/acsami.5b04589
ACS Appl. Mater. Interfaces 2015, 7, 17363−17370

$Bi(IO_3)_3$-based thermite complex in killing spores compared with simple rapid heating.

4. CONCLUSION

This work reports the formation of metal-iodate-based thermites which have superior performance as sporicidal agents. Three different metal iodate nanoparticles were synthesized and incorporated into energetic composites with nanoaluminum by electrospray or physical mixing, forming highly reactive nanothermites. We characterized the reactivity using combustion cell and fast-heating wire experiments. The pressure and pressurization rate of metal-iodate-based thermites are several times higher than the corresponding oxide-based thermites, and the reactivity could be further promoted by using the electrospray technique to assemble the metal-iodate-based thermites. The thermal decomposition properties of metal iodates, as well as the reaction mechanisms of the related thermites, were separately investigated by TGA/DSC, and TOF-MS. The results show that the metal iodates decompose into their corresponding metal oxide, oxygen, and iodine before the aluminothermic reaction takes place. The sporicidal performance of the metal-iodate-based thermites was also assessed, and the results showed that they outperform the corresponding metal-oxide-based thermites. The working mechanism was proposed as a synergistic effect of heat/pressure and iodine production from the highly reactive metal-iodate-based thermite reaction. This combination has a much higher sporicidal rate than the individual effect of either heat/pressure (from the metal-oxide-based thermite reaction) or iodine (from the burning residue of metal-iodate-based thermite reaction).

■ ASSOCIATED CONTENT

Supporting Information

Characterization of the three different metal iodates nanoparticles was shown, including SEM and TEM images, as well as thermal decomposition results. The SEM images of electrosprayed metal-oxide-based thermites and physically mixed metal-iodate-based thermites. The combustion cell results of all three kinds of metal-iodate-based thermites and corresponding metal-oxide-based thermites. The burning snapshots of $Al/Cu(IO_3)_2$ and $Al/Fe(IO_3)_3$ composites on the wire. The SEM images and EDS results of the postcombustion products from $Al/Cu(IO_3)_2$ and $Al/Fe(IO_3)_3$ composite thermite reaction. The Supporting Information is available free of charge on the ACS Publications website at DOI: 10.1021/acsami.5b04589.

■ AUTHOR INFORMATION

Corresponding Author

*Phone: 301-405-4311. E-mail: mrz@umd.edu.

Present Address

§Department of Safety Engineering, Nanjing University of Science and Technology, Nanjing, Jiangsu 210094, China.

Author Contributions

The manuscript was written through contributions of all authors. All authors have given approval to the final version of the manuscript.

Notes

The authors declare no competing financial interest.

■ ACKNOWLEDGMENTS

This work was supported by the Defense Threat Reduction Agency and the Army Research Office. We acknowledge the support of the Maryland Nanocenter and its NispLab. The NispLab is supported in part by the NSF as a MRSEC Shared Experimental Facility. H.-Y.W. is grateful for the financial support from China Scholarship Council.

■ REFERENCES

(1) Rossi, C.; Estéve, A.; Vashishta, P. Nanoscale Energetic Materials. *J. Phys. Chem. Solids* **2010**, *71*, 57−58.

(2) Weismiller, M. R.; Malchi, J. Y.; Lee, J. G.; Yetter, R. A.; Foley, T. J. Effects of Fuel and Oxidizer Particle Dimensions on the Propagation of Aluminum Containing Thermites. *Proc. Combust. Inst.* **2011**, *33*, 1989−1996.

(3) Moore, K.; Pantoya, M. L.; Son, S. F. Combustion Behaviors Resulting from Bimodal Aluminum Size Distributions in Thermites. *J. Propul. Power* **2007**, *23*, 181−185.

(4) Pantoya, M. L.; Granier, J. J. Combustion Behavior of Highly Energetic Thermites: Nano versus Micron Composites. *Propellants, Explos., Pyrotech.* **2005**, *30*, 53−62.

(5) Jian, G. Q.; Feng, J. Y.; Jacob, R. J.; Egan, G. C.; Zachariah, M. R. Super-reactive Nanoenergetic Gas Generators Based on Periodate Salts. *Angew. Chem., Int. Ed.* **2013**, *52*, 9743−9746.

(6) Granier, J. J.; Pantoya, M. L. Laser Ignition of Nanocomposite Thermites. *Combust. Flame* **2004**, *138*, 373−383.

(7) Blobaum, K. J.; Reiss, M. E.; Plitzko, J. M.; Weihs, T. P. Deposition and Characterization of a Self-propagating CuO_x/Al Thermite Reaction in a Multilayer Foil Geometry. *J. Appl. Phys.* **2003**, *94*, 2915−2922.

(8) Schoenitz, M.; Ward, T. S.; Dreizin, E. L. Fully dense Nano-Composite Energetic Powders Prepared by Arrested Reactive Milling. *Proc. Combust. Inst.* **2005**, *30*, 2071−2078.

(9) Blobaum, K. J.; Wagner, A. J.; Plitzko, J. M.; Van Heerden, D.; Fairbrother, D. H.; Weihs, T. P. Investigating the Reaction Path and Growth Kinetics in CuOx/Al Multilayer Foils. *J. Appl. Phys.* **2003**, *94*, 2923−2929.

(10) Petrantoni, M.; Rossi, C.; Salvagnac, L.; Conédéra, V.; Estève, A.; Tenailleau, C.; Alphonse, P.; Chabal, Y. J. Multilayered Al/CuO Thermite Formation by Reactive Magnetron Sputtering: Nano versus Micro. *J. Appl. Phys.* **2010**, *108*, 084323.

(11) Zhang, K.; Rossi, C.; Ardila Rodriguez, G. A. Development of a Nano-Al/CuO Based Energetic Material on Silicon Substrate. *Appl. Phys. Lett.* **2007**, *91*, 113117.

(12) Umbrajkar, S. M.; Seshadri, S.; Schoenitz, M.; Hoffmann, V. K.; Dreizin, E. L. Aluminum-Rich Al-MoO_3 Nanocomposite Powders Prepared by Arrested Reactive Milling. *J. Propul. Power* **2008**, *24*, 192−198.

(13) Ward, T. S.; Chen, W.; Schoenitz, M.; Dave, R. N.; Dreizin, E. L. A Study of Mechanical Alloying Processes Using Reactive Milling and Discrete Element Modeling. *Acta Mater.* **2005**, *53*, 2909−2918.

(14) Kim, S. H.; Zachariah, M. R. Enhancing the Rate of Energy Release from Nanoenergetic Materials by Electrostatically Enhanced Assembly. *Adv. Mater.* **2004**, *16*, 1821−1825.

(15) Tillotson, T. M.; Gash, A. E.; Simpson, R. L.; Hrubesh, L. W.; Satcher, J. H., Jr.; Poco, J. F. Nanostructured Energetic Materials Using Sol−Gel Methodologies. *J. Non-Cryst. Solids* **2001**, *285*, 338−345.

(16) Seo, H. S.; Kim, J. K.; Kim, J. W.; Kim, H. S.; Koo, K. K. Thermal Behavior of Al/MoO_3 Xerogel Nanocomposites. *J. Ind. Eng. Chem.* **2014**, *20*, 189−193.

(17) Rossi, C.; Zhang, K.; Esteve, D.; Alphonse, P.; Tailhades, P.; Vahlas, C. Nanoenergetic Materials for MEMS: a Review. *J. Microelectromech. Syst.* **2007**, *16*, 919−931.

(18) Subramanium, S.; Hasan, S.; Bhattacharya, S.; Gao, Y.; Apperson, S.; Hossain, M.; Shede, R. V.; Gangopadhyay, S.; Render, R.; Kapper, P.; Nicolich, S. Self-assembled Ordered Energetic Composites of CuO Nanorods and Nanowells and Al Nanoparticles with High Burn Rates. *Mater. Res. Soc. Symp. Proc.* **2005**, *896*, 9.

DOI: 10.1021/acsami.5b04589
ACS Appl. Mater. Interfaces 2015, 7, 17363−17370

(19) Shende, R.; Subramanian, S.; Hasan, S.; Apperson, S.; Thiruvengadathan, R.; Gangopadhyay, K.; Gangopadhyay, S.; Redner, P.; Kapoor, D.; Nicolich, S.; Balas, W. Nanoenergetic Composites of CuO Nanorods, Nanowires, and Al-Nanoparticles. *Propellants, Explos., Pyrotech.* **2008**, *33*, 122−130.
(20) Malchi, J. Y.; Foley, T. J.; Yetter, R. A. Electrostatically Self-assembled Nanocomposite Reactive Microspheres. *ACS Appl. Mater. Interfaces* **2009**, *1*, 2420−2423.
(21) Séverac, F.; Alphonse, P.; Estève, A.; Bancaud, A.; Rossi, C. High-Energy Al/CuO Nanocomposites Obtained by DNA-Directed Assembly. *Adv. Funct. Mater.* **2012**, *22*, 323−329.
(22) Wang, H. Y.; Jian, G. Q.; Egan, G. C.; Zachariah, M. R. Assembly and Reactive Properties of Al/CuO Based Nanothermite Microparticles. *Combust. Flame* **2014**, *161*, 2203−2208.
(23) Nicholson, W. L.; Munakata, N.; Horneck, G.; Melosh, H. J.; Setlow, P. Resistance of Bacillus Endospores to Extreme Terrestrial and Extraterrestrial Environments. *Microbiol. Mol. Biol. Rev.* **2000**, *64*, 548−572.
(24) Setlow, P. Spores of Bacillus Subtilis: their Resistance to and Killing by Radiation, Heat and Chemicals. *J. Appl. Microbiol.* **2006**, *101*, 514−525.
(25) Leggett, M. J.; McDonnell, G.; Denyer, S. P.; Setlow, P.; Maillard, J. Y. Bacterial Spore Structures and their Protective Role in Biocide Resistance. *J. Appl. Microbiol.* **2012**, *113*, 485−498.
(26) Johnson, C. E.; Higa, K. T. Presented at *MRS Meeting Iodine-Rich Biocidal Reactive Materials*, Boston, 25−30 (11, 2012).
(27) Mulamba, O.; Hunt, E. M.; Pantoya, M. L. Neutralizing Bacterial Spores Using Halogenated Energetic Reactions. *Biotechnol. Bioprocess Eng.* **2013**, *18*, 918−925.
(28) He, C.; Zhang, J.; Shreeve, J. M. Dense Iodine-Rich Compounds with Low Detonation Pressures as Biocidal Agents. *Chem. - Eur. J.* **2013**, *19*, 7503−7509.
(29) Fischer, D.; Klapotke, T.; Stierstorfer, J. R. Synthesis and Characterization of Guanidinium Difluoroiodate, $[C(NH2)-3]^{+}[IF2O2]^{-}$ and its Evaluation as an Ingredient in Agent Defeat Weapons. *Z. Anorg. Allg. Chem.* **2011**, *637*, 660−665.
(30) Aly, Y.; Zhang, S.; Schoenitz, M.; Hoffmann, V. K.; Dreizin, E. L.; Yermakov, M.; Indugula, R.; Grinshpun, S. A. Iodine-containing Aluminum-based Fuels for Inactivation of Bioaerosols. *Combust. Flame* **2014**, *161*, 303−310.
(31) Feng, J. Y.; Jian, G. Q.; Liu, Q.; Zachariah, M. R. Passivated Iodine Pentoxide Oxidizer for Potential Biocidal Nanoenergetic Applications. *ACS Appl. Mater. Interfaces* **2013**, *5*, 8875−8880.
(32) Sullivan, K. T.; Piekiel, N. W.; Chowdhury, S.; Wu, C.; Zachariah, M. R.; Johnson, C. E. Ignition and Combustion Characteristics of Nanoscale Al/$AgIO_3$: A Potential Energetic Biocidal System. *Combust. Sci. Technol.* **2010**, *183*, 285−302.
(33) Jian, G. Q.; Chowdhury, S.; Sullivan, K.; Zachariah, M. R. Nanothermite Reactions: Is Gas Phase Oxygen Generation from the Oxygen Carrier an Essential Prerequisite to Ignition? *Combust. Flame* **2013**, *160*, 432−437.
(34) Jian, G. Q.; Piekiel, N. W.; Zachariah, M. R. Time-resolved Mass Spectrometry of Nano-Al and Nano-Al/CuO Thermite under Rapid Heating: a Mechanistic Study. *J. Phys. Chem. C* **2012**, *116*, 26881−26887.
(35) Zhou, L.; Piekiel, N.; Chowdhury, S.; Zachariah, M. R. T-Jump/time-of-flight Mass Spectrometry for Time-Resolved Analysis of Energetic Materials. *Rapid Commun. Mass Spectrom.* **2009**, *23*, 194−202.
(36) Wang, H. Y.; Jian, G. Q.; Yan, S.; DeLisio, J. B.; Huang, C.; Zachariah, M. R. Electrospray Formation of Gelled Nano-Aluminum Microspheres with Superior Reactivity. *ACS Appl. Mater. Interfaces* **2013**, *5*, 6797−6801.
(37) Sullivan, K. T.; Piekiel, N. W.; Wu, C.; Chowdhury, S.; Kelly, S. T.; Hufnagel, T. C.; Fezzaa, K.; Zachariah, M. R. Reactive Sintering: an Important Component in the Combustion of Nanocomposite Thermites. *Combust. Flame* **2012**, *159*, 2−15.
(38) Sullivan, K.; Zachariah, M. R. Simultaneous Pressure and Optical Measurements of Nanoaluminum Thermites: Investigating the Reaction Mechanism. *J. Propul. Power* **2010**, *26*, 467−472.
(39) Jain, A.; Ong, S. P.; Hautier, G.; Chen, W.; Richards, W. D.; Dacek, S.; Cholia, S.; Gunter, D.; Skinner, D.; Ceder, G.; Persson, K. A. The Materials Project: A materials genome approach to accelerating materials innovation. *APL Mater.* **2013**, *1*, 011002.
(40) Howard, W. M.; Souers, P. C.; Vitello, P. A. *Cheetah 6.0 User Manual*; LLNL-SM-416166; Lawrence Livermore National Laboratory: Livermore, CA, 2010.
(41) Hobbs, M. L.; Baer, M. R.; McGee, B. C. JCZS: An Intermolecular Potential Database for Performing Accurate Detonation and Expansion Calculations. *Propellants, Explos., Pyrotech.* **1999**, *24*, 269−279.
(42) Zhou, L.; Piekiel, N. W.; Chowdhury, S.; Zachariah, M. R. Time-resolved Mass Spectrometry of the Exothermic Reaction between Nanoaluminum and Metal Oxides: the Role of Oxygen Release. *J. Phys. Chem. C* **2010**, *114*, 14269−14275.
(43) Davis, C. Enumeration of Probiotic Strains: Review of Culture Dependent and Alternative Techniques to Quantify Viable Bacteria. *J. Microbiol. Methods* **2014**, *103*, 9−17.
(44) Zhou, W. B.; Wu, M. O.; Watt, S. K.; Jian, G. Q.; Lee, V. T.; Zachariah, M. R. Inactivation of Bacterial Spores Subjected to Sub-second Thermal Stress. *Chem. Eng. J.* **2014**, *279*, 578−588.

DOI: 10.1021/acsami.5b04589
ACS Appl. Mater. Interfaces 2015, 7, 17363−17370

Synergistic Effects of Ultrafast Heating and Gaseous Chlorine on the Neutralization of Bacterial Spores

Wenbo Zhou [a], Mona W. Orr [b], Vincent T. Lee [b*], Michael R. Zachariah [a*]

[a] Department of Chemical and Biomolecular Engineering, and Department of Chemistry and Biochemistry, University of Maryland, College Park, MD 20742, USA

[b] Department of Cell Biology & Molecular Genetics, University of Maryland, College Park, MD 20742, USA

[*] Corresponding authors:

Department of Chemical and Biomolecular Engineering, and Department of Chemistry and Biochemistry, University of Maryland, College Park, MD 20742, USA.

Tel: +1 301 405 4311.

E-mail address: mrz@umd.edu (M.R. Zachariah).

Department of Cell Biology & Molecular Genetics, University of Maryland, College Park, MD 20742, USA.

Tel: +1 301 405 9397; fax: +1 301 314 1248.

E-mail address: vtlee@umd.edu (V.T. Lee).

ABSTRACT

Improving the neutralization of bacterial spores is important in a variety of clinical, industrial, and biodefense applications. In this study, we investigate the synergism between rapid heating (~10^4 ˚C/s to ~10^5 ˚C/s) and chlorine gas in the neutralization of *Bacillus thuringiensis* (Bt) spores – a close relative of *B. anthracis* (Ba), which is a known biowarfare agent. Bt spores were heated in a gas chamber with defined concentrations of Cl_2 gas and relative humidity (RH). The critical peak temperature (T_c) of spores, which corresponds to 50% reduction in viability, was decreased from 405 ˚C when heated at ~10^4 ˚C/s in air to 250 ˚C when heated at the same rate in 100 ppm Cl_2. SEM results show no obvious difference between the morphologies of spores heated in air or in Cl_2 at ~10^4 ˚C/s. These results indicate that Cl_2 gas acts in synergy with high temperatures (>300 ˚C) to neutralize Bt spores. Similarly, the T_c for Bt spores heated at the faster rate of ~10^5 ˚C/s was reduced from 230 ˚C when heated in air to 175˚C when heated in 100 ppm Cl_2. At temperatures below 300 ˚C, Cl_2 treatment did not alter spore morphology. At temperatures above 450 ˚C with Cl_2, the spore coat detached from the underlying core. The effect of Cl_2 was further examined by changing the RH of Cl_2 gas. The results show that highly humidified Cl_2 (RH = 100%) reduced T_c by 170 ˚C and 70 ˚C at ~10^4 ˚C/s and ~10^5 ˚C/s, respectively, as compared to dry Cl_2 (RH = 0%). Energy dispersive spectrometric (EDS) results demonstrate that Cl_2 on the spore increased with elevated peak temperature, with the majority of the Cl located in the shed spore coat. This study indicates that the major mechanism of spore neutralization by the synergism of Cl_2 and rapid heat is chlorine reacting with the spore surface.

KEYWORDS

Bacterial spores; Neutralization; Ultrafast heating; Chlorine; Hydrogen Chloride

1. Introduction

Bacterial spores are importance since they pose a risk to public health and military biodefense [1-3]. Neutralization of spores is a significant challenge since they are much more resistant than their vegetative counterparts to a variety of external stresses such as UV irradiation, extreme pH values, chemicals, and temperature extremes [4-6]. Studies have shown that spore longevity and resilience is correlated to physical features of spores, including a tight proteinaceous spore coat that inhibits chemicals penetration, low water content in the spore core to reduce metabolism, as well as the production of proteins for DNA stabilization (e.g. α/β-type small acid soluble proteins (SASPs)) [6]. One of the primary strategies for spore neutralization is to expose them to autoclaving heat (120-150 ˚C) for minutes to hours [7-9]; however, this approach is not appropriate for the large-scale neutralization of spores. To further improve the killing efficacy, aerosol based techniques are being developed to rapidly inactivate airborne bacterial spores by rapid heating (>200 ˚C within a timescale of a second) [10-16]. At this timescale, more than 3-logs reduction in spore population can be achieved when the peak temperature ranges from 200 to 400 ˚C. An analogous approach of spore inactivation by heat has been tested using heat generated from exothermic reactions of energetic materials such as aluminum-based thermites [17]. This approach is able to produce even higher peak temperatures (> 2200 ˚C) over a shorter period (~0.1 s), and leads to a 7-log reduction of spore viability. Although these methods are capable of neutralize spores, an accurate and quantitative relationship of time-temperature-kill for spores is not available due to the variability in temperature distribution and the resident exposure time of these heating schemes. Nevertheless, a precise time-temperature-kill relationship is needed for predicting and ensuring a successful outcome of large-scale neutralization events. In order to improve the accuracy of measurements of the temperature

history on spores, an alternative approach has been developed by heating spores deposited on conductive surfaces [18] that allows measurement of the transient temperature using the standard electric resistance-temperature relationships [18]. Since the transient temperature of immobilized spores can approximate that on the immobilizing surface [19], the time-temperature-kill relationship for spores can be accurately measured. Results showed that a 6-log reduction in spore counts could be achieved by rapidly heating spores to 600 ˚C within 50 ms at a heating rate of ~10^4 ˚C/s. The neutralization mechanism was likely due to DNA damage as mutants in *sspA sspB* are sensitized for killing [14]. Faster heating rates (~10^5 ˚C/s) also improved spore neutralization, which was associated with increased structural destruction of spore coat through increased pressure of vaporization [19].

In addition to heat, another commonly used disinfection procedure for spores utilizes biocidal chemicals [20]. Commonly used biocides (antibiotics, detergents, alcohol) have little effect on spore viability [21]. In contrast, strong oxidation agents, such as chlorine, iodine, sulfur, silver, and compounds containing these elements, have demonstrated efficacy in spore inactivation [20]. Among these spore sterilants, Cl_2 is one of the few agents that is gaseous at room temperature. The main advantage of Cl_2 over other aqueous sterilants is that gas provides greater coverage, thus facilitating the neutralization of both airborne and surface-associated spores. Cl_2 can directly chlonrinate functional groups on macromolecules in cells to damage proteins, nucleic acids and lipids [22,23]. In addition, Cl_2 can react with water to form hypochlorous acid (HOCl) and hydrogen chloride (HCl). Both compounds can also react with the spore to inactivate them [24][25].

The performance criteria of Cl_2 depends on two characteristic factors: concentration ("C") and inactivation time ("T"). The US Enivronmental Protection Agency and the water treatment industry has set the units of Cl_2 concentration in parts per million (ppm) and the inactivation time in minutes [26]. In general, the "CT" product is a constant for spores of a specific *Bacillus* strain required to achieve a defined reduction of viability [27]. Table 1S presents some documented "CT" results for different *Bacillus* spores [24, 26-38]. The "CT" product for a 4-log reduction in spore viability is ~3×10^4 ppm·min (~100 mg·min/l) for most of *Bacillus* spores when the Cl_2 concentration is below 3×10^3 ppm [26-30]. At much higher Cl_2 concentrations (*e.g.* 7×10^6 ppm), this "CT" value is significantly larger than ~3×10^4 ppm·min, and the minimum exposure time is 5 min [24, 31, 32]. In order to improve the neutralization efficiency at exposure times under a second, which according to the "CT" rule would require concentrations of Cl_2 >10^8 ppm (close to that of pure Cl_2 liquid). The use of these concentrations of Cl_2 would be impractical as a method to safely neutralize spores [39]. To meet the guidelines set by the U.S. Food and Drug Administration (FDA) for food and drinking water processing (Code of Federal Regulations Title 21 Part 173/178) [40, 41], new approaches are in development to combine heat with 100 - 2000 ppm Cl_2.

One such potent, more environment-friendly and safer approach is to synergize the neutralization of spores by Cl_2 with heat. Xu et al. [42] studied the inactivation of *Bacillus* spores by Cl_2 (~1000 ppm) under high-temperature short-time pasteurization conditions (~80 ˚C, ~1min), and found a viability reduction of 6-logs. Further tests using a higher temperature of 120 ˚C resulted in inactivation of spores by 6-logs within 16s, whereas it took >30 mins to achieve viability reduction of 6-logs by employing either Cl_2 gas (1000 ppm) (Table S1) or heat (120 ˚C)

[7-9]. Based on these results, higher temperatures (>200 ˚C), and diluted Cl_2 gas (< 2000 ppm) synergistically inactivated Ba spores.

In this work, we investigated the synergistic effects of ultrafast heating and Cl_2 gas on the inactivation of Bt spores. Bt spores, while closely related to *Bacillus anthracis* (Ba) spores that are considered as a serious bioterrorist weapon, is not pathogenic to humans. Both Bt and Ba spores were reported to have similar sensitivity to biocides [43], so we expect the results in this study can be utilized for the neutralization of Ba spores in the future. For these studies, Bt spores were electrophoretically deposited onto a fine Pt wire [19]. By tuning the heat pulse time (2 ms and 50 ms) and peak temperature (~1200 ˚C) for the Pt wire, the heating rate (~10^4 ˚C/s and ~10^5 ˚C/s) and time-resolved temperature for individual spores were measured [19]. Using this thermal approach, we evaluated the effect of 100 ppm (0.3 mg/l) Cl_2, a concentration below the FDA safety guidelines, in combination with different peak temperatures and heating rates, on the neutralization of spores. Spore viability and morphology were assessed after these treatments by determining the viable number of colony forming units (CFU) and scanning electron microscopy (SEM). To investigate the neutralization mechanism of Cl_2, spores were also heated in Cl_2 gas with different relative humidities, to see the roles of the hydrolysis products of Cl_2 (hydrogen chloride (HCl) and hypochlorous acid (HOCl)). Energy dispersive X-ray spectroscopy (EDS) was employed to determine the elemental changes of Cl and carbon (C) in spores.

2. Materials and methods

2.1. Spore attachment on platinum wires

Bt spores were sporulated in Difco Sporulation Medium (DSM) at 30 ˚C for 48 h. The 250 ml of DSM included 2 g Bacto nutrient broth, 2.5 ml 10% KCl, 0.375 ml 1 M NaOH and 2.5 ml 1.2% $MgSO_4 \cdot 7H_2O$. The spore concentration was enumerated by plating to be 8×10^9 colony-forming units per milliliter (CFU/ml). The purity of spores was found more than 99%. Bt spores were electrophoretically immobilized onto a sterilized platinum (Pt) wire with a diameter of 76.8 μm (Omega Engineering, Inc.). The electroplating experiments were conducted in an in-house spore deposition cell [44]. By controlling the biased deposition voltage, pulse frequency and overall charging time (from a 6340 sub-femtoamp remote sourcemeter, Keithley), we are able to prepare a uniform monolayer of Bt spores on the wire after 5 pulses [44]. More information of the spore deposition cell and spore coating scenarios in detail can be found in our previous studies [19, 44].

2.2. Wire heating test in Cl_2 gas filled chamber

The spore coated wire was connected to an in-house built power source, working as a temperature jump probe (Fig. S1). The wire was then inserted into a gas chamber that is connected to a vacuum pump and a Cl_2 gas tank (Fig. S1). Prior to the pulse heating of the wire, the chamber was emptied by vacuum and replenish with the appropriate concentrations of Cl_2 gas. For evaluating the effect of relative humidity (RH) of Cl_2 gas, the chamber is also connected to a water bubbler that can supply water vapor into the chamber. RH was monitored using an attached humidity meter. A defined thermal history for spores on wire during the heating period was measured through the dynamic electric resistance-temperature relationship for Pt (Callendar-Van Dusen equation [18]). The peak temperature (~200 ˚C to ~700 ˚C) and the heating rate (~10^4

˚C/s to ~10^5 ˚C/s) can be precisely controlled by tuning the applied voltage and the pulse time (2 ms to 50 ms). The temperature-time profile for spores in the cooled region was calculated according to an energy balance equation which was dominated by the heat conduction. It is estimated that the cooling time scale is between ~300 ms and ~500 ms [19]. The detailed description of the transient temperature measurement on spores can be found in our previous study [19].

2.3. Determination of colony forming units

The viable spores after various heat and Cl_2 treatments were enumerated by determining CFUs. Spore-coated wires were completely submerged in 1 ml of Lysogeny Broth (LB) media (10 g tryptone, 5 g yeast extract and 5 g NaCl per liter) and placed on a shaker at the 37 ˚C for three hours to allow for the germination and detachment of viable spores from the wire surface. After incubation, samples were serially diluted and plated on LB agar plates to count viable CFUs.

2.4. Characterization of morphology of spores

The surface morphology of spores with or without treatment of Cl_2 and rapid heat was investigated by SEM (Hitachi S-4700) using an accelerating voltage of 5 kV. Prior to imaging, the spore-coated wire was attached to stubs and then sputtered with gold/palladium alloy.

2.5. Characterization of hydrocarbon and chlorine contents inside spores

171 Quantitative EDS X-ray microanalysis using SEM was employed to analyze the elemental
172 contents (carbon, chlorine and calcium) inside spores. Since calcium will not escape from spores
173 by evaporation (boiling point at ~1500 ˚C) during the rapid heating in our temperature regimen
174 (<700 ˚C), the detected calcium content was used as a control to measure the relative Cl and C
175 contents. The tests were conducted in the line scan mode by detecting the elemental intensity
176 along a line drawn across one spore. The ratio of mass fractions of Cl/Ca or C/Ca was calculated
177 by comparing the integrated intensities of Cl/Ca or C/Ca along the line, respectively. For spores
178 with their coats detached, a line was across either the cracked coat or the exposed core, to
179 analyze the distribution of elemental masses in both compartments. Statistical analyses are based
180 on a spore population of ~10.

181

182 **3. Results and discussion**

183 *3.1. Spore viability heated at two ramp rates in air and in Cl_2*

184 The neat effect of fast heating on the viability of Bt spores in air was determined and the
185 relationship between peak temperature and spore viability was plotted in Fig. 1. The viability
186 data fit a sigmoidal model [45] as:

187 $$S = \frac{1}{1 + \exp(k(T - T_c))} \quad (1)$$

188 where S is the survival ratio of spores (CFU_{final} / $CFU_{initial}$), T is the peak temperature, T_c is the
189 critical peak temperature to induce viability reduction by half, and k is the heat resistance
190 parameter. The fitted values of T_c and k are listed in Table 1. Compared to T_c (405 ˚C) at the

191 temperature rate of ~10^4 ˚C/s, T_c at ~10^5 ˚C/s decreases to 230 ˚C. In addition, a reduction of 6-
192 logs was achieved at the peak temperatures of 400 ˚C and 600 ˚C at ~10^5 ˚C/s and ~10^4 ˚C/s,
193 respectively. These neutralization data for Bt spores resemble those for Bs spores in our previous
194 studies [19], indicating that the faster heating rate of ~10^5 ˚C/s is able to effectively decrease the
195 peak temperature required for spore neutralization when compared to the heating rate of ~10^4
196 ˚C/s. In addition, the *k* value of the neutralization curve at the higher heating rate (~10^5 ˚C/s) was
197 larger than that at the lower heating rate (~10^4 ˚C/s), indicating that Bt spores are more sensitive
198 to higher heating rates. These results show a better neutralization effect for Bt spores by higher
199 heating rates and higher peak temperatures.

200 The effect of Cl_2 gas and rapid heat was evaluated for their ability to synergistically neutralize
201 Bt spores. The resistance of Bt spores to Cl_2 gas at room temperature was first assessed. After 15
202 minutes of exposure, spore viability was not affected when exposed to 1 ppm (0.003 mg/l) to 100
203 ppm (0.3 mg/l) of Cl_2 (Fig. S2), whereas spores were completely neutralized by 1000 ppm of Cl_2.
204 We used 100 ppm of Cl_2 for the rest of this study since this concentration did not neutralize Bt
205 spores in the absence of heat and is within the FDA guidelines (200 – 2000 ppm) [41, 42].
206 Heating to 250 ˚C at 10^4 ˚C/s, and 170 ˚C at 10^5 ˚C/s (Fig. 1) reduced spore viability. Compared
207 to the viability results by heat treatment alone, the critical peak temperatures T_c decrease by 150
208 ˚C and 50 ˚C at heating rates of 10^4 ˚C/s and 10^5 ˚C/s, respectively (Table 1). In addition, a 6-log
209 viability reduction was achieved at lower temperatures of 300 ˚C at 10^5 ˚C/s, and 450 ˚C at 10^4
210 ˚C/s. These results show a synergistic effect of rapid heat pulses and Cl_2 gas in the neutralization
211 of Bt spores in both heating schemes. It should be noted that the *k* values for the neutralization
212 curves of spores treated with Cl_2 and without Cl_2 are similar at the same heating rate (> 0.1 for 50

ms pulse and < 0.1 for 2 ms pulse), indicating that the temperature sensitivity of spore neutralization is primarily controlled by the heating rate instead of the addition of Cl_2.

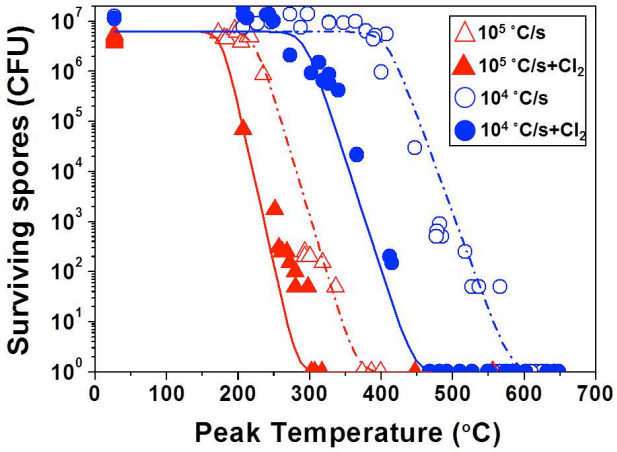

Fig. 1. *Survival curves of Bt spores versus peak temperature for 2 ms (10^5 °C/s) and 50 ms (10^4 °C/s) heat pulses, and with or without the presence of Cl_2 (100 ppm). The relative humidity was kept at 40%.*

Table 1.
Fitting results for the variables in Eq. 1.

Heating conditions	Cl_2 (+, -)	RH	k (°C^{-1})	T_c (°C)
50 ms heating pulse (~10^4 °C/s)	-	40%	0.090	407
50 ms heating pulse (~10^4 °C/s)	+	40%	0.065	252
50 ms heating pulse (~10^4 °C/s)	+	0%	0.065	352
50 ms heating pulse (~10^4 °C/s)	+	100%	0.083	180
2 ms heating pulse (~10^5 °C/s)	-	40%	0.109	232
2 ms heating pulse (~10^5 °C/s)	+	40%	0.146	176
2 ms heating pulse (~10^5 °C/s)	+	0%	0.136	247

2 ms heating pulse (~10^5 ˚C/s)	+	100%	0.131	177

222 Note: "+" represents the presence of Cl_2 during heating of spores, while "-" represents no Cl_2 during heating of spores.

223

224 *3.2. Spore viability heated in Cl_2 gas of different RH at two ramp rates*

225 To understand the mechanism of spore inactivation by Cl_2, different humidities were
226 supplemented to the 100 ppm of Cl_2 in the gas chamber used for heat inactivation of Bt spores.
227 The gas chamber for the results described in Section 3.1 has a relative humidity of ~40%, similar
228 to that of ambient air. At ~10^4 ˚C/s, the critical peak temperature for spores heated in dry Cl_2 (0%
229 RH) is 100 ˚C higher than that in moderately humidified Cl_2 (40% RH), whereas the critical peak
230 temperature for spores heated in moist Cl_2 (100% RH) is 70 ˚C lower (Table 1). These results
231 show that the T_c is reduced as the humidity of Cl_2 increases indicating that the synergistic effect
232 of Cl_2 and rapid heat is potentiated by high humidity.

233 When the heating rate for Bt spores increases to ~10^5 ˚C/s, T_c increased for Bt spores treated
234 with dry Cl_2 (0% RH) (Fig. 2B), similar to spores heated at ~10^4 ˚C/s heating rate (Fig. 2A). In
235 contrast, moderately humidified Cl_2 (40% RH), and moist Cl_2 (100% RH) resulted in similar T_c,
236 176 ˚C and 177 ˚C, respectively (Table 1). These ~10^5 ˚C/s results are distinct from those at ~10^4
237 ˚C/s since there is minimal change of spore neutralization when RH of Cl_2 increases from 40% to
238 100% (Fig. 2B). Thus, the synergistic effect of Cl_2 in different humidities at 10^5 ˚C/s is reduced
239 as compared to the lower heating rates of ~10^4 ˚C/s. The reduction in the effect of humidity can
240 be in part attributed to the reduced change in T_c (~60 ˚C) for spores heated in air and in Cl_2 at
241 ~10^5 ˚C/s, which is much smaller than that (~160 ˚C) at ~10^4 ˚C/s (Fig. 1 and Table 1). To

evaluate the heating-rate-dependent synergistic effects of Cl_2, we assessed the changes to Bt spore morphology and composition in response to Cl_2 and rapid heat.

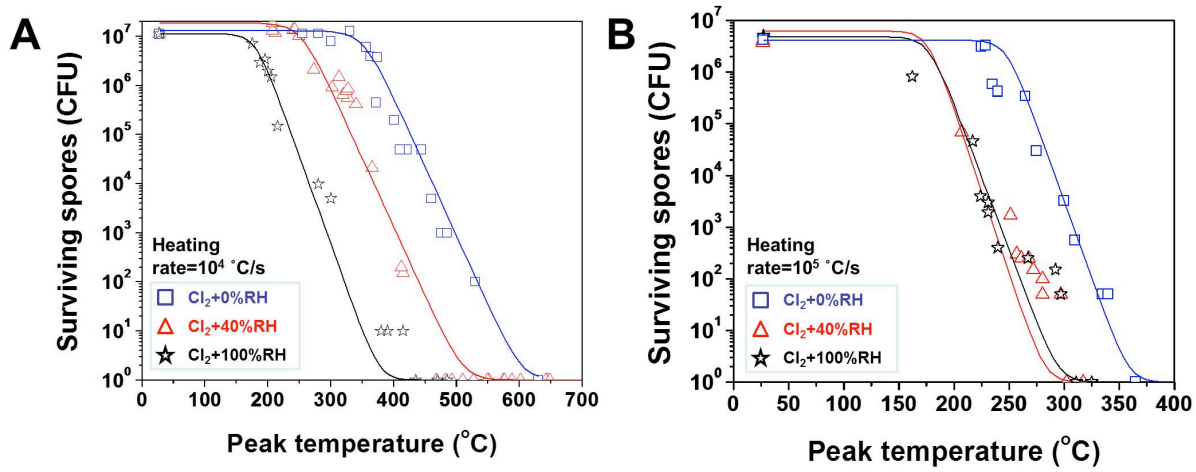

Fig. 2. *Survival curves of Bt spores versus peak temperature for 50 ms (10^4 °C/s) (A) and 2 ms (10^5 °C/s) (B) heat pulses. The blue, red, and black curves fit the survival of spores in response to Cl_2 and heat at 0%, 40%, and 100% relative humidities.*

3.3. Spore morphology after treatment of rapid heat and Cl_2 gas

Cl_2 vapors in the chamber surround the immobilized spores and is in contact with the surface of the spores. The effect of Cl_2 and heat on Bt spores was assessed by scanning electron microscopy (SEM). The unheated spores had a general dimension of 1.5 μm (longitudinal) times 1.0 μm (transversal) with wrinkly protrusions along their surfaces (Fig. 3A and Fig. S2B). In the absence of heat, treatment with Cl_2 gas up to 1000 ppm, which was sufficient to completely inactivate Bt spores, did not alter spore morphology (Fig. S2C). The relationship between spore morphology and peak temperature was investigated first for Bt spores exposed to the higher heating rates (~10^5 °C/s). The spore coat remains unaffected when heated to a peak temperature

of 200 ˚C at ~10^5 ˚C/s (Fig. 3B). When heated to 300 ˚C at ~10^5 ˚C/s, the spore surface started to melt and the surface protrusions were reduced (Fig. 3C). Further increases in the peak temperature to ~400 ˚C at ~10^5 ˚C/s caused the surfaces of Bt spores to melt (Fig. 3D). At higher peak temperatures of >450 ˚C, the surface coat was completely melted and only the underlying core remains (Fig. 3E and 3F). When 100 ppm Cl_2 was used, Bt spores were morphological indistinguishable from the spores treated by heat alone when the peak temperature is below ~400 ˚C (Fig. 3G-3I and Fig. 3A-3C). However, a distinct morphology emerged after ~400 ˚C when additional surface cracks were formed and the spore coat were detached from the underlying core (Fig. 3J-3K) in contrast to the spore coat melting in the absence of Cl_2. The disintegration of spore coat was further deteriorated when the humidity of Cl_2 increased to 100% at 400 ˚C (Fig. S3), suggesting that the effect of Cl_2 on the destruction of spore coat is associated with RH. Together these results indicate that Cl_2 acts on the surface of the spore to alter the fluidity of the spore coat.

The SEM images of Bt spores at a lower ramp rate of ~10^4 ˚C/s revealed similar morphological changes (Fig. 4A-4D) as that at a higher ramp rate of ~10^4 ˚C/s (Fig. 3A-3D). Bt spores started to melt at the peak temperature of ~300 ˚C, and completely melted at the peak temperature of ~400 ˚C. The addition of Cl_2 did not alter Bt spore morphology (Fig. 4E-4H) compared to the effect of heat alone (Fig. 4A-4D). These results indicate that the morphological changes were determined by peak temperatures at ~10^4 ˚C/s.

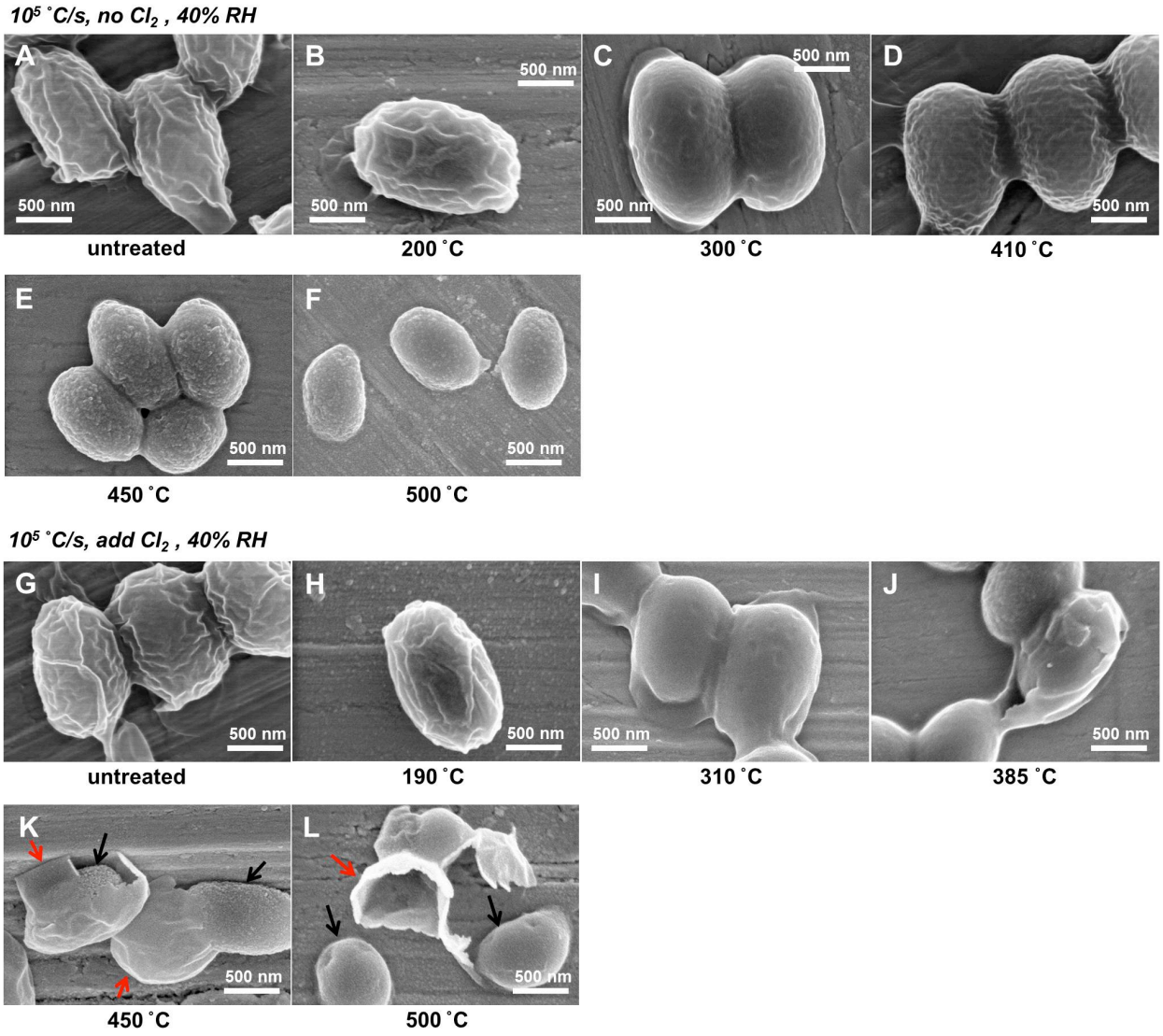

278

279 ***Fig. 3.*** *Spore morphologies when heated to different peak temperatures at 10^5 ˚C/s without (A-F)*
280 *or with (G-L) the presence of Cl_2. The relative humidity was kept at 40%. The red arrows and the*
281 *black arrows in image 4K and 4L designate detached spore coats and exposed inner spore*
282 *structures, respectively.*

283

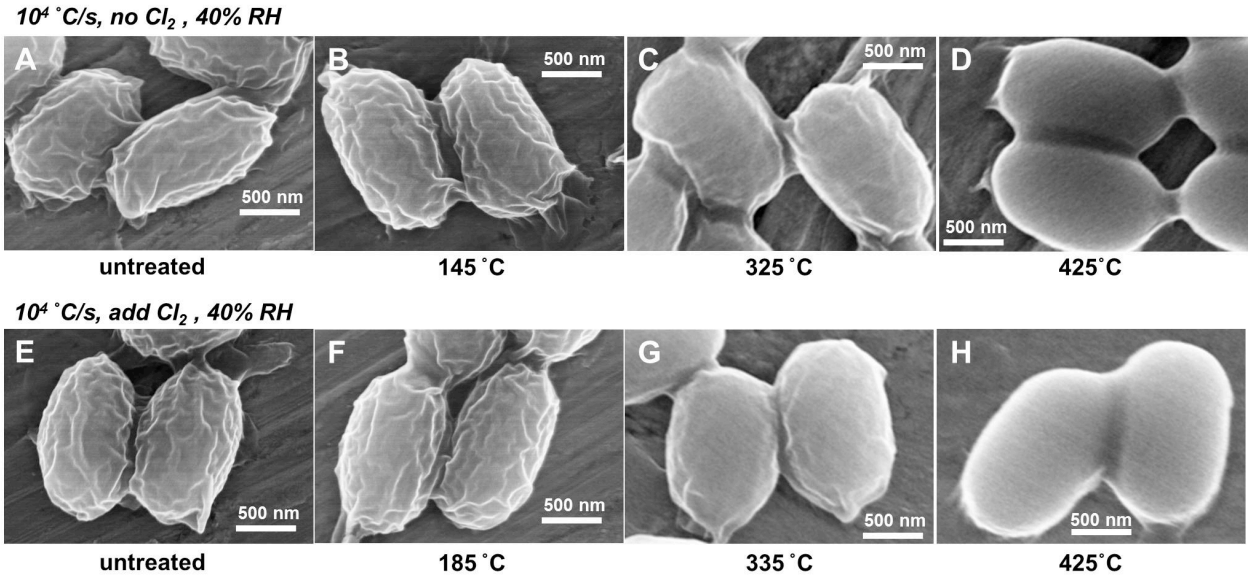

Fig. 4. *Spore morphologies when heated to different peak temperatures at 10^4 ˚C/s without (A-D) or with (E-H) the presence of Cl_2. The relative humidity is was kept at 40%.*

3.4. Changes in C and Cl contents inside Bt spores exposed to rapid heat and Cl_2

To evaluate the effect of Cl_2 on spores, the mass fractions of chlorine (Cl) and carbon (C) within spores treated by different heating schemes were measured using EDS. Calcium was used in these experiments as a standard since the calcium content inside spores will not change within our experimental temperature range (< 700 ˚C) (Fig. 5). The Cl content of the spores exposed to Cl_2 at room temperature was low indicating that Cl_2 gas does not react readily with the spores at ambient temperatures. The Cl content was increased as the peak temperature rose at ~10^4 ˚C/s, with the mass concentration of Cl for spores heated to 400 ˚C ~50 folds higher than that at room temperature. At the higher ramp rate of ~10^5 ˚C/s, a similar trend of increased Cl content was observed for spores exposed to higher peak temperature. At each temperature, the Cl content of spores exposed to ~10^5 ˚C/s heating rate was higher than spores exposed to the ~10^4 ˚C/s heating

299 rate (Fig. 5B). These results demonstrate that both heat and heating rate enhance the reaction of
300 Cl_2 with the spores. To determine the location on the spore that is reacting with Cl_2, we took
301 advantage of the SEM observation that the spore coat detaches from the core when heated to 500
302 °C at ~10^5 °C/s heating rate in the presence of Cl_2. EDS of the detached spore coat revealed that
303 there is a Cl/Ca ratio of 0.335 as compared to 0.005 Cl/Ca ratio in the core (Fig 5B). The 70-fold
304 increase in Cl concentration in the spore coat indicates that Cl_2 is reacting primarily with the
305 surface of the spores during the rapid heating event.
306 Since SEM images reveal that the spores disintegrated at high temperatures, the carbon content
307 within spores was evaluated. Spores heated either in air or in Cl_2 at ~10^4 °C/s did not lose carbon
308 content (Fig. 5C). Given that the spore coat was not completely melted until 400 °C (Fig. 4), this
309 result shows that the intact spore surface inhibits the release of volatile carbons. When rapidly
310 heated at ~10^5 °C/s, the C content in spores decreased starting at 300 °C and 400 °C for Bt spores
311 heated in Cl_2 and in air, respectively (Fig. 5D). The decrease in carbon content correlates with
312 the SEM images of revealing damage to the Bt spores heated both in air and in Cl_2 at 400 °C (Fig.
313 3D and 3J). In addition, at 300 °C the remaining C content for spores heated in 100% RH Cl_2 is
314 40% less than that for spores heated in 0% RH Cl_2 (Fig. S4), indicating that the carbon release
315 increase at a higher RH. This is consistent with the fact that heating in the presence of Cl_2 gas at
316 a higher RH induces more damage to the spore surface (Fig. S3). The carbon release occurred at
317 peak temperatures that are higher than the corresponding T_c for Bt spores, indicating that release
318 of volatile carbons is not the primary factor for spore neutralization at both temperature rates.
319

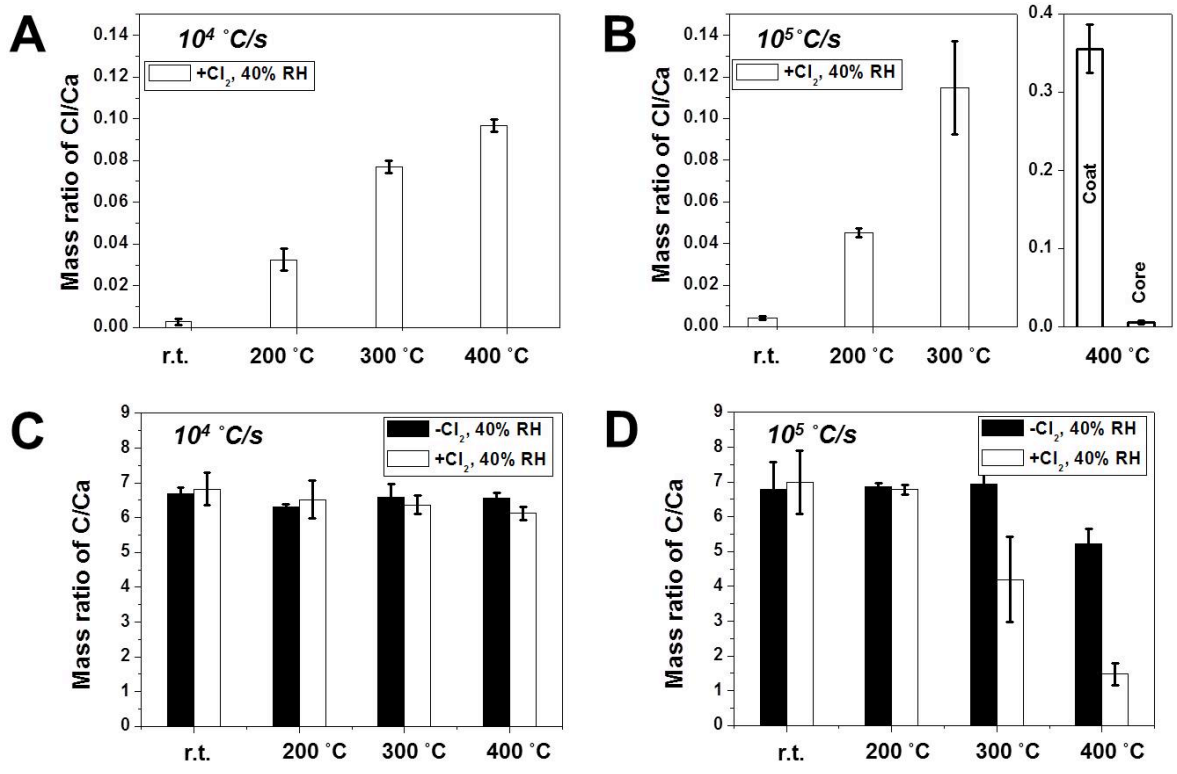

320

321 ***Fig. 5.*** *EDS (energy dispersive spectroscopic) results on the chlorine (A and B) and carbon (C*
322 *and D) mass contents in spores heated at ~10^4 °C/s (A and C) and ~10^5 °C/s (B and D) rates. The*
323 *right side of the graph (B) shows the relative mass contents of Cl in the coat and core of spores*
324 *heated to 400 °C at 10^5 °C/s. The constant content of Ca inside spores is taken as a control and*
325 *normalized to 1. Both the relative contents of Cl and C are presented as the mass ratios of Cl/Ca*
326 *and C/Ca, respectively.*

327

328 **4. Discussion**

329 4.1. Neutralization of Bt *vs* Bs spores at two heating rates without Cl_2

330 Our results (Fig. 1 and Table 1) show that the neutralization of Bt spores by rapid heat
331 treatment alone is determined by the peak temperature and heating rate. The critical peak
332 temperatures for Bt spores heated at ~10^4 °C/s and at ~10^5 °C/s are 407 °C and 232 °C,
333 respectively (Table 1). Previously, we have also studied the neutralization of Bs spores under

similar heating schemes [19]. The critical peak temperatures for Bs spores heated at these two ramp rates are 20 - 30 ˚C lower, indicating that Bs spores are more sensitive to rapid heat than Bt spores. SEM observations of Bs and Bt spores heated at ~10^4 ˚C/s show that spore coats melt at 410 ˚C [19] and 425 ˚C, respectively. When heated at ~10^5 ˚C/s, the coats of Bs spores started to generate visible fissures at a peak temperature of 300 ˚C [19]. In contrast, at the same heating rate and temperature, there are only very small pin holes observed on the surface of Bt spores (Fig. 3C). Together, these results indicate that the spore coat of Bt is less temperature sensitive, which corresponds to the fact that Bt spores possess a higher T_c to rapid heat.

The previously reported neutralization mechanisms for Bs spores depend on the heating rate [19]. At ~10^4 ˚C/s, inactivation is likely due to the thermal damage to DNA since mutants lacking small acid-soluble proteins that protect the DNA within spore showed enhanced sensitivity to heat. At ~10^5 ˚C/s, the spore coat was compromised by elevated internal vapor pressurization from rapid heating [19]. Since neutralization of Bt and Bs was increased at the elevated ~10^5 ˚C/s heating rate, Bt spores likely undergo the same neutralization mechanism as Bs spores. This is supported by the similarity of SEM morphological changes in response to heating at ~10^4 ˚C/s. Furthermore, heating of Bt at ~10^5 ˚C/s to 300 ˚C caused the emergence of holes on the surface of the spores indicating that the Bt spores experienced a similar pressurization event as the Bs spores (Fig. 3C). Although the size of the holes on the surface of Bt spores are reduced in size, heating of Bt spores at ~10^5 ˚C/s to > 400˚C in the presence of Cl_2 led to the entire spore coat detaching from the underlying core. This phenomenon also supports the idea that internal pressure lead to rupture of the fixed spore coat. Results presented here and in earlier studies demonstrate that Bs and Bt spores undergoing rapid heat treatments can be neutralized through two different mechanisms depending on the rate of heating.

4.2. The interaction of Cl_2 and spores

Cl_2 synergizes with rapid heat pulses to inactivate spores at both the ~10^4 ˚C/s and ~10^5 ˚C/s heating rates (Fig. 1). Our results thus raise two central questions: 1) which form of Cl_2 is enhancing the synergistic killing of Bt spores? 2) where is this form of Cl_2 acting on the spore? The mechanism by which Cl_2 synergizes with heat pulses is not completely understood. Cl_2 gas, in addition to being a potent oxidizer, can form chemical bonds with numerous organic and non-organic molecules [23]. Our study has revealed several important findings regarding the form of Cl_2 that is enhancing synergistic killing with heat. First, increased water vapor concentrations in the chamber enhanced the potency of Cl_2 (Fig. 2). Cl_2 can readily react with H_2O to form HCl and HOCl [23]. Since Cl_2 synergizes with heat pulses minimally in the absence of humidity (Fig. 2), the compounds that actively enhance neutralization are likely HCl or HOCl rather than Cl_2 gas. Additional evidence for the higher neutralization activity of HCl/HOCl than Cl_2 is that when the peak temperature increases from 100 ˚C to 300 ˚C, the molar ratio of Cl_2/HCl decreases from ~4 to ~0.13 due to a biased reaction equilibrium from Cl_2+H_2O towards HCl+HOCl at high temperatures (according to CEA (NASA Chemical Equilibrium with Applications) calculations [46] given that the initial concentration of Cl_2 is 4.2×10^{-3} mol/m^3 with a RH of 40 %). Correspondingly, the spore viability reduced significantly as the temperature increased suggesting that HCl/HOCl is more effective in spore neutralization. HCl and HOCl have unique chemical properties. HCl is a strong acid that can act to denature proteins on the spore coat [47-49]. In contrast, HOCl can react with organic molecules leading to chlorine covalently attached to the molecules on and in the spores [23]. But neither at room temperature appears to be efficient at neutralizing Bt spores (Fig. S2) suggesting that the reaction of HCl or HOCl with spores is promoted by heat. For reasons described below, we believe that HOCl is likely the

active form of chlorine. Nonetheless, future studies with HCl alone, HOCl alone, or the combination of the two will provide definitive data regarding the specific form of chlorine that promotes synergistic killing with rapid heat pulses.

The target of Cl_2 inactivation on the spore is also an area of interest since this can reveal vulnerabilities of *Bacillus* spores that can be exploited in biodefense. The EDS data on Cl support the idea that the heat treatment with Cl_2 leads to an accumulation of Cl on the detached spore coat (Fig. 5) indicating the chlorine is interacting primarily with the surface of the spore during the heating pulse. The Cl detected in the spore coat by EDS is either deposited as Cl^- anion from deprotonated HCl or covalently attached through chemical reactions of HOCl to cellular organic molecules. There are two reasons, one chemical and one biological, that favor covalently attached chlorine through HOCl. Our observation that heat synergizes with the form of chlorine that attacks the spore suggests that HOCl rather than HCl is the active agent. This is because the electrophilic attack on biological molecules by $Cl^{\delta+}$ (partially polarized chlorine) from the HOCl molecule possesses a high reaction rate constant and is thus more temperature-dependent, with an increased reaction rate in a high temperature range (> 100 ˚C) [23]. In contrast, even though deprotonation of HCl occurs rapidly at room temperature, the electrophilic attack by H+ is less dependent on temperature and more dependent on the pH value of the system. Supporting the theory that HOCl rather than HCL is responsible is the observation that spores are quite resistant to acid stress alone [6]. The observed synergistic effect of heat pulse and Cl_2 only at elevated temperatures argues against the pH change caused by HCl, which would occur even at ambient temperature. Future studies of the synergistic effect of HOCl with rapid heat pulse would provide direct evidence to support the active compound that inactivates spores.

402 Furthermore, future identification of the spore coat protein(s) that are covalently modified by
403 chlorine will reveal the bacterial target(s) that confers sensitivity.

404

405 4.3. Synergistic neutralization mechanisms for Bt spores by rapid heat and Cl_2

406 There are two potential mechanisms for the observed synergistic effect in spore neutralization
407 between rapid heat and Cl_2: 1). A chemical mechanism in which heat activates chlorine to
408 become a more potent biocide or 2). A biological mechanism in which chlorine and heat damage
409 different targets in the spores to enhance inactivation. Although these two potential mechanisms
410 are not mutually exclusive, the synergistic effect of heat and chlorine is at least in part due to the
411 heat pulse overcoming the activation energy of reactions between chlorine and the spore. The
412 EDS data shows that exposure to Cl_2 alone does not increase Cl content in the spore. Only when
413 heated does the Cl content of the spore increase, supporting the idea that heat enhances the
414 reactivity of chlorine. In addition to the increase in chlorine reactivity, the biological targets of
415 heat and chlorine act on different parts of the spore. Heat pulses at ~10^4 °C/s damage DNA [44],
416 whereas chlorine targets the spore coat. The combination of coat damage and DNA damage can
417 act synergistically neutralize spores. Support for this model of inactivation is that heat pulses at
418 ~10^5 °C/s, which inactivates spores primarily through physical damage of the spore coat,
419 synergizes minimally with chlorine. Thus damaging different targets within the spores, rather
420 than the same target, enhances synergistic neutralization.

421 Another feature of the synergism of Cl_2 with heat pulses is that this effect occurs at peak
422 temperatures and heating rate far below what was required to fix and detach the spore coat (Fig
423 5). An open question is whether the effect observed at the higher peak temperature (>500°C) and

high heating rate (~10^5 ˚C/s) applies to the lower peak temperature and heating rates, which nonetheless synergize with chlorine to neutralize Bt spores. Despite the lack of visual changes of the spores as detected by SEM at peak temperatures of under 300 ˚C, the Cl content on the spore increases as detected by EDS. One interpretation of these results is that at heat pulses between 200-300 ˚C activates chlorine to interact with spores. Even this lower level of chlorine modification of the spore surface can negatively impact the function of the spore coat and increase spore inactivation.

5. Conclusion

Surface immobilized Bt spores subjected to the synergistic effects of ultrafast heating and biocidal chlorine gas were characterized by several observations including changes in viability, morphology, and composition. At the heating rates of ~10^4 ˚C/s, the critical peak temperatures for spore neutralization were reduced from 407 ˚C in air to 252 ˚C when exposed to 100 ppm Cl_2. At the higher heating rates of ~10^5 ˚C/s, the critical peak temperatures for spore neutralization are decreased from 232 ˚C in air to 176 ˚C when exposed to 100 ppm Cl_2. Cl_2 synergizes with rapid heat pulse to enhance spore neutralization. Additional experiments revealed that the synergistic effect of Cl_2 and heat was increased in high humidity, whereas the synergistic effect decreased in low humidity. Cl_2 can react with water to generate HCl and HOCl, which in turn react with the spore. Despite enhancing neutralization, Cl_2 and heat pulses under 300 ˚C did not alter the morphology of the spores. However, treatment of spores at peak temperatures >450 ˚C at ~10^5 ˚C/s caused the spore coat to detach completely from the endospore. EDS results showed that Cl is present in heated spores and the majority of the chlorine is present in detached spore coat indicating that chlorine is acting on the surface of the spores. Our results suggest that the spore surface damage caused by Cl_2, via HOCl and/or HCl, was found to be the major mechanism in enhanced spore neutralization by rapid heat.

Acknowledgements

This work was funded by a grant from DOD/DTRA (BRBAA08-Per5-H-2-0065). We thank Mr. Tim Maugel in the Laboratory for Biological Ultrastructure at the University of Maryland, College Park for his assistance in SEM imaging.

References

[1] E. Nadasi, T. Varjas, I. Prantner, V. Virag, I. Ember, Bioterrorism: Warfare of the 21st century, Gene Ther. Mol. Biol. 11 (2007) 315-320.

[2] Y. Gilbert, C. Duchaine, Bioaerosols in industrial environments: a review, Can. J. Civ. Eng. 36 (2009) 1873-1886.

[3] V. Kummer, W.R. Thiel, Bioaerosols – Sources and control measures, Int. J. Hyg. Environ – Health. 211 (2008) 299-307.

[4] G.W. Gould, History of science – spores Lewis B Perry memorial lecture 2005, J. Appl. Microbiol. 101 (2006) 507-513.

[5] W.L. Nicholson, N. Munakata, G. Horneck, H.J. Melosh, P. Setlow. Resistance of *Bacillus* endospores to extreme terrestrial and extraterrestrial environments, Microbiol. Mol. Biol. Rev. 64 (2000) 548-572.

[6] P. Setlow, Spores of *Bacillus subtilis*: their resistance to and killing by radiation, heat and chemicals, J. Appl. Microbiol. 101 (2006) 514-525.

[7] R. Conesa, P.M. Periago, A. Esnoz, A. Lopez, A. Palop, Prediction of *Bacillus subtilis* spore survival after a combined non-isothermal-isothermal heat treatment, Eur. Food Res. Technol. 217 (2003) 319-324.

[8] O. Couvert, S. Gaillard, N. Savy, P. Mafart, I. Leguerinel, Survival curves of heated bacterial spores: effect of environmental factors on Weibull parameters, Int. J. Food Microbiol. 101 (2005) 73-81.

[9] W.H. Coleman, D. Chen, Y-Q. Li, A.E. Cowan, P. Setlow P, How moist heat kills spores of *Bacillus subtilis*, J. Bacteriol. 189 (2007) 8458-8466.

[10] S.D. Gates, A.D. McCartt, P. Lappas, J.B. Jeffries, R.K. Hanson, L.A. Hokama, K.E. Mortelmans, *Bacillus* endospores resistance to gas dynamic heating, J. Appl. Microbiol. 109 (2010) 1591-1598.

[11] S.D. Gates, A.D. McCartt, J.B. Jeffries, R.K. Hanson, L.A. Hokama, K.E. Mortelmans, Extension of *Bacillus* endospore gas dynamic heating studies to multiple species and test conditions, J. Appl. Microbiol. 111 (2011) 925-931.

[12] S.A. Grinshpun, A. Adhikari, C. Li, T. Reponen, M. Yermakov, M. Schoenitz, E. Dreizin, M. Trunov, S. Mohan, Thermal inactivation of airborne viable *Bacillus subtilis* spores by short-term exposure in axially heated air flow, J. Aerosol Sci. 41 (2010) 352-363.

[13] S.A. Grinshpun, C. Li, A. Adhikari, M. Yermakov, T. Reponen, M. Schoenitz, E. Dreizin, V. Hoffmann, M. Trunov, Method for studying survival of airborne viable microorganisms in combustion environments: development and evaluation, Aerosol Air Qual. Res. 10 (2010) 414-424.

[14] E. Johansson, A. Adhikari, T. Reponen, M. Yermakov, S.A. Grinshpun, Association between increased DNA mutational frequency and thermal inactivation of aerosolized *Bacillus* spores exposed to dry heat, Aerosol Sci. Technol. 45 (2011) 376-381.

493 [15] J.H. Jung, J.E. Lee, S.S. Kim, Thermal effects on bacterial bioaerosols in continuous air
494 flow, Sci. Total Environ. 407 (2009) 4723-4730.

495 [16] Y.H. Lee, B.U. Lee, Inactivation of airborne *E. coli* and *B. subtilis* bioaerosols utilizing
496 thermal energy, J. Microbiol. Biotechnol. 16 (2006) 1684-1689.

497 [17] B-D. Lee, R. Thiruvengadathan, S. Puttaswamy, B.M. Smith, K. Gangopadhyay, S.
498 Gangopadhyay, S. Sengupta, Ultra-rapid elimination of biofilms via the combustion of a
499 nanoenergetic coating, BMC Biotechnol. 13 (2013) 30.

500 [18] P.R.N. Childs, Practical Temperature Measurement, Butterworth Heinemann, London, UK,
501 2001.

502 [19] W. Zhou, M.W. Orr, G. Jian, S.K. Watt, V.T. Lee, M.R. Zachariah, Inactivation of bacterial
503 spores subjected to sub-second thermal stress, Chem. Eng. J. 279 (2015) 578-588.

504 [20] G. McDonnell, A.D. Russell, Antiseptics and disinfectants: activity, action, and resistance,
505 Clin. Microbiol. Rev. 12 (1999) 147-179.

506 [21] A. Fraise, Currently available sporicides for use in healthcare, and their limitations, J. Hosp.
507 Infect. 77 (2011) 210-212.

508 [22] M.M. Coombs, J.F. Danielli, Chlorination of proteins as a method of increasing their
509 opacity in the electron microscope, Nature. 183 (1959) 1257-1258.

510 [23] M. Deborde, U. von Gunten, Reactions of chlorine with inorganic and organic compounds
511 during water treatment – kinetics and mechanisms: a critical review, Water Res. 42 (2008) 13-51.

512 [24] G.A. DeQueiroz, D.F. Day, Disinfection of *Bacillus subtilis* spore-contaminated surface
513 materials with a sodium hypochlorite and a hydrogen peroxide-based sanitizer, Lett. Appl.
514 Microbiol. 46 (2008) 176-180.

515 [25] S.B. Young, P. Setlow, Mechanisms of killing of *Bacillus subtilis* spores by hypochlorite
516 and chlorine dioxide, Appl. Environ. Microbiol. 95 (2003) 54-67.

517 [26] L.J. Rose, E.W. Rice, B. Jensen, R. Murga, A. Peterson, R.M. Donlan, M.J. Arduino,
518 Chlorine inactivation of bacterial bioterrorism agents, Appl. Environ. Microbiol. 71 (2005) 566-
519 568.

520 [27] A.R. Brazis, J.E. Leslie, P.W. Kabler, R.L. Woodward, The inactivation of spores of
521 Bacillus globigii and Bacillus anthracis by free available chlorine, Appl. Microbiol. 6 (1958)
522 338-342.

523 [28] E.W. Rice, N.J. Adcock, M. Sivaganesan, L.J. Rose, Inactivation of spores of *Bacillus*
524 *anthracis* Sterne, *Bacillus cereus*, and *Bacillus thuringiensis* subsp. *israelensis* by chlorination,
525 Appl. Environ. Microbiol. 71 (2005) 5587-5589.

526 [29] G.M. Fair, J.C. Morris, S.L. Chang, The dynamics of chlorination, J. New Engl. Water
527 Works Assoc. 61 (1947) 285-301.

528 [30] A.A. Hosni, W.T. Shane, J.G. Szabo, P.L. Bishop, The disinfection efficacy of chlorine and
529 chlorine dioxide as disinfectants of *Bacillus globigii*, a surrogate for *Bacillus anthracis*, in water
530 networks: a comparative study, Can. J. Civ. Eng. 36 (2009) 732-737.

[31] J. Szabo, S. Minamyer, Decomtamination of biological agents from drinking water infrastructure: a literature review and summary, Environ. Int. 72 (2014) 124-128.

[32] A.C. Kreske, J-H. Ryu, C.A. Pettigrew, L.R. Beuchat, Lethality of chlorine, chlorine dioxide, and a commercial produce sanitizer to *Bacillus cereus* and *Pseudomonas* in a liquid detergent, on stainless steel, and in biofilm, J. Food Prot. 69 (2006) 2621-2634.

[33] L.V. Venczel, M. Arrowood, M. Hurd, M.D. Sobsey, Inactivation of Cryptosporidium parvum oocysts and Clostridium perfringens spores by a mixed-oxidant disinfectant and by free chlorine, Appl. Environ. Microbiol. 63 (1997) 1598-1601.

[34] C.H. Johnson, M.M. Marshall, L.A. DeMaria, J.M. Moffet, D.G. Korich, Chlorine inactivation of spores of *Encephalitozoon* spp., Appl. Environ. Microbiol. 69 (2003) 1325-1326.

[35] H. Son, M. Cho, H. Chung, S. Choi, J. Yoon, Bactericidal activity of mixed oxidants: comparison with free chlorine, J. Ind. Eng. Chem. 10 (2004) 705-709.

[36] J. Perez, S. Springthorpe, S.A. Sattar, Activity of selected oxidizing microbiocides against the spores of *Clostridium difficile*: relevance to environmental control, Am. J. Infect. Control. 33 (2005) 320-325.

[37] D.E. John, C.N. Haas, N. Nwachuku, C.P. Gerba, Chlorine and ozone disinfection of *Encephalitozoon intestinalis* spores, Water Res. 39 (2005) 2369-2375.

[38] R.M.S. Thorn, G.M. Robinson, D.M. Reynolds, Comparative antimicrobial activities of aerosolized sodium hypochlorite, chlorine dioxide, and electrochemically activated solutions

550 evaluated using a novel standardized assay, Antimicrob. Agents Chemother. 57 (2013) 2216-
551 2225.

552 [39] http://emergency.cdc.gov/agent/chlorine/basics/facts.asp

553 [40] http://www.accessdata.fda.gov/scripts/cdrh/cfdocs/cfCFR/CFRSearch.cfm?CFRPart=173

554 [41] http://www.accessdata.fda.gov/scripts/cdrh/cfdocs/cfcfr/CFRSearch.cfm?CFRPart=178

555 [42] S. Xu, T.P. Labuza, F. Diez-Gonzalez, Inactivation of *Bacillus anthracis* spores by a
556 combination of biocides and heating under high-temperature short-time pasteurization conditions,
557 Appl. Environ. Microbiol. 74 (2008) 3336-3341.

558 [43] J-L. Sagripanti, M. Carrera, J. Insalaco, M. Ziemski, J. Rogers, R. Zandomeni, Virulent
559 spores of Bacillus anthracis and other Bacillus species deposited on solid surfaces have similar
560 sensitivity to chemical decontaminants, J. Appl. Microbiol. 102 (2007) 11-21.

561 [44] W. Zhou, S.K. Watt, D-H. Tsai, V.T. Lee, M.R. Zachariah, Quantitative attachment and
562 detachment of bacterial spores from fine wires through continuous and pulsed DC
563 electrophoretic deposition, J. Phys. Chem. B. 117 (2013) 1738-1745.

564 [45] J.N. Junior, P.R. de Massaguer, Thermal death kinetics of *B. stearothermophilus* spores in
565 sugarcane must, J. Food Proc. Eng. 30 (2007) 625-639.

566 [46] http://www.grc.nasa.gov/WWW/CEAWeb/ceaHome.htm

567 [47] L.R. Wyatt, W.M. Waites, The effect of chlorine on spores of *Clostridium bifermentans*,
568 *Bacillus subtilis* and *Bacillus cereus*, J. Gen. Microbiol. 89 (1975) 337-344.

569 [48] B. Setlow, C.A. Loshon, P.C. Genest, A.E. Cowan, C. Setlow, P. Setlow, Mechanisms of
570 killing spores of *Bacillus subtilis* by acid, alkali and ethanol, J. Appl. Microbiol. 92 (2002) 362-
571 375.

572 [49] M. Cho, J-H. Kim, J. Yoon, Investigating synergism during sequential inactivation of
573 Bacillus subtilis spores with several disinfectants, Water Res. 40 (2006) 2911-2920.

574

575

576

577 Supplemental information:

578 Synergistic Effects of Ultrafast Heating and Gaseous
579 Halogen Biocides on the Neutralization of Bacterial
580 Spores

Wenbo Zhou,[a] Mona W. Orr,[b] Vincent T. Lee,[b] Michael R. Zachariah[a]

Department of Chemical and Biomolecular Engineering and Department of Chemistry and Biochemistry, University of Maryland, College Park, Maryland 20742, USA[a]; Department of Cell Biology & Molecular Genetics, University of Maryland, College Park, Maryland 20742, USA[b]

LIST OF FIGURE AND TABLE CAPTIONS

TABLE S1. Chlorine concentration-exposure time-kill relationships for *Bacillus* spores in solution. All measurements were done at the room temperature.

FIGURE S1. Schemetic of the T-jump probe involving one Bt spores coated wire, as well as the gas chamber supplemented with a humidity meter.

FIGURE S2. (A) The survivability of Bt spores exposed to Cl_2 gas with different concentrations for 15 mins in ambient air. (B) and (C) are SEM images of original Bt spores and Bt spores after treated with 1000 ppm Cl_2 for 15 mins.

FIGURE S3. Spore morphologies when heated to ~400 ˚C at 10^5 ˚C/s in Cl_2. The relative humidities are controlled as 0% (A), 40% (B) and 100% (C), respectively.

FIGURE S4. EDS (energy dispersive spectroscopic) results on the carbon mass contents in spores heated to 300 ˚C at ~10^5 ˚C/s. The RH was changed from 0% to 100%. The constant content of Ca inside spores is taken as a control and normalized to 1. The relative contents of C are presented as the mass ratios of C/Ca.

Table S1.

Chlorine concentration-exposure time-kill relationships for *Bacillus* spores in solution. All measurements were done at the room temperature.

Reference	Bacillus spore	Cl_2 concentration (ppm)	Exposure time (min)	Viability reduction
Brazis et al. [27]	*B. anthracis*	63-110	420	4-log
Brazis et al. [27]	*B. globigii*	50-113	1080	4-log

Rice et al. [28]	*B. anthracis*	267	120	2-log
Fair et al. [29]	*B. anthracis*	333	60	3-log
Rose et al. [26]	*B. anthracis*, *B. cereus*, *B. thuringiensis*	667	45-61	>4-log
Hosni et al. [30]	*B. globigii*	500-667	118-234	3-log
Brazis et al. [27]	*B. anthracis*	767-800	49	4-log
Brazis et al. [27]	*B. globigii*	833-867	82	4-log
Fair et al. [29]	*B. anthracis*	1000	30	3-log
Szabo et al. [31]	*B. anthracis*	3333	60	4-log
Kreske et al. [32]	*B. cereus*	6.7×10^4	5	>3.8-log
DeQueiroz et al. [24]	*B. subtilis*	8.3×10^6	5	4-log

619

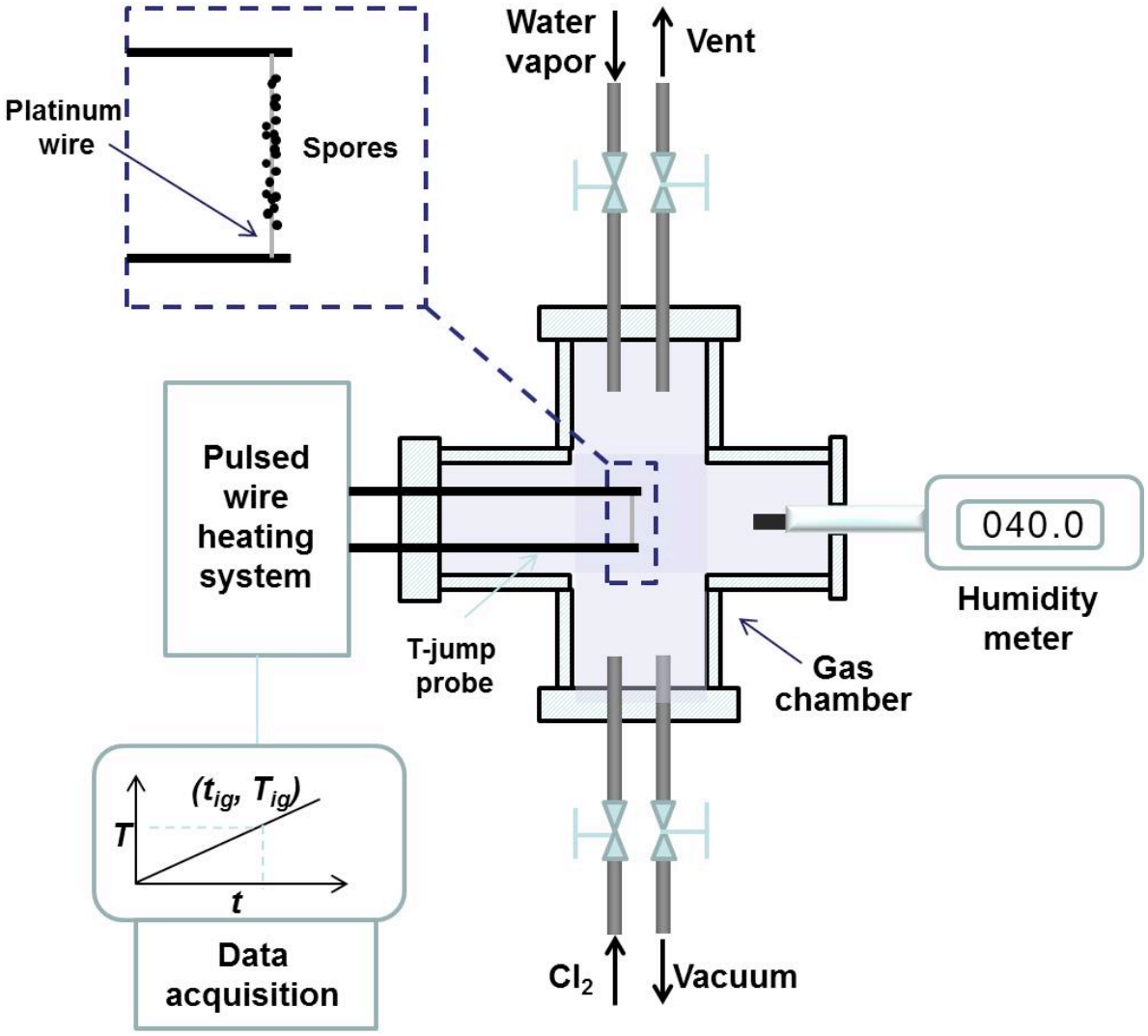

620

621 **Fig. S1.** Schemetic of the T-jump probe involving one Bt spores coated wire, as well as the gas
622 chamber supplemented with a humidity meter.

623

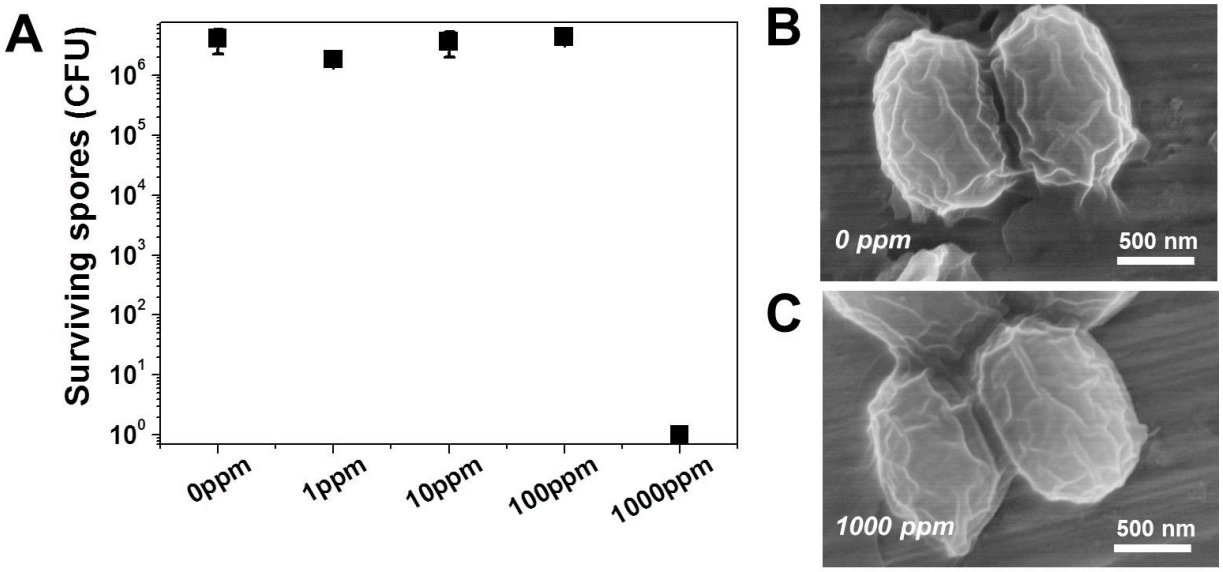

624

625 **Fig. S2.** (A) The survivability of Bt spores exposed to Cl_2 gas with different concentrations for
626 15 mins in ambient air. (B) and (C) are SEM images of original Bt spores and Bt spores after
627 treated with 1000 ppm Cl_2 for 15 mins.

628

629

630

631

632

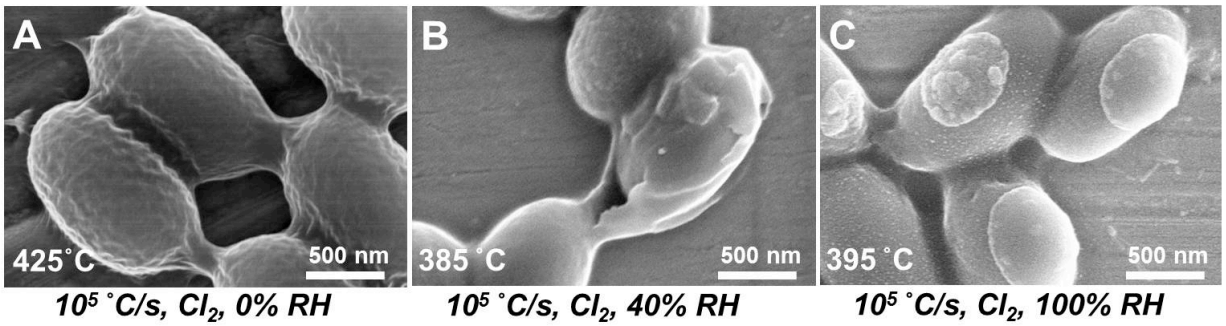

Fig. S3. Spore morphologies when heated to ~400 ˚C at 10^5 ˚C/s in Cl_2. The relative humidities are controlled as 0% (A), 40% (B) and 100% (C), respectively.

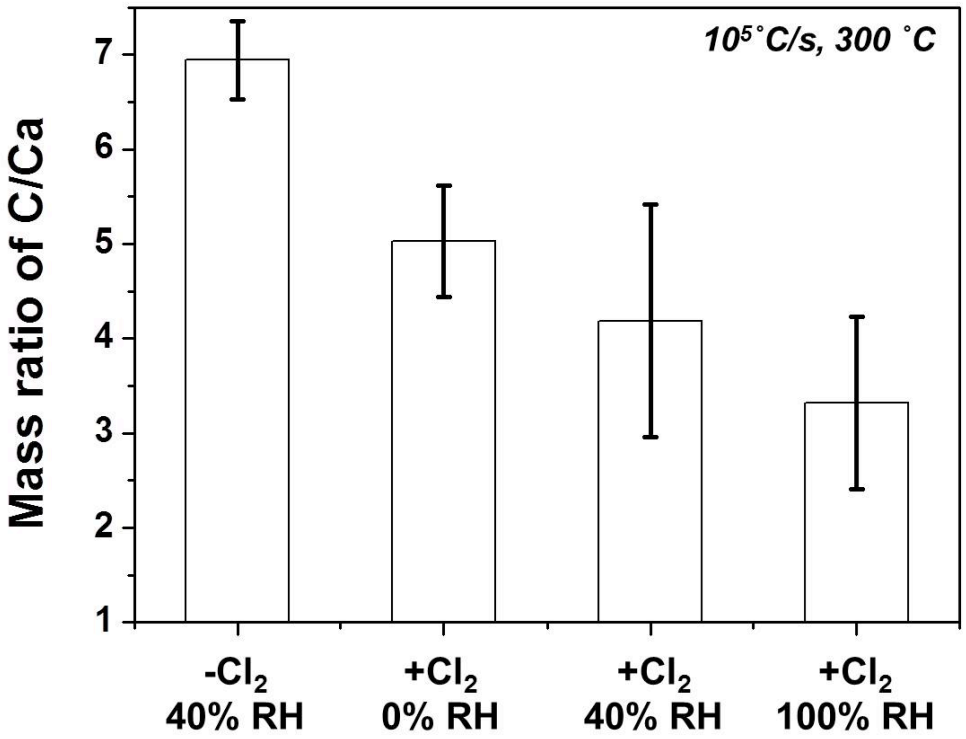

Fig. S4. EDS (energy dispersive spectroscopic) results on the carbon mass contents in spores heated to 300 ˚C at ~10^5 ˚C/s. The RH was changed from 0% to 100%. The constant content of Ca inside spores is taken as a control and normalized to 1. The relative contents of C are presented as the mass ratios of C/Ca.

DEPARTMENT OF DEFENSE

DEFENSE THREAT REDUCTION
AGENCY
8725 JOHN J. KINGMAN ROAD
STOP 6201
FORT BELVOIR, VA 22060
ATTN: D. DALTON

DEFENSE TECHNICAL
INFORMATION CENTER
8725 JOHN J. KINGMAN ROAD,
SUITE 0944
FT. BELVOIR, VA 22060-6201
ATTN: DTIC/OCA

DEPARTMENT OF DEFENSE CONTRACTORS

QUANTERION SOLUTIONS, INC.
1680 TEXAS STREET, SE
KIRTLAND AFB, NM 87117-5669
ATTN: DTRIAC